Developments in biomedical sensors based on electrical impedance

Improvements in electrodes, instrumentation and signal processing technology for new and existing biomedical sensors for clinical use.

Christian Tronstad

Thesis for the degree of Doctor Philosophiae

Department of Clinical and Biomedical Engineering

Oslo Hospital Services

Oslo University Hospital

Series of dissertations submitted to the
Faculty of Mathematics and Natural Sciences, University of Oslo
No. 1252

ISSN 1501-7710

Cover: Inger Sandved Anfinsen.
Printed in Norway: AIT Oslo AS.

Produced in co-operation with Akademika publishing.
The thesis is produced by Akademika publishing merely in connection with the thesis defence. Kindly direct all inquiries regarding the thesis to the copyright holder or the unit which grants the doctorate.

TABLE OF CONTENTS

PREFACE

Foreword

This is the summary of research over five years within different projects related to impedance-based biomedical sensors. An introduction to this technology is given in CH1, leading to the general aim of the work given in CH2. The content is then divided into three parts: *electrodes*, *instrumentation* and *signal processing*, which are introduced in CH1. For a gradual insight into this work, it is advised to first continue with CH3 on instrumentation, and then go on to CH4 and CH5. These are the main chapters which summarize all the technological papers with an introduction to the topic followed by specific problems, aims, results, discussion and conclusion. In order to discuss the potential for clinical benefit of the technology, a whole chapter (CH6) is dedicated to the clinical perspective of the biomedical sensors including the clinical and pre-clinical papers. In CH7, some of the ongoing and unpublished related work is mentioned before the general discussion and conclusion is given in CH8. Among the included papers, papers I, II, III and VIII are related to instrumentation, papers IV, V and VI are related to electrodes, papers VII, IX, X and XI are related to signal processing, and papers XII, XIII and XIV are related to clinical or pre-clinical testing. A poster relevant to the clinical use of one of the biomedical sensors is attached as an appendix.

Timeline, projects and funding

This work started with the continuation of the Author's Master's degree project where a prototype instrumentation was developed for measurement of sweat activity [Tronstad 2005]. Since then, the development of this sensor has continued towards the final goal of clinical use. In 2007, the further developed sensor was presented at the ICEBI XII conference in Graz. The Author was then motivated to pursue a doctoral degree, and a paper was submitted to Physiological Measurement later the same year. A 3-year hyperhidrosis project was described by Sverre Grimnes, Erik Fosse and Anne-Lene Krogstad at Oslo University Hospital (OUS), but funding was not granted. At this time, the Author was funded on 40% salary from BioGauge A/S only. In 2008, the Author was included in a bioimpedance sensor project led by Håvard Kalvøy at the Department of Clinical and Biomedical Engineering, OUS, and partly funded by this project together with 20% consultancy work for Alertis Medical ASA. In 2009, the Author was 80% funded as a research fellow in a biomedical sensor project led by Alertis Medical ASA, which had 50% funding from the Norwegian Research Council. Due to bankruptcy, this lasted only a year, and the Author was offered a 100% temporary position for 2010 at the Department of Clinical and Biomedical Engineering, with 50% time for research and development. A 50% position was extended in 2011 for clinical research assistance and completion of the doctorate work. Since January 2012, the Author has worked in a full-time position at the Department of Clinical and Biomedical engineering. Hence, from 2007 until 2012, the Author has jumped between several projects due to funding, but the research and development has always been on impedance-based biomedical sensors for clinical use, which is the theme of this thesis.

Acknowledgements
It is a privilege to have had the conditions to work with, and now write about, some of the very things that fascinates one in life. These conditions are the foundation of this work, and there are many contributors to this foundation whom all deserve mentioning. Hence, this list is long.

First, my thanks go to professor emeritus Sverre Grimnes, my first supervisor before his retirement. His vast knowledge, dedication, enthusiasm and completely unselfish attitude in research inspired me as a role model of a scientist, and he has been a great support over the years. Although he is retired, he is still producing important contributions to his fields of research, and his presence at the department is greatly valued by many.

Secondly, my sincere thanks go to associate professor Jan Olav Høgetveit, who completely boosted the motivation of a slacking student within only days after starting my trainee job at his department back in 2004. He is today my superior, and I could not imagine a better leader for all aspects that includes. Specifically thanks for providing the time and resources to complete this work.

Next, my second supervisor, professor Ørjan G. Martinsen, who gave me a gentle push into the doctorate work which I am now grateful for. I soon found out that he can also use more force, as he is a 3rd Dan in karate, which is a common interest. Another trait is his unique and intelligent humor which paralleled with his scientific expertise constitutes a person who is great to work together with.

This work has been conducted at the Department of Clinical and Biomedical Engineering, Division of Oslo Hospital Services, Oslo University Hospital in collaboration with researchers from the following departments at the hospital: Department of Dermatology, The Interventional Centre, The Department of Neuropsychiatry and Psychosomatic Medicine, Department of Plastic and Reconstructive Surgery, Department of Neurology, Department of Nephrology, Division of Emergencies and Critical Care and the Division of Mental Health and Addiction.

It has been especially interesting for someone with an engineering background to work so tightly together with clinicians, which has provided a unique learning experience. Being included in research together with the anesthesiologists professor Tor Inge Tønnessen and Søren Pischke has been very enriching to my understanding of the clinical side of biomedical engineering. Their sheer skill and competence has been very educational to a becoming researcher. Special thanks to professors Anne-Lene Krogstad and Erik Fosse for their interest in the sweat activity sensor since the beginning, and to Anne-Lene and Per Helsing for including me in their research and helping me with dermatologically-related questions. Further thanks go to professor Trond Jenssen, Bjørn Christian Østberg, Slawomir Wojniusz and professor Ellen Jørum for collaboration or support within their respective fields of diabetes, stress disorders, neuropsychiatry and neurology relevant to this work. Also thanks to the nurses Laila Elmholt, Oddrun Sarong and Hilde Hestvaag for their assistance during experiments.

On the technical side, I have had the pleasure to work together with skilled colleagues both at the department of Clinical and Biomedical Engineering at the hospital and at the Department of Physics, University of Oslo. Special thanks to: Håvard Kalvøy, who included me in his interesting projects, and also supported me greatly in mine. Gorm Krogh Johnsen and Bernt Nordbotten, with whom I greatly appreciate working together with. From the Department of Clinical and Biomedical Engineering, I would also like to thank my close colleagues Tormod Martinsen and Fred-Johan Pettersen for contributing to a great work environment. Bård Henningsen for giving me time to finish this work. Øyvind Stenshagen for providing me with computer equipment which greatly enhanced the data analysis capabilities in this work. Andre Bakken for sharing his expertise in electronic circuitry. Cecilie Langvik for proof-reading. Aman Osmani for help with laboratory equipment. The rock climbing group for the annual mountaineering adventures. Lars-Fredrik Aronsen (the lønningspils general) for keeping up social arrangements. And last but not least, the head of department, Øystein Jensen and his chief of staff, Per-Arne Jørgensen, for providing this great work environment and for their general emphasis on research.

Sincere thanks to the director of Oslo Hospital Services, Geir Teigstad, for managing to prioritize research during a tight budget and for approving my position during this time.

Thanks go to those I had the pleasure to work together with from the previous Alertis Medical ASA: Lars Holhjem, Tore Omtveit, Lars Guntveit, Martin Krekling and Kristin Eivindvik, giving me some new insights into sensor design, manufacturing, regulations and marketing.

Among all the conditions for doing research work, funding is major. Although my funding has been variable and short-sighted during these five years, it has always been sufficient and I have never experienced it as a problem. My sincere gratitude goes to the following people for their efforts in providing me and my doctorate work with funding: Jan Olav Høgetveit, Sverre Grimnes, Ørjan Martinsen, Øystein Jensen, Tor Inge Tønnessen, Kristin Eivindvik, Martin Krekling, Bård Henningsen, André Nygård, Anne-Lene Krogstad, Erik Fosse, Per Ludvigsen and Bjørn Christian Østberg.

Thanks to Stein Stabelfelt Nielsen and his electronics workshop at the Department of Physics, University of Oslo, for assistance with production of instrumentation.

Thanks to all international colleagues within the fields of biomedical engineering and bioimpedance who have shown interest, shared expertise and given opinion on our work.

Finally, even though you have no clue what I work with: Sincere thanks to my closest friends, my dear parents Grete and Sverre, my brother Andreas and sister-in-law Kristin, and my beautiful girlfriend Shelly for their support, wisdom, different perspectives and for getting the most out of my limited spare-time during this work.

Oslo, July 1st 2012

LIST OF ORIGINAL PAPERS

I. **Tronstad C**, Gjein G E, Grimnes S, Martinsen Ø G, Krogstad A L and Fosse E 2008 Electrical measurement of sweat activity. Physiol. Meas. 29 S407–15

II. **Tronstad C**, Martinsen Ø G and Grimnes S 2008 Embedded instrumentation for skin admittance measurement. Engineering in Medicine and Biology Society, 2008. EMBS 2008. 30th Annual International Conference of the IEEE S2373 - 2376

III. **Tronstad C**, Grimnes S, Martinsen Ø G, Amundsen V and Wojniusz S 2010 PC-based instrumentation for electrodermal activity measurement. J. Phys.: Conf. Ser. 224 012093

IV. **Tronstad C**, Johnsen G K, Grimnes S and Martinsen Ø G 2010 A study on electrode gels for skin conductance measurement. Physiol.Meas 31 S1395-1410

V. Kalvøy H, **Tronstad C**, Nordbotten B, Martinsen Ø G and Grimnes S 2010 Electrical impedance of stainless steel needle electrodes. Ann. Biomed. Eng. 38 2371–82

VI. **Tronstad C**, Pischke S, Holhjem L, Tønnessen T I, Martinsen Ø G and Grimnes S 2010 Early detection of cardiac ischemia using a conductometric pCO2 sensor: real-time drift correction and parameterization. Physiol.Meas 31 S1241-1255

VII. Martinsen Ø G, Grimnes S, Nilsen J K, **Tronstad C**, Wooyoung J, Hongsig K, Kunsoo S, Naderi M, Thielmann F 2008 Gravimetric method for in vitro calibration of skin hydration measurements IEEE trans.biomed.eng. 55 S728-732

VIII. Grimnes S, Jabbari A, Martinsen Ø G, **Tronstad C** 2010 Electrodermal activity by DC potential and AC conductance measured simultaneously at the same skin site. Skin Res.Tech. DOI: 10.1111/j.1600-0846.2010.00459.x

IX. **Tronstad C,** Kalvøy H, Martinsen Ø G and Grimnes S 2012 Improved estimation of sweating based on electrical properties of skin. *Submitted to Annals of Biomedical Engineering.*

X. **Tronstad C**, Kalvøy H, Martinsen Ø G and Grimnes S 2012 Waveform difference between skin conductance and skin potential responses in relation to electrical and evaporative properties of skin. *Submitted to Psychophysiology.*

XI. Nordbotten BJ, **Tronstad C**, Martinsen Ø G and Grimnes S 2011 Evaluation of algorithms for calculating bioimpedance phase angle values from measured whole-body impedance modulus. Physiol Meas 32 S755-765.

XII. **Tronstad C**, Helsing P, Tønseth K A, Sverre Grimnes and Krogstad A L 2012 Tumescent suction curettage versus curettage only for the treatment of axillary hyperhidrosis evaluated by subjective and new objective methods. *Submitted to Skin Research and Technology.*

XIII. Pischke S E, **Tronstad C**, Holhjem L, Halvorsen P S, Tønnessen T I 2012 Perioperative detection of myocardial ischemia/reperfusion with a novel tissue CO2 monitoring technology. *European Journal of Cardio-Thoracic Surgery. In press.*

XIV. Pischke S E, **Tronstad C**, Holhjem L, Line P D, Haugaa H and Tønnessen T I 2012 Hepatic and Abdominal PCO2 Measurement Detects and Discriminates Hepatic Artery and Portal Vein Occlusion in Pigs. *Submitted to Liver Transplantation.*

1.0 GENERAL INTRODUCTION

For a clear understanding of the topic of this work, it is necessary to first give a definition of a *biomedical sensor*. To begin with, consider an object with a property of interest, and a tool which can be applied in order to sense this property. In this context, the object is the human body and the tool is called a *sensor*. A *sensor is a mediator able to convert one or more measurands (properties) or physical variables into an equivalent signal variable of another type of quantity within a frame of a given unity* [Pallàs-Areny & Webster, 2001, pp.3-4]. When the sensor is used for purposes within the fields of biology or medicine, the sensor is a biomedical sensor. Grimnes and Høgetveit 2011 gave the following definition of a biomedical sensor: *A biomedical sensor is a device converting any signal related to the science of any living tissue into other quantities, usually an electrical signal, and thereby representing a connection between a biomedical and a recording system.* This work concerns biomedical sensors where this signal of interest is physiological and clinically relevant information from the human body.

In many cases, the human senses of the physician will suffice to gather the necessary information about the condition of the patient, for example when inspecting a wound. However, biomedical sensors provide a door into important information which is not accessible with the senses of either physician or patient. Some biomedical sensors simply just amplify the senses of the physician, such as the stethoscope which enables diagnostics of heart or lung function by the amplified sounds generated by these organs. Nevertheless, most biomedical sensors measure another physical property which is translated into the property of interest. As an example, the pulse-oxymeter measures absorbance of light emitted through the finger, but converts this optical property into a number which quite accurately represents the oxygen saturation in the blood. Table 1 gives a list of different physical properties which are translated into important biomedical parameters by biomedical sensor methods.

Table 1. Examples of different physical properties which are translated to important biomedical parameters by biomedical sensor methods.

Physical property	Sensor method	Biomedical parameter
Pressure	Doppler ultrasound	Blood flow velocity
Light	Pulse oxymeter	Blood oxygen saturation
Temperature	Thermodilution	Cardiac output
Electrical potential	Electrocardiogram (ECG)	Heart function
Electrical impedance	Electrical impedance tomography	Lung function

The device which converts the physical property into a signal which can be more easily handled and quantified (e.g. voltage) is called a *transducer*.The transducer represents the first line in the flow of information from the body to the output which displays the biomedical parameter of interest, e.g. a patient monitor. Without proper transducers, the measurement will be useless. Second in line is the instrumentation which controls the measurement. This part usually consists of electronic circuitry with one or more microchips which are

programmed to perform measurements. A poorly designed instrumentation part will reduce the accuracy of the measurement. The third line is the step which converts the measured signal into useful information for the physician. This process involves removing redundant information, enhancing the information of interest and estimating the biomedical parameter by mathematical operations. The processing may take place within the microchips of the instrument, in the software on the monitoring unit which receives data and displays the result, or as a separate post-processing tool for analysis of stored measurement. In its simplest form, this step only filters noise, amplifies the signal of interest and leaves the interpretation to the eye of a trained physician, such as in ECG monitoring. In more advanced sensor systems, large amounts of data are used to automatically suggest a decision for the physician, such as with malignant melanoma detection [Aberg et al 2011]. The development of signal processing algorithms is a very important part of biomedical sensor engineering, and much of the innovation today lies in this part as many measurement technologies are approaching their limit and microprosessor computing capabilities have increased vastly. The final parameter shown on the screen can never be more accurate than the accuracy of the parameter estimation algorithm, which can never be more accurate than what is provided by the instrumentation, which again can never be more accurate than what the transducer can pick up from the body. Thus, all the parts shown in figure 1 are critical to a biomedical sensor.

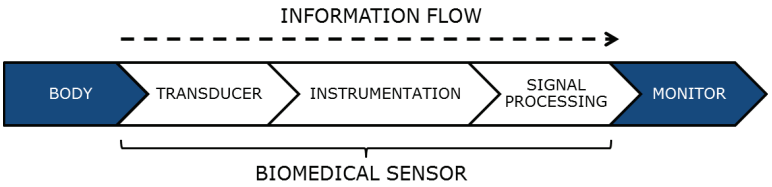

Figure 1. Information flow from the body to the monitor provided by the biomedical sensor.

Depending on definition, the biomedical sensor can either be regarded as the transducer, the transducer together with the instrumentation, or all three parts as in figure 1. In this work, we consider everything in between the body and the final parameter displayed on the screen as the biomedical sensor. The work in this thesis concerns developments within these three parts for biomedical sensors being based on the physical property of *electrical impedance,* which is briefly explained below:

Electrical impedance means to which degree something opposes the flow of electrons or ions. In order to have an electrical current through an object, there needs to be an electrical potential difference (voltage) between two points. The impedance is found from this voltage divided by the current, and is a *passive* property of the object. This is different from electrical potentials which are generated by the object itself, which is an *active* property. When electrical impedance is measured in a biological material such as the human body, it is called *bioimpedance*, and represents the opposition to the flow of *ions* through the body, not electrons as in a copper wire. The transducers which connect the biosensor to the body, apply the electrical potential and facilitate the transfer between electronic and ionic current are called *electrodes*. In bioimpedance measurement, the same electrodes can also be used to pick up the current which can be measured in order to calculate the impedance. More advanced

solutions use different electrodes for voltage excitation and pick-up. For an electrical impedance measurement, the instrumentation governs both the generation of voltage between the electrodes and the measurement of the current passing between them. The signal processing of bioimpedance measurement depends on the biomedical parameter of interest, and the raw bioimpedance values are rarely of clinical interest.

2.0 GENERAL AIM

The vision at the author's workplace, the Department of Clinical and Biomedical Engineering, is *development of technology for the benefit of the patient*. This implies that the technology must have potential for clinical use, and also that the technology must work. The focus technology in this work is impedance-based biomedical sensors, and this means that the sensors must have clinical significance, and that the measurement of the biological parameter must be accurate. As outlined in the introduction, the electrodes, instrumentation and signal processing are critical to this accuracy. Hence, the general aim of this work was:

Improvements in electrodes, instrumentation and signal processing for biomedical sensors based on electrical impedance.

Within each of these biomedical sensor parts, the aims were:

- Electrodes: *Assess how different electrode types influence measurement, both for non-invasive and invasive electrical impedance measurement.*
- Instrumentation: *To develop instrumentation suitable for portable and long-term recording of skin admittance in patients.*
- Signal processing: *To improve the estimation of biological parameters based on electrical impedance signals coming from skin, tissue metabolism and the whole body.*

These aims are further specified within their respective chapters.

3.0 INSTRUMENTATION

3.1 Introduction to instrumentation for impedance measurement

Electrical impedance is a material property which has two components – the resistive and the reactive part. Thus, mathematically the impedance (Z) is expressed as a complex number by the sum of the resistance (R) and the imaginary reactance (X):

$$Z = R + jX \quad (1)$$

When a known electrical current is applied to a material, the impedance is found by measuring the voltage between the electrodes and dividing this by the current. In many cases, applying a known voltage to the material and measuring the current between the electrodes is more practical. The signal (current) then becomes inversely proportional to the impedance. This quantity is called electrical *admittance (Y)*, which is also expressed as a complex number with two components *conductance (G)* and *susceptance (B)*:

$$Y = \frac{1}{Z} = G + jB \quad (2)$$

Depending on which of these electrical properties that is most interesting for the type of sensor in question, the Z, Y, R, X, G, B or a combination of these is extracted from the measurement. The X and B are dependent on the frequency (ω) of the current which is applied through the material and can only be measured by alternating the direction of the current. B is proportional to this frequency and the electrical *capacitance (C)* of the material can be found from B/ω. Thus, the first basic part needed for impedance measurement is a generator which applies controlled alternating current (AC) or voltage through the electrodes and the material.

The second most important part is the acquisition of the resulting voltage between the electrodes from the applied current, or the resulting current through the electrodes from the applied voltage, which is needed to calculate Z or Y, respectively. The voltage can be read directly by an analog-to-digital converter (ADC), but the current needs to be converted to voltage before the acquisition. In both cases, the instrument will acquire an AC voltage signal which in amplitude is proportional to the Z or Y.

Because the conductive (R or G) and the capacitive (X or B) components represent different properties of the material, the decomposition of these from the Z or Y signal is a part of most impedance measurement instrumentation. The preferred method for this third basic part is called phase-sensitive rectification (PSR), which implies extraction of only the component of a signal which has the same phase (temporal shift) and frequency as a reference signal. A purely conductive material will not change the phase between the applied and response signal, but a purely capacitive material will shift the phase by a quarter of the AC cycle (90˚). Thus, the conductive part can be extracted by PSR with a 0˚ reference signal, while the capacitive part is extracted in the same way using a 90˚ reference signal.

This *phase angle* of the signal is often used directly as a parameter for interpreting impedance measurements. Further information about the material, and especially for biological materials, can be gained by measuring impedance at multiple frequencies. This requires more advanced instrumentation for current/voltage application and acquisition.

For bioimpedance measurement where the instrument is connected to e.g. patients, additional steps must be taken for electrical safety of the equipment.

In summary, there are three basic parts or functions needed for impedance measurement instrumentation:

1. AC voltage or current generator
2. Signal acquisition
3. Phase-sensitive rectifier (PSR)

3.2 Problems with instrumentation for impedance measurement

An advantage with impedance measurement is that the instrument requires only electrical components, as the physical property of interest is electrical or ionic and no transducers other than electrodes are needed. With 21st century electronics, utilization of smart components enables miniaturized and cost-effective design. However, most available impedance analyzers are still large and expensive. Stationary equipment for research or industrial process-control should still be as accurate as possible with no compromise for size or cost, but for biomedical sensors, portability or wearability of the sensor is often a key requirement.

3.3 Aims of the instrumentation work

The aim of this work was to design and develop instrumentation which is suitable for portable and long-term recording of skin admittance in patients. This included the following requirements:

- The instrument had to be small enough to fit into a pocket or carried attached to a belt.
- The instrument had to be continuously operative for 24 h.
- The instrument had to be able to record skin admittance at four skin sites simultaneously.
- The instrument had to satisfy hospital requirements for electrical safety.

3.4 Summary of the results on instrumentation work

3.4.1 Embedded design

An embedded design was created with emphasis on performing most of the measurement functions within a microcontroller (μC) (Paper II). Instead of using a dedicated component for voltage generation, a μC was used to generate a sine-wave voltage using a combination of a lookup-table, an internal pulse-with modulator (PWM), a voltage divider and a low-pass filter. Signal acquisition of the current through the measuring electrode was implemented by current-to-voltage conversion using an operational amplifier and sampling of the converted signal by an ADC. The PSR function was implemented by digital processing of the sampled

current signal within the µC. Figure 2 shows the component layout of the solution in a) and the µC measurement process in b). Compared to conventional instrumentation using analogue components for specific functions, this design reduces the number of components needed and thereby the size, current usage and cost of the sensor. The digital solution with software control also provides flexible configuration of measurement parameters such as the applied voltage amplitude and frequency.

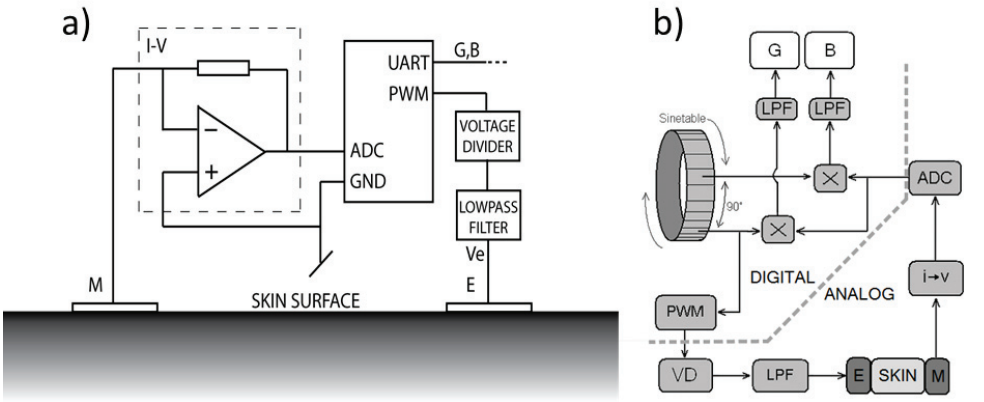

Figure 2. Overview of the embedded design for skin admittance measurement instrumentation. a) Component layout with current-to-voltage conversion (I-V) of the current picked up at M, a microcontroller with ADC, PWM and serial port (UART), and external voltage divider and low-pass filter for controlled voltage between the electrodes (E and M). b) principle of the measurement process run by the microcontroller, in which most of the measurement processes are run digitally in software © 2008 IEEE.

3.4.2 Portable skin conductance sensor for clinical use

Based on the embedded solution (Paper II), a portable device for multichannel skin conductance measurement was built (Paper I).

In order to provide measurements which are sensitive to the skin rather than deeper tissue, the frequency of the applied voltage was carefully selected based on previous research by Martinsen et al [Martinsen et al 1999].

To facilitate measurements at different skin sites simultaneously which are sensitive only to the conductance of the skin below each measuring electrode, a special electrode system was used based on the earlier work by Grimnes in 1983 [Grimnes 1983]. For a sensor system with four measurement channels, a total of six electrode terminals were used, in which one is for current injection, another for voltage feedback sensing, and the rest for the measuring electrodes. In this way, simultaneous recording of skin conductance every second at four different skin sites was obtained.

For portability and to cover the aspects of electrical safety for clinical use, wireless transfer of data was implemented in addition to on-board storage of measurements. In this way, the

patient is not electrically connected to the main power supply, and can move around freely. In addition, safety resistors were added at each terminal in order to reduce current exposure if breakdown of electrical components should occur. Software was developed for realtime monitoring of measurements on a PC. A photograph of the instrument which was built and a screenshot from the PC software is presented in figure 3.

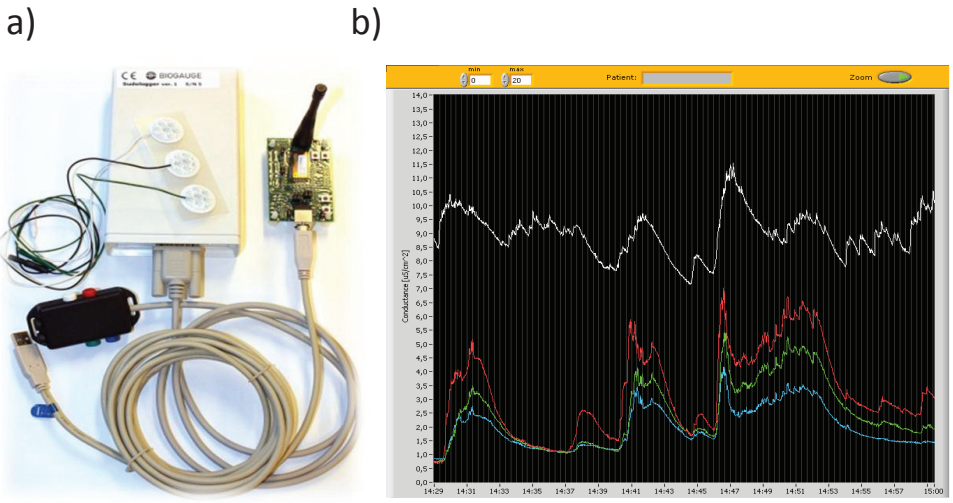

Figure 3. The developed multichannel skin conductance sensor system. a) Photograph of the instrument box (size 157 x 95 x 33 mm) with cables, electrodes, and a wireless reception module for PC connection. b) Screenshot from the PC software of a skin conductance recording at four different skin sites.

This sensor was named the *Sudologger* and is today CE-marked and marketed by BioGauge A/S.

3.4.3 PC-based instrumentation

In some cases, PC-based instrumentation is practical, especially for prototyping or demonstration of new instrumentation ideas. The PC together with a data-acquisition (DAQ) card then replaces the microcontroller, and a front-end of electronics between the electrodes and the DAQ-card completes the system. A PC-based skin conductance instrument was developed (Paper III), consisting of a laptop, a PCMCIA DAQ-Card (Type 6062E, National Instruments) and matchbox-size front-end electronics, shown in figure 4a. For the purpose of demonstrating tissue type discrimination by needle bioimpedance [Kalvøy 2009 and Paper V], a PC-based demonstrator was developed from the same components and similar front-end circuitry (figure 4b).

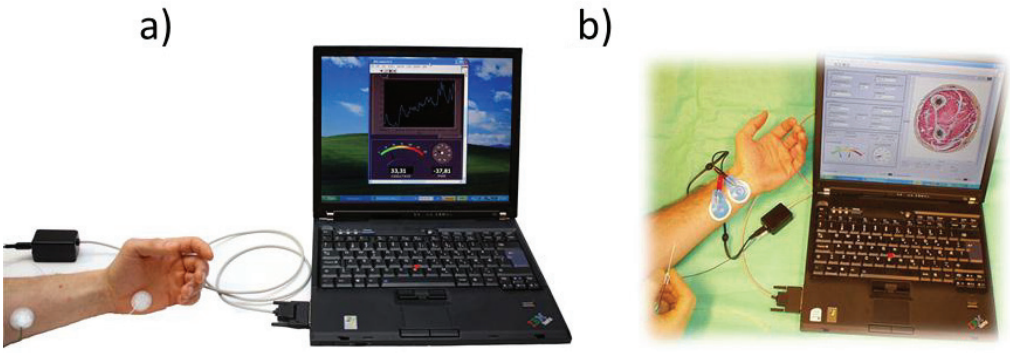

Figure 4. PC-based instrumentation for skin conductance (a) and tissue impedance (b) measurement.

3.5 Discussion of the instrumentation work

The Sudologger, which was developed based on the presented instrumentation design, has enabled recording of the skin conductance parameter in situations which have previously been impractical. Within our hospital, recordings for research have been done during exercise, heat exposure in a sauna, and ten patients have worn the system ambulatory for 48h. Other research groups have used the Sudologger for research on treatment of excessive sweating, research on night sweats, stress research, psychological research, diabetes research and research in basal physiology. Chapter 6 covers the clinical applications of the sensor in detail.

The development of the system which is presented in Paper I took place from 2005-2007. Since then, electronic components and modules for embedded instrumentation have become even smaller, smarter and with low power consumption, in line with the developments in smart-phones. With today's technology, the sensor could be miniaturized into e.g. a matchbox size of the instrumentation box. In 2011, the EEPROM in the Sudologger was replaced by mico-SD card storage, and a special version with fMRI compatibility is in development.

A future version will include a redesign of the electronics, miniaturization, better ergonomic design and the inclusion of an accelerometer for registration of physical activity. In 2010, Grimnes et al [Paper VIII] developed a method for measuring skin potential in addition to the skin conductance and skin susceptance, simultaneously at the same skin site. PC-based instrumentation similar to Paper III and figure 4 was built for this purpose (not published), and was used in Papers IX and X to investigate the benefit of this feature. Due to findings in favor of this method, it will be implemented in a future version of the Sudologger.

The PC-based instrumentation solution for skin conductance was published (Paper III, 2010) with the intention that other engineers and researchers could easily put together skin conductance instrumentation using a PC with LabVIEW®, a DAQ-card and a few standard electrical components. However, to our knowledge no other group has yet used this solution.

The demonstrator for bioimpedance measurement tissue discrimination provided accurate tissue discrimination between muscle and fat in pilot studies on in vivo porcine models after calibration (not published).

3.6 Conclusion on the instrumentation work

Instrumentation for portable skin admittance measurement which fits into a pocket was developed. The device is operative for 24h, can measure at four skin sites simultaneously and satisfies the requirements for electrical safety and patient use.

4.0 ELECTRODES

4.1 Introduction to electrodes for impedance measurement

Electrodes are critical to any impedance-based biosensor, as they serve as the physical connection between the material and the instrumentation and facilitate the transfer between electronic and ionic conduction. This makes the electrode material very important, as different materials have different charge transfer properties. Any electrically conducting material can serve as an electrode, but the material properties can have large effects on the measurement. For human use, the measurement can either be non-invasive or invasive, depending on whether the electrode is attached to the surface of the skin, or if the electrode is placed within the body. For non-invasive bioimpedance measurements, standard ECG electrodes are usually very suitable as they contain an electrolyte (ion containing) gel layer below the metallic part of the electrode, which serves to enhance skin contact and charge transfer across the skin. This gel also helps reduce the impedance from the skin, which is often an unwanted effect in the measurement. For invasive biompedance measurements, small metallic electrodes are used i.e. pacemaker leads, where the biocompatibility and long-term stability of the electrode material is important [Shepard 2009]. A third use of electrodes and impedance measurement in biomedical sensors is the sensing of electrochemical reactions. Biomedical sensors may utilize the chemical reactions between biological molecules and a reagent sensor solution in which ions are formed upon reaction and the changes can be picked up by the impedance of the solution. Although the electrodes are not in direct contact with the tissue in this case, the electrode properties are important regarding sensitivity and stability of the measurement, especially because such sensors often need miniaturization for clinical use, and the concentration of biomolecules and thereby the changes in impedance may be very small. This type of electrode shares the same requirement as the invasive bioimpedance electrode regarding stability. Figure 5 gives an illustrative overview of these three electrode applications.

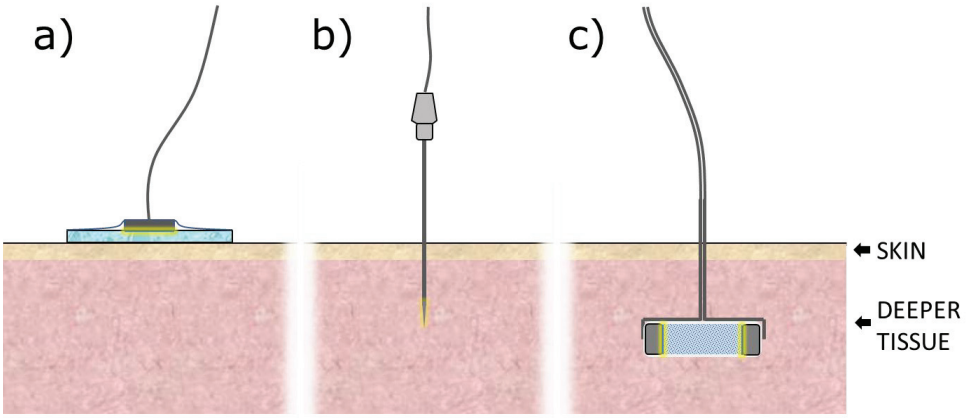

Figure 5. Illustration of three different electrode applications. a) Skin surface electrode with an electrolyte gel layer for skin impedance measurement. b) Needle electrode for invasive bioimpedance measurement. The needle is insulated down to the tip. c) Electrodes for an

electrochemical biomedical sensor measuring the impedance of a reagent solution interacting with the tissue. The yellow glow indicates the interfaces between electronic and ionic conduction.

The work on electrodes in this thesis is divided into two electrode categories:

1. Gel-based skin surface electrodes for non-invasive bioimpedance measurement.
2. Small (<1mm^2) metallic electrodes for invasive bioimpedance or electrochemical biomedical sensors.

4.2 Problems with electrodes for impedance measurement

4.2.1 Gel-based electrodes

Gel-based electrodes have the benefit that they reduce the skin impedance, which is very large compared to deeper tissue and often introduce an unwanted effect in the measurement. However, for measurements where the skin impedance itself is the interesting property, the electrode should not influence the skin impedance. The skin conductance parameter is frequently used within psychological research, and a certain type of gel-paste has been recommended as an electrode-gel. However, many different types of standard or custom-made gels are still being used for these sensors. Differences in these include electrolyte concentration, water sorption properties and viscosity. It has been unknown how differences in electrode gels affect the skin conductance measurement, as this has not been studied in detail before.

4.2.2 Metallic electrodes

Depending on the electrode and the material it is in contact with, there is an impedance of the interface between the electronic conduction in the electrode and the ionic conduction in the material. This impedance is called electrode polarization impedance (EPI) [Grimnes and martinsen 2008]. For the small metal-based electrodes, EPI may become relatively large compared to the tissue or electrochemical solution, which reduces the sensitivity of the measurement. As the electrode area decreases, the EPI increases, but depending on the surface structure of the electrode material, the effective electrode area may be manifold that of the geometrical area. Thus, the ideal electrode should have a rough surface structure rather than a flat, and the relation between surface structure and bioimpedance measurement has not been studied in detail before. Consequently, the first problem is sensitivity, and the second problem is stability. If the EPI is changing during the measurement, which can be over several days for such a sensor, the measurement will suffer from a drift which changes the baseline level over time. This can be due to reactions between the electrode material and the tissue or with the electrochemical solution. The two problems are connected, as a continuous increase in EPI will not only introduce a drift, but also gradually reduce the sensitivity of the measurement.

The EPI is also dependent on the frequency of the current across the interface, and the EPI contribution may thus be reduced by increasing the measurement frequency. However, parasitic capacitances dominate the higher frequencies, especially for miniature sensors. Thus,

the optimal measurement frequency must generally be selected based on a compromise between these two effects [Mirtaheri et al 2004]. Another way to overcome the EPI is to use separate electrodes for current injection and voltage pick-up (4-electrode system), but this is more difficult to assemble in a miniature sensor [Mirtaheri et al 2004].

4.3 Aims for the work on electrodes

4.3.1 Gel-based electrodes

For the gel electrodes, the aim was to compare different types of gels with respect to skin conductance measurement. This included:

- Assessment of water sorption characteristics for different gel types.
- Measurement of area-corrected gel electrolyte impedance.
- Simultaneous recording of skin conductance (SC) at palmar and abdominal skin, using electrode pairs with different gel at bilaterally equal sites.
- Comparison of stability, responsiveness to skin impedance changes and susceptibility to pressure-induced artifacts.
- Assessment of skin impedance change and skin irritation from 24 h adhesion of the electrodes.

4.3.2 Metallic electrodes

For the metallic electrodes, the aim was to compare the EPI of electrodes from the same material, but with different surface properties. These properties were contact area, alloy composition, surface structure and electrolytic treatment of the electrode. This included:

- Impedance frequency spectrum measurement of different stainless steel electrodes in vitro, repeated over 48h to gather data on stability.
- Investigation of impedance stability with respect to contact area, alloy composition, surface structure and electrolytic treatment.
- Determination of the optimal measurement frequency.

4.4 Summary of the results on electrode work

4.4.1 Gel-based electrodes

Electrodes with the following gel types were investigated:

Table 2. Overview of the electrode gel types examined in this study according to gel material, the intended use, effective electrode area (EEA) and type of adhesion.

Type	Gel material	Intended use	EEA [cm^2]	Adhesion
A	Solid hydrogel	ECG, neonatal	5.05	Adhesive gel
B	Wet gel	ECG, short-term	2.54	Outer adhesive part
C	Isotonic EDA jelly	EDA	1.95	Outer adhesive part
D	Karaya solid gel	ECG, hypoallergenic	6.16	Adhesive gel

Water sorption characteristics of one sample from each gel was measured gravimetrically using a dynamic vapor sorption instrument (DVS). From these measurements, the relative water uptake from steps in 10% relative humidity (RH) was calculated along with the time-constant of the weight change of the sample. Types B and C contained high amounts of water initially of approx. 6 and 4 times the 0% weight respectively, while types A and D were very similar with less than 10% water depleted to the environment. Types B and C did not regain their original water content even at 90% RH. No hysteresis was observed between increasing and decreasing RH steps, except for type B between 60% and 80% RH.

Type B had the highest conductivity, followed by type C, A, and type D with lowest conductivity as shown in table 3.

Table 3. Gel AC conductivity [µS/cm] at low and high frequencies for all the gel types presented as median (bold), 25% and 75% quartiles.

Frequency	A	B	C	D
1 Hz	**166.0** (162.8, 174.4)	**313.8** (301.3, 320.6)	**282.0** (265.7, 290.5)	**3.600** (3.299, 3.676)
100 kHz	**399.1** (390.3, 407.4)	**1480** (1445, 1523)	**670.6** (597.9, 737.1)	**71.81** (70.58, 73.27)

From SC recordings on 18 subjects, several significant differences in time-series parameters were found between the electrode types. Type B had significantly higher initial drift than type A, C and D at palmar skin, and significantly higher drift than type A and D at abdominal skin. Type B was significantly different from all the others with respect to responsiveness to skin impedance changes, which were induced by sweating. On palmar skin, the SC response was significantly higher in magnitude than for the other gels, which was also the case on abdominal skin, but with the response in the negative direction, which only occurred for type B. On palmar skin, the offset between SC at baseline and at 15 minutes after sweating was significantly larger for type B than the others. On abdominal skin, this offset was significantly larger for type B compared with type A and D, while the type C offset was also significantly larger than for type A. Applied pressure to the electrodes generated a significantly larger SC response for type B and C compared to type A on palmar skin, while the type B response was significantly larger than for type A and D on abdominal skin. The initial SC drift correlated

positively with the initial desorption measurement (R=0.988, p<0.05 for palmar skin and R=0.901, p<0.1 for abdominal skin).

Figure 6 shows an example recording from both skin sites where SC has been measured with type A and B electrodes simultaneously. On both sites, type B introduced a drift which was not present for type A, and type B gives a negative SC response during sweating at abdominal skin.

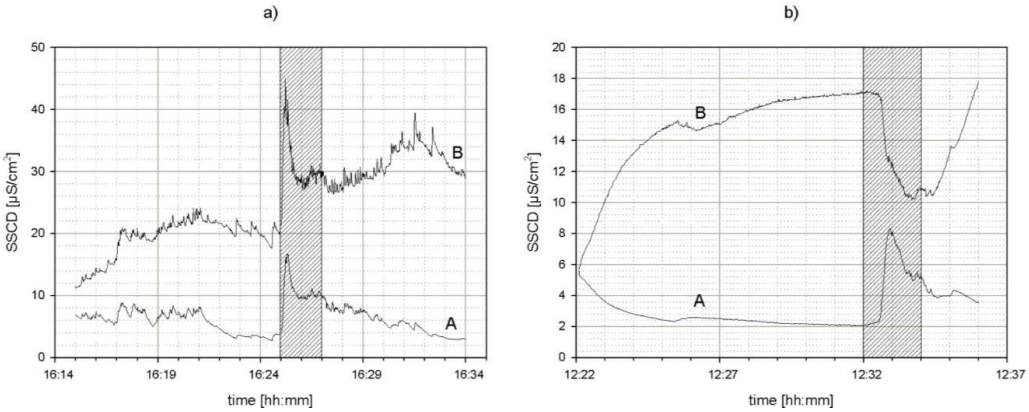

Figure 6. Example recordings using different electrode type A and B on the same subject on palmar skin in a) and abdominal skin in b). The hatched area indicates the interval of sweating by physical exercise.

No clear results were found for the skin impedance change from 24h of adhesion, except for a reduction in the resistance of gel type D, and no signs of skin irritation were found by photographic evaluation by a dermatologist.

4.4.2 Metallic electrodes

Electrodes of the following types were investigated:

Table 4. Electrodes of medical grade stainless steel (MGSS) used in the study.

Type	Name	Company	Length x Diam.	Active area
1	Disposable Monopolar needle electrode	Medtronic Inc.	37 x 0.33 mm	0.3 mm^2
2	Disposable Monopolar needle electrode	Medtronic Inc.	50 x 0.40 mm	0.3 mm^2
3	TECA Needles Disposable monopolar needle electrode	VIASYS Healthcare	37 x 0.36 mm	0.28 mm^2
4	Pirouette, Disposable EMG Needle	Technomed Europe	40 x 0.35 mm	Not given (0.5 mm^2)
5	Stimuplex A	B.Braun Melsungen AG	50 x 0.7 mm	Not given (0.7 mm^2)

For new and untreated electrodes, significant differences among all the types were found for the impedance at all frequencies except for the highest (0.56 and 1MHz). As shown in figure 7, the impedance spectra for these electrodes showed a clear increase in the impedance as the frequency decreased below 100-200 kHz for types 1 and 2, and below 10-20 kHz for types 3,4 and 5. Although types 1, 2 and 3 had similar electrode areas, differences in impedance at low frequencies were up to 3-fold.

Based on scanning electron microscopy (SEM) analysis of the electrodes, an alloy composition with no more than roughly 1% differences between electrode types was found, and the relation between the composition and the electrode impedance was thus not further investigated.

Based on electrolytic treatment by applying positive (anodic) or negative (cathodic) DC current through the electrodes, large differences in impedance was measured. Cathodic treatment lead to decreased impedance and drift for all electrode types, and the impedance of type 1 and 2 was also reduced by anodic treatment. Types 3 and 5 had only minor impedance changes from the electrolytic treatment.

Regarding stability, repeated measurements over 48h in a physiological saline tank revealed that type 4 was the most stable with no significant drift in impedance. The impedance of types 1,2 and 3 increased during all repeated measurements and ended at twice or higher after 48h.

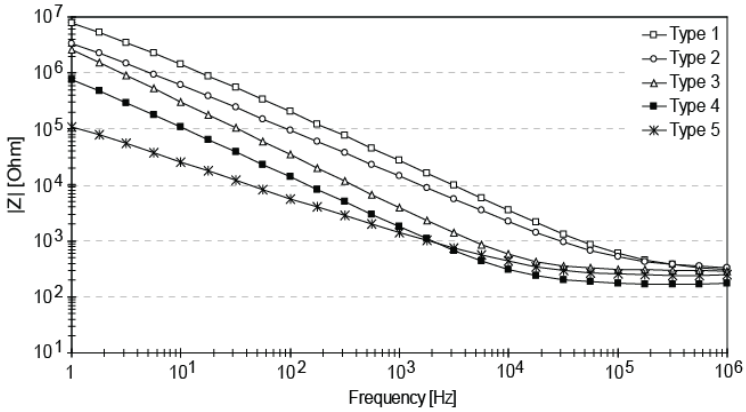

Figure 7.Mean impedance vs frequency for new, untreated needles, sorted by type. (From Paper V by Kalvøy et al)

4.5 Discussion of the electrode work

Different electrode properties strongly and significantly affect the sensitivity and the stability of the measurement for both the gel-based and the metallic electrodes.

4.5.1 Gel-based electrodes

The results show that the choice of electrode gel can severely affect the SC measurement due to the gel reacting with the skin, and that this effect is correlated to the amount of water which

the gel can release. Differences in initial drift, response amplitudes and their directions, recovery offset and susceptibility to pressure artifacts indicate that an inappropriate choice of electrodes could lead to implications with clinical decisions based on SC measurement. The findings are summarized as follows:

- Electrode gels can introduce large changes in the level of skin conductance over time, corresponding with the amount of free water in the gel and its viscosity.
- Sweating can lead to negative skin conductance responses for wet gels with low viscosity. This inverse sweating response effect probably depends on the thickness of the SC.
- Wet gels may provide an increased sensitivity to sweat activity in partially filled ducts.
- Solid gels have in general a better ability than the wetter gels to return the skin conductance to baseline during recovery after a period of sweating.
- Wet gels seem to give less repeatable measurements due to the changes introduced by the gel which likely depend on the interindividual SC properties.
- Expectedly, the gels with lower mechanical stability are more susceptible to pressure artifacts.
- The karaya-based solid gel (Type D) may introduce a drift in the skin conductance measurement due to lowering of its initially high resistivity.
- The Isotonic EDA Jelly (Type C) may be completely absorbed by the skin during long-term wear.

Based on these findings, electrode type A is used for the measurements in following studies (Paper III, IX, X and XII).

4.5.2 Metallic electrodes

The increase in impedance as the frequency is decreased, as seen in figure 7, is due to the EPI. Thus, the optimal measuring frequency should be above 200kHz for types 1 and 2, and above 20 kHz for types 3,4 and 5. Stray capacitances are however likely to influence the measurement at 200 kHz for sensors with small distances between the electrodes.

From SEM images of the electrode surface, large variations in surface roughness were seen among electrode types. Although the shape of the type 3 surface was different from type 1 and 2, the increased real surface area was not large enough to explain the large impedance differences. Both the geometrical area and the roughness was larger for type 4 compared to 1,2 and 3, in agreement with the lower impedance of this electrode. Type 5 had the largest geometrical area, and also a large surface roughness factor, in agreement with the lowest impedance at lower frequencies.

Although the variation in contact area and roughness of the electrode surface was in agreement with the variation in EPI among the electrodes, not all of the observations could be explained, suggesting that factors not included in this study have significant influence on the electrode properties.

The effect of treatment suggests that cathodic DC current generates processes at the electrode surface which reduces the EPI and the drift. Electrolytic pretreatment of electrodes could thus be a recommended procedure before impedance measurement.

There was in general an agreement between lower EPI and increased stability. Differences in long-term stability among the electrode types suggests that electrodes for impedance measurement should not be picked randomly although the differences in given producer characteristics may seem negligible.

4.6 Conclusion on the electrode work

The properties of electrodes are critical both for non-invasive and invasive impedance-based biomedical sensors. Inappropriate electrode choice leads to drift, altered sensitivity or other artefacts in the measurement.

For skin impedance or skin conductance measurement, solid hydrogel electrodes are recommended due to the least disturbance on the innate skin impedance.

For impedance measurements using small metallic electrodes, more stable and sensitive measurements are obtained by electrodes with rougher surface area, by cathodic pretreatment, and by using higher frequencies for the impedance measurement.

5.0 SIGNAL PROCESSING

5.1 Introduction to biomedical signal processing

5.1.1 Scope

There are two general rationales for performing signal processing: (1) for the acquisition and processing of signals to extract a priori desired information; and (2) for interpreting the nature of a physical process based either on observation of a signal or on observation of how the process alters the characteristics of a signal. [Bruce 2001]. The work in this thesis concerns both of these rationales. After a physical property has been converted to an electrical signal by a transducer and acquired by the instrumentation, the biological signal will often contain both desired and unwanted components. The first part deals with extraction of the desired components or removal of the unwanted components, which is called *filtering*. Unwanted signal components may either originate from the body, i.e. when the electrical activity of the heart disturbs the measurement of respiratory muscle activity, or in the instrumentation as electrical noise from the circuitry or from external fields i.e. the power supply. In both cases, knowledge of the nature of both the desired and unwanted signals will improve the filtering.

Filtering can either be done in hardware using analogue components, or digitally in software. The phase-sensitive rectification (PSR) described in CH3.1 is a form of filtering, and was implemented digitally in the microcontroller of the skin admittance instrumentation. This is considered pre-processing in order to acquire the physical property (electrical admittance) which is being measured. The work in this part is limited to the mathematical processing of an acquired physical property into a biomedical parameter, in agreement with table 1 and figure 1 in CH1.

5.1.2 Examples

In an ideal world, both the transducer and the instrumentation work perfectly, providing the sensor software with undistorted signals from the body. However, a number of factors such as transducer contact with the body, may distort the measurement although the physical property is correctly measured by the instrumentation. To give an example, given a wearable biomedical sensor which is used during physical activity, the transducer may occasionally lose contact with the body, creating outliers in the series of measurements. Calculating the mathematical median of a number of consecutive measurements can in this case give a better representation of the desired property, as the median is not affected by the magnitude of the outliers. This median filter can be implemented in the software of the microcontroller or monitoring unit for real-time processing of the signal, or in post-processing software for analysis of saved recordings. To elaborate further, the filtered signal may be used to estimate a biomedical parameter based on a known mathematical model for the relation between the physical property and the biomedical parameter. An example is a temperature sensor which uses the resistance of a temperature-dependent resistor (thermistor) to estimate the temperature by a known formula. For most accurate measurements, this formula needs calibration before use for adjustment to the individual transducer and the desired temperature

range. The functionality of the biomedical sensor may extend further with alarms being triggered if the measurement crosses a certain threshold. The biomedical sensor may go even further with reporting these measurements or alarms to a treatment device, creating a completely autonomous system which replaces the physician, such as with rate-responsive pacemakers which continuously tune the pacing signal according to sensor inputs of physical activity.

5.1.3 Signals

In order to correctly process the signal of a physical property into a biomedical parameter, it is important to know its source and signal characteristics. This work concerns signals of the following sources, physical properties and signal types:

Table 5. Overview of the types of biomedical signals included in this work.

Source	Physical property	Type of signal	Biomedical parameter
Skin	Electrical conductance	Time-series	Sweat gland activity
Skin	Electrical potential	Time-series	Sweat gland activity
Skin	Electrical susceptance	Time-series	Skin moisture content
Tissue (metabolism)	Electrical conductance	Time-series	Tissue carbon dioxide
Whole body	Electrical impedance	Spectrum	Body composition

The first four signals in table 5 are time-series, meaning that the physical property is measured successively in uniformly spaced time-intervals, and that the variation over time is of interest either for the signal processing, as with the median filter, or for the monitoring of the biomedical parameter. The electrical properties of skin are influenced by the skin moisture content and the sweat gland activity, and large variations occur within seconds as the sweat pores are filled with sweat [Paper I]. The skin susceptance is however not influenced by the sweat glands and is correlated to the skin moisture content [Paper V].

The fourth signal in the table comes from a biomedical sensor for conductometric measurement of the partial pressure of carbon dioxide (pCO_2), in which pCO_2 increase is a marker of organ ischemia [Tønnessen 1997]. The sensor is based on a water-filled chamber enclosed by a semi-permeable membrane which allows diffusion of CO_2 molecules into the water which dissolves into ions and thereby changes its conductivity. The conductivity is found by impedance measurement between two electrodes in the solution, as was outlined in CH4.1, and figure 5 c).

The last signal in table 5 is not a time-series signal, but a spectrum of impedance measurements at different frequencies, such as figure 7, CH4.4. The bioimpedance spectrum measured over the whole body can be used to estimate the total body water, the extracellular / intracellular fluid balance, muscle mass and fat mass [Grimnes and Martinsen 2008].

5.2 Problems with impedance signals

5.2.1 Electrical properties of skin

It is known that the skin conductance (SC) and the skin potential (SP) are related to sweat gland activity [Boucsein 2012], and that the skin susceptance (SB) is related to the skin moisture content [Paper VII], but it is not known if these electrical properties can be used to estimate the amount of sweating, as water evaporated from the skin.

Due to the link between sweat gland activity and the central nervous system (CNS) which regulates it, skin conductance (SC) or skin potential (SP) measurements are used to calculate parameters of CNS activity [Boucsein 2012]. A CNS burst to the sweat glands generates a SC response (SCR) and a SP response (SPR), and the frequency or the shape features of the responses are used to quantify the CNS activity. The SCR and SPR have similar shapes in some cases, but can also have very different shapes. This difference is not completely understood, as methods for comparing them have been lacking, but comprehensive theories have been proposed [Edelberg 1993].

5.2.2 pCO_2 measurement

Long-term instability is a well-known problem for the conductometric pCO_2 sensor [Varlan and Sansen 1997, Mirtaheri et al 2004a, 2004b], and also for pCO_2 and pH sensors which are based on voltage (potentiometric) measurements [Zhao and Cai 1997, Gumbrell et al 1997, Mindt et al 1978, Drake and Treasure 1986]. Based on the findings in Paper V and work by others on electrode polarization impedance [Franks et al 2005], the electrodes are a likely source of this instability, which is observed as drift and sensitivity reduction over time for the pCO_2 sensor. For clinical use, such a sensor should ideally be stable for 3 or more days. Until this issue is solved at the transducer part of the sensor (Figure 1, CH1), signal processing methods may offer an alternative solution to the problem. For the purpose of ischemia detection, an appropriate signal processing algorithm may provide early and accurate automatic detection despite the instability of the signal.

5.2.3. Bioimpedance analysis

As described in CH3.1, the PSR function of impedance sensor instrumentation derives the conductive and capacitive components from the impedance signal. These components can be used to calculate the phase angle of the impedance, which is often used in estimation of the biomedical parameter in bioimpedance measurements. However, not all commercial instruments have this function embedded, and they provide only the magnitude of the impedance. When an impedance spectrum is available, there are methods for estimating the phase angle based on the information inherent in the frequency dependency of the impedance magnitude. It is however unknown which of these methods produce the most accurate estimate.

5.3 Aims of the work on signal processing

5.3.1 Electrical properties of skin

In 2011, Grimnes et al introduced a method for measuring SC and SP simultaneously at the same skin site, and also presented recordings which showed that these two parameters are different in nature [Paper VIII]. Utilizing this method, the aims were to:

- Determine how accurate the amount of sweating can be estimated based on simultaneous recordings of SC, SP and SB during variations in sweating.
- Investigate the waveform difference between SCR and SPR in relation to sweating, skin hydration and other features of the electrical properties of skin, and to compare the findings with existing theories.

5.3.2 pCO_2 measurement

The aim for the pCO_2 sensor was to develop a real-time signal processing method for the earliest accurate detection of cardiac ischemia given the properties of the sensor, based on measurements from a porcine cardiac ischemia model.

5.3.3 Bioimpedance analysis

The aim on the bioimpedance signal processing part was to determine which of two methods, the Kramers-Kronig method and the Cole parameter method, provides the most accurate estimation of the phase angle parameter.

5.4 Summary of the results on signal processing

5.4.1 Electrical properties of skin

PC-based instrumentation, similar to the system presented in Paper III, was built based on the method in Paper VIII in order to measure SC, SP and SB simultaneously at the same skin site. Using a QSweat® device as a reference for the amount of sweating, measurements were done on 40 healthy subjects during relaxation and mental stress. A multilinear regression model based on a combination of SC, SP and SB features was found by stepwise regression and model validation. The model estimated the sweating with an average error of 15.4%. Figure 8 shows a plot of the measured vs estimated sweating.

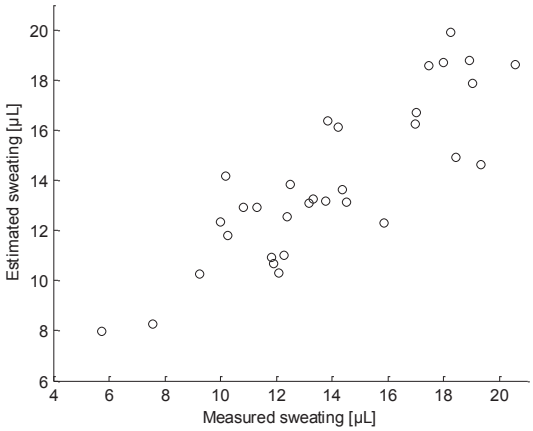

Figure 8. Measured sweating vs estimated sweating based on SC, SP and SB.

The same measurements were used to compare the SCR and SPR waveforms by the percent-wise difference between their peaks, as shown in figure 9 as the SPRET.

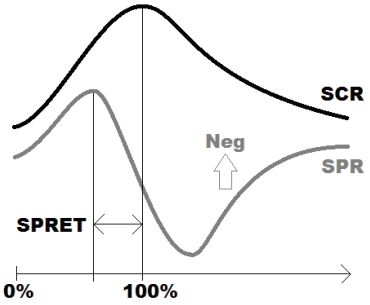

Figure 9. Illustration of the skin potential relative turning time (SPRET). The onset and peak of the SCR defines the 0% and 100% and the SPRET is found from the percent-wise difference from the SCR peak to the SPR peak.

Roughly 30% of all SPRs were similar to the SCR (SPRET<10%), and the rest had SPRETs which were more evenly distributed towards 100%. Typical SPRs in different SPRET categories were constructed and presented. Within subject, the SPRET was found to correlate strongly with the slope and curvature of the increasing part of the SCR. Between subjects, SPRET was negatively correlated with the SB. As shown in figure 10, the median SPRET was positively correlated to mean sweat rate.

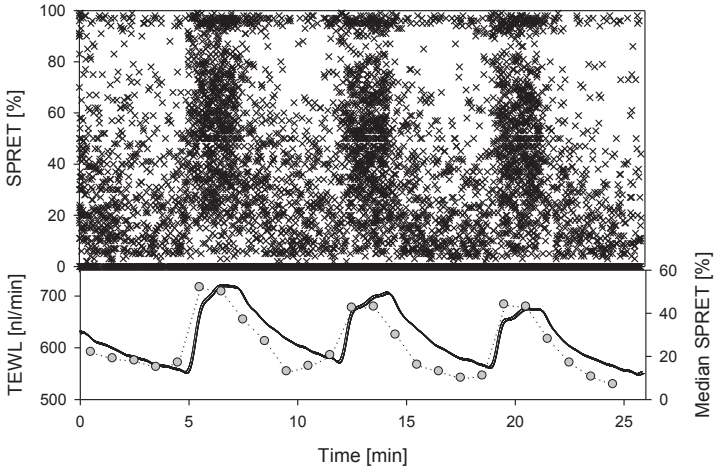

Figure 10. SPRET for all responses from all subjects vs time (above) for comparison with mean sweat rate (solid line below). The grey circles represent the median SPRET during each minute interval. The subjects were given arithmetic problems during minutes 5 to 7, 12 to 14 and 19 to 21.

Another important finding was that under periods of increasing sweating, the SPRs were easier to detect than the SCRs, as shown by example in figure 11.

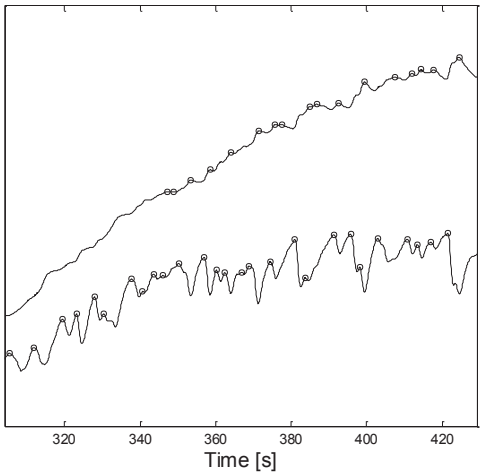

Figure 11. An example recording showing the SP (lower) yielding more detected peaks (circles) than for the SC (upper).

5.4.2 pCO_2 measurement

Based on a dataset of measurements from 17 sensors in tissue with induced ischemia by arterial occlusion, and 6 control sensors in non-ischemic tissue, an algorithm was developed for real-time drift correction. Figure 12 shows a comparison between the uncorrected and drift-corrected signals.

The drift-correction led to earlier and more accurate detection of ischemia. Based on the drift-corrected signal, ischemia could have been detected with 100% accuracy after 7 minutes of occlusion. The rate of change (the time-derivative mathematically) of the signal was also analyzed, which could provide earlier detection alone, but with lower specificity. Combining these two enabled a 96% accuracy of detecting occlusions lasting from 1 min to 15 min.

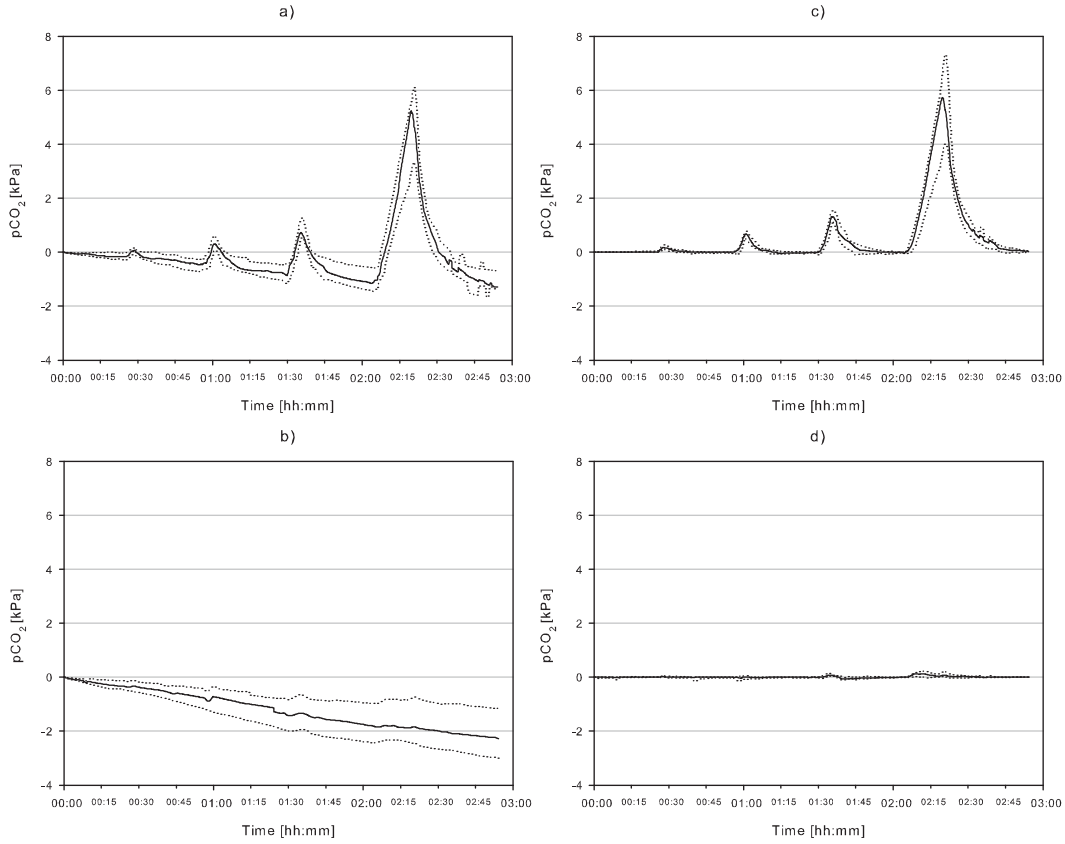

Figure 12. Uncorrected signal from sensors in tissue exposed to ischemia (a) and non-ischemic tissue (b), compared to drift-corrected signals from the same sensors in c) and d).

5.4.3 Bioimpedance analysis

By comparing the estimated phase angles based on the two methods against the measured phase angle for 20 subjects, it was found that the Cole method was significantly more accurate for two of the investigated frequencies (50 kHz and 100 kHz), and that the two methods were not significantly different for 5 kHz and 200 kHz estimations (figure 13).

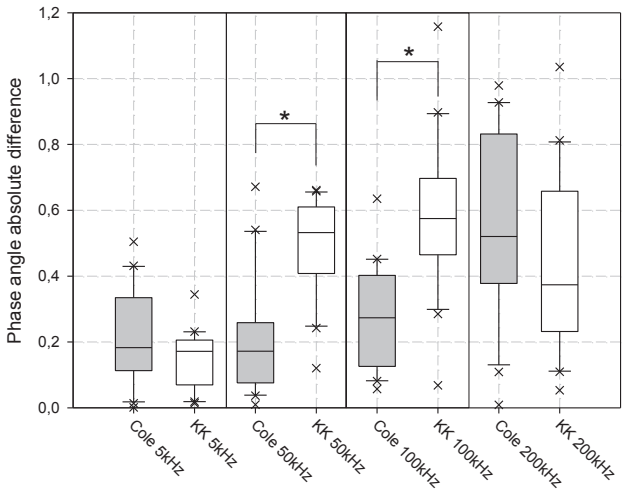

Figure 13. The absolute difference between estimated and measured phase angle using the Cole (grey) and Kramers-Kronig (white) approaches for four selected frequencies.

5.5 Discussion of the results on signal processing

5.5.1 Electrical properties of skin

The results speak in favor of usefulness of the Grimnes method for simultaneous SC and SP measurement, whether it is for estimation of sweating, identification of CNS responses or basal research on the electrical properties of skin.

A 15% error must be interpreted with regard to the intended application, but is nevertheless a significant improvement to estimation by the raw SC signal only (26% error). The most important parameter for the estimation was the sum of positive increments in the SC time-series. For sensors with only SC measurements, an estimation with 18% error could be obtained by using this parameter only.

Roughly 30% of the variation in sweating could not be explained by the electrical parameters, which suggests that factors such as the electrolyte concentration of sweat produce large variations which affect the electrical properties, but are not directly related to sweat production.

Interpretation of the SPRET and the factors which it was correlated to, in light of existing biophysical theories of the SCR and SPR, suggests that the SPRET itself represents the hydraulic capacity state of the sweat ducts. Although the SPRET was strongly correlated with several factors, these factors did not completely explain its variance, suggesting that this parameter may contain additional physiological information not accounted for by the investigated effects.

The larger number of SP peaks than SC peak suggests that simultaneous recording of the two properties can improve the quantification of biomedical parameters for CNS activity.

5.5.2 pCO_2 measurement

The detection accuracy indicates that the signal processing algorithm removed the unwanted component (drift) and preserved the desired signal (pCO_2 changes). This is also supported by the measurements on the same animals using a different pCO_2 sensor in Paper XIII, which shows flat curves between each occlusion (Figure 2). Although the data were not processed in real-time, the developed algorithm is suitable for real-time monitoring. However, this work has several limitations:

1. The algorithm was developed in order to obtain the best possible early detection accuracy for a given dataset, and not evaluated on another independent dataset. Thus, the reported accuracy is a best-case result. (The number of measurements was too low to divide the dataset in two).
2. The data came from recordings lasting only a few hours, which is vastly less than for the intended clinical use.
3. The ischemia pig model which produced the data does not completely represent a real clinical setting, and real signals may include components which could be incorrectly filtered by the algorithm.

Thus, the presented signal processing method is a start in correcting the errors which are not solved by improvements in the transducer technology.

5.5.3 Bioimpedance analysis

Although the Cole method produced the most accurate estimation, the results obtained are however good for both methods. The Cole method has the advantage that it requires measurements at only four frequencies (5, 50, 100 and 200 kHz), while the Kramers-Kronig method needs measurements up to at least 500 kHz.

5.6 Conclusions from the signal processing work

The following conclusions are drawn from the signal processing work:

- The amount of sweating can be estimated from the skin electrical properties with acceptable accuracy (15% mean error) depending on the application.
- The mechanisms of the electrical signals from the skin are now better explained.

- The Grimnes instrumentation for SC and SP measurement provides extended physiological information from the skin and CNS.
- Sensor drift from electrode instability may be removed by signal processing methods.
- The Cole Parameter approach is more accurate than the Kramers-Kronig approach for estimating the phase-angle from bioimpedance spectra.

6.0 CLINICAL APPLICATIONS

6.1 Clinical use of impedance-based biomedical sensors as of 2012

Sensor methods based on electrical impedance have been proposed for a wide range of clinical uses, covering most organs, tissue types and functions within the body, but few of these technologies have yet made it into routine clinical use. Table 6 lists some of those who have made it far in this respect as of 2012.

Table 6. Some of the most successful impedance-based sensor methods with respect to clinical use as of 2012.

Biomedical parameter	Sensor method	Invasiveness	Status
Lung ventilation distribution	Electrical impedance tomography (EIT)	Non-invasive	On market for clinical use as the Pulmovista® 500 by Dräger Medical GmbH.
Cardiac output	Impedance cardiography (ICG)	Non-invasive	Part of the Task Force® monitor by APC cardiovascular, on market for clinical use.
Body composition	Bioimpedance spectroscopy (BIS)	Non-invasive	On market for clinical use as the SFB7 by Impedimed.
Cellular analysis	Microelectrode array bioimpedance	Cell culture sample	On market for pre-clinical use as the xCELLigence system by Roche Diagnostics.
Melanoma classification	Skin BIS	Minimally invasive	Undergoing clinical trials, planned market release in 2012 by SciBase AB.
Fluid status	Intrathoracic impedance by pacemaker	Invasive	On market for clinical use as a feature in St. Jude and Medtronic pacemakers.

Although not used as sensors on their own, impedance measurement is also integrated in some clinical treatment devices such as electrosurgery equipment where vessel fusion feedback is given by the tissue impedance (Ligasure™) and in defibrillators where the shock delivery is adjusted based on chest impedance measurement (Philips HeartStart defibrillators).

In addition, several promising impedance-based methods have potential for clinical use in the near future, such as multichannel intraluminal esophageal impedance for diagnosis of gastroesophageal reflux [Hernani et al 2011], microfiltrometer method for red blood cell deformability measurement [Amoussou-Guenou KM et al 2004], the dielectrophoresis method for cell characterization [Chung et al 2011] and non-invasive assessment of gastric motility by bioimpedance [Huerta-Franco 2012] to name a few.

In general, impedance-based sensors have the advantage that the instrumentation is cheap, safe, and that measurements can be taken rapidly and often non-invasively, which are all attractive features for clinical use. However, although bioimpedance is a parameter which is

very sensitive to many properties within the body or in tissue samples, it is often limited by the specificity, in other words failing to discriminate between these properties, which brings the sensor below the accuracy requirements for introduction to the clinic.

The papers in this thesis are related to different types of clinical applications, and the following chapters put the work in a clinical perspective by description of the related clinical problems and discussion of the potential for clinical applications based on the sensor methods.

6.2 Sweating and hyperhidrosis

6.2.1 Introduction to hyperhidrosis

Hyperhidrosis is a disease causing excessive sweating, and was the original motivation for developing the portable skin conductance sensor. Hyperhidrosis has a prevalence of 2.8% in the US, and the patients often report very poor quality of life with occupational, emotional, psychological and physical impairment [Strutton et al 2004]. The cause of hyperhidrosis is not completely understood, although there are indications of elevated sympathetic nervous activity in patients with this disease [Iwase et al 1997]. The disease can be psychologically conditioned and a connection has been shown between anxiety and hyperhidrosis [Ramos et al 2006a,b]. The most effective of the many different treatment options is sympathectomy, where the sympathetic nerve trunk in the chest is dissected. However, compensatory sweating where the patients report of increases in sweating at non-treated areas after receiving the procedure is extremely common [Ojimba and Cameron 2004]. One of the great challenges for the attending physician today is the lack of a useful method to quantitatively and objectively estimate the degree of sweating before and after treatment, and consequently there is no way to supply the subjective assessment of the patient when it comes to the degree of suffering and the result of treatment. Grading of sweating before treatment is exclusively based on the patient's subjective evaluation, making it difficult to determine the indication for treatment and the treatment result. In addition to sympathectomy, there are other treatment options such as antiperspirants, iontosphoresis, drugs, botulinum toxin injection and surgical excision of sweat glands in the axilla. It is important that each patient receives the correct type of treatment corresponding to the severity of their symptoms and to avoid offering the more risky and costly procedures to patients with few objective symptoms [Kreyden et al 2002]. It is especially important to separate the patients with a real need for medical or surgical treatment from those who are better suited for a different approach. For palmar hyperhidrosis, little is known about the daily pattern of sweating [Krogstad et al 2006] and there is no consensus based on objective criteria as to when treatment should be given [Krogstad et al 2004]. Iodine starch test, gravimetry, evaporation and skin conduction have all been proposed as objective estimates, but are limited to controlled laboratory research [Krogstad et al 2006]. Hence, there is a need for portable equipment for long-term measurement of sweat activity.

6.2.2 The link between sweating and skin conductance

There are several sources influencing the electrical properties of skin, but the sudomotor (movement of sweat) activity generates the largest changes in its electrical admittance. The skin has both conductive and capacitive properties, and as shown in figure 14a, sweating

mainly changes the conductive part of the admittance. A simplified electrical model for the electrical properties of skin is shown in figure 14b, where the resistors R1 and R2 represent the conductive pathway through the sweat duct, which changes in conductance as the duct is filled with sweat. It is thus R1+R2 which is of interest for measuring the sudomotor or sweat activity. A and B are terminals for the measuring and counter-electrodes respectively. R3 and C1 represents the epidermal admittance, while R6 represents the resistance from the deeper layers of the skin to the counter-electrode. R4 and R5 represents duct wall resistances at the epidermal and sub-epidermal levels, connected to biopotentials E2 and E1, where E1<E2. Due to C1, which increasingly admits current according to frequency, the sensitivity depth of the measurement also increases with the frequency of the signal used for measurement. Thus, a low excitation frequency yields a measurement sensitive to the epidermal skin properties, and especially the highly resistive corneum layer, while the contribution from R6 becomes negligible. A too low excitation frequency will however let the AC measurement signal fall within the frequency range of the skin biopotential activity, making it difficult or impossible to discriminate between the two. As shown in papers VIII, IX and X, these two signals are different, and a too low AC frequency or DC measurement would thus not correctly reflect the sweat activity. Hence, using an excitation frequency above the skin biopotential range while also keeping the C1 admittance low, e.g. 10 Hz, yields an admittance measurement sensitive to R1, R2, R3, R4, R5 and C1. Using the phase-sensitive rectifier technique, as described in CH3.1, cancels out the C1 contribution, leaving only the resistors. The resistances R3, R4 and R5 are either very large or constant compared to R1 and R2, making the temporal variation in the low-frequency skin AC conductance measurement selectively reflect the sudomotor activity. A great deal of this knowledge on electrical properties of skin comes from the many years of research in bioimpedance by S Grimnes and ØG Martinsen.

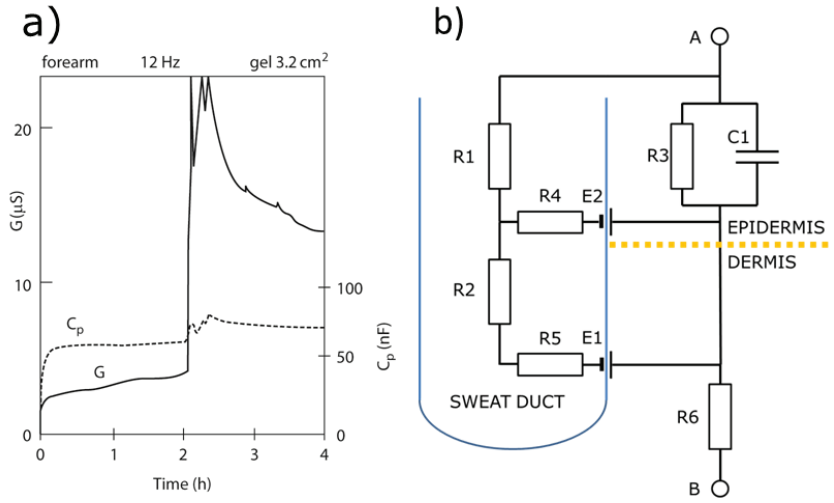

Figure 14. Electrical properties of skin and sweating. a) skin conductance (G) and skin capacitance (C_p) during sweating induced by physical exercise (at 2h), from Grimnes (1984) by permission. b) An electrical equivalent model for the skin based on the Fowles model [Fowles 1974] and modified for AC measurement.

6.2.3 The potential for clinical use

As presented in CH3 and in depth in Papers I and II, a portable skin conductance (SC) sensor (the Sudologger) was developed for clinical use. In paper I, the sensor was tested on 24 healthy subjects who wore the system during relaxation and physical exercise. Shown by examples, the SC measurements were visibly correlated with periods of exercise, although no other reference parameter than heart rate was used in this study. In paper IX, the correlation to a reference method for quantitative sweating measurement was studied in detail, and a high within-subject correlation was found (median r=0.77). Recordings from 28 subjects are presented in figure 2, where the mean SC vs mean sweat rate correlated with r=0.94.

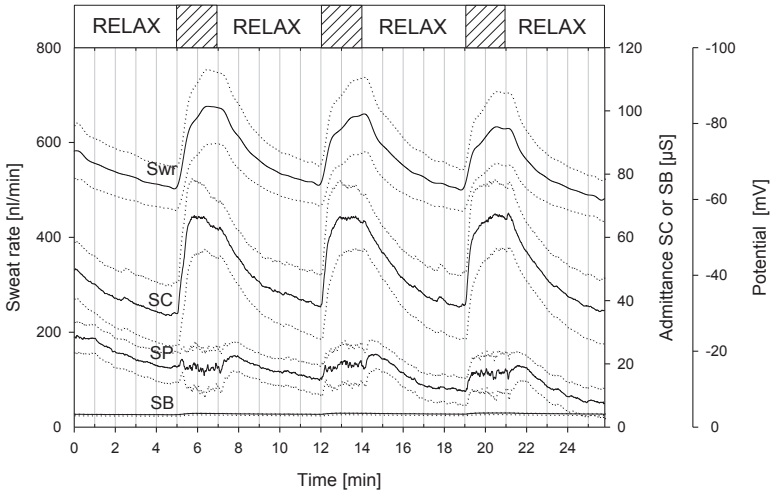

Figure 2. Mean time series of sweat rate (Swr), skin conductance (SC), skin potential (SP) and skin susceptance (SB) with 95% confidence intervals (dotted lines). The upper boxes indicates the intervals of relaxation and stress by arithmetics (hatched).

The Sudologger was included as an objective measurement in a study on the treatment of axillary hyperhidrosis at Oslo University Hospital (Paper XII). The main purpose of the study was to compare the effect of two surgical techniques. Secondary goals were to evaluate the Sudologger method and to compare subjective scoring with objective measurements. The study was longitudinal, implying within-subject comparisons before and after treatment. Comparisons were also done between the types of treatment, but these observations were paired as each patient received one type of treatment at each armpit. The Sudologger measurements were also compared with a traditional measurement of weight absorption of filter papers attached to the armpits.

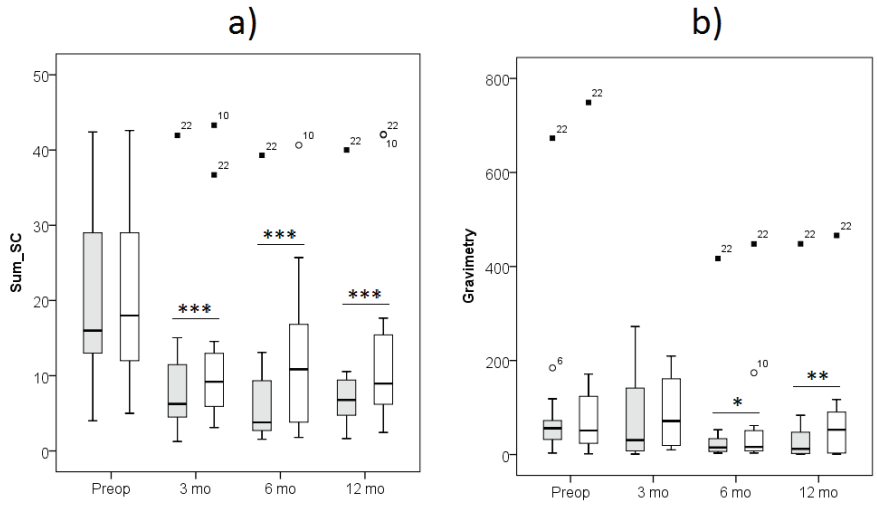

*Figure 15. Sudologger (a) and gravimetric (b) scores before treatment and at 3 months, 6 months and 12 months after treatment (gray=type A, white=type B). *p<0.05 **p<0.01 ***p<0.001 significantly lower than preop.*

As shown in figure 15, the Sudologger provided measurements which suggested a clear improvement in sweating after treatment, which was not as significant for the gravimetric method. A stronger correlation to subjective scores (Table 7) for the Sudologger than the gravimetric measurement suggests that the Sudologger measurements may have been more correct.

Table 7. Spearman rho correlation matrix for Sudologger, gravimetry, visual analogue scale (VAS) scoring of sweating and life quality, and dermatological life quality index (DLQI).

Spearman rho	Gravimetry	VAS sweating	VAS life quality	DLQI
Sudologger	0.66**	0.54**	-0.12	0.60**
Gravimetry		0.38**	-0.18	0.41**
VAS sweating			-0.34**	0.52**
VAS life quality				-0.44**

Both the Sudologger and the gravimetric measurement, along with the subjective scores, agreed that treatment type A was significantly more effective than type B.

The Sudologger had several advantages compared to the filter paper method:

- Less uncertainties during measurement, such as the pressure against the armpit during filter paper attachment.
- Time-series recording allowing registration of sweating reactions to different types of stimuli.

- The multichannel system allows simultaneous measurement at other control sites, such as the palm which was used in this study as a control for different degrees of nervousness from visit to visit (inclusion of this covariate produced the same result).

A disadvantage was saturation of the measurement in a few cases of extreme sweating, but this was due to equipment calibration and is not a methodological limitation.

The Sudologger is currently being used in a study on thoracoscopic sympathectomy treatment of palmar hyperhidrosis at Akershus University Hospital by E.Øvensen et al. While patients are still being recruited, the group presented preliminary results (46 patients) as a poster [Appendix] at the 9th international symposium on sympathetic surgery, Odense 2011. The multi-channel sweat activity recording of the Sudologger enabled quantitative assessment of both the intended treatment of the palmar hyperhidrosis and side-effects of compensatory sweating at other skin sites.

In conclusion, these results suggest that the Sudologger is clinically useful for treatment evaluation of hyperhidrosis. Implementation of the estimation model presented in Paper IX will also allow for between-subjects comparisons, which can offer physicians assistance in diagnosis as well. Before clinical routine use, some aspects need further consideration:

- For long-term (24h+) recording on hyperhidrosis patients, the electrode fixation needs improvement. It is unlikely that the electrode will keep stable contact with the skin over long periods for heavy sweaters.
- The estimation accuracy needs to be validated also for repeated measurements under different conditions in order to determine its repeatability and reproducibility.
- The device should be ergonomically improved for unobtrusiveness during wearable use.

Although sweating-related diseases are not highly prioritized and the market potential of the sensor is not huge, the technology can help certain groups of patients in the long-term. An objective screening of patients for appropriate treatment selection can also be beneficial for the healthcare economy.

6.3 Electrodermal activity and the sympathetic nervous system

The previous chapter dealt with the SC with respect to the amount of sweating, but a SC recording can also be used to extract information about the activity in in the central nervous system (CNS). The sweat glands are innervated by the sympathetic branch of the CNS, and a nervous impulse to the sweat glands trigger a sudomotor response which can be picked up by a response in the SC signal [Kunimoto et al 1991]. Thus, counting the number of SC responses (SCRs) during a time window can give an estimate of the sympathetic nervous system (SNS) activity, or the reaction to a certain stimulus can be estimated by looking at the following SCR amplitude. The regulating mechanism of the SNS activity is complex, and it is difficult to determine the source or cause of the activity (see Boucsein 2012 CH 1.3.4 for details). These parameters are much used within the field of psychophysiology as indices of e.g. arousal or stress, where the measurement is known as electrodermal activity (EDA).

Within this field, EDA has been used in applications such as biofeedback, assessment of personality traits, psychopathology and detection of deception [Boucsein 2012 CH3], to name a few. EDA is not well established in clinical use, and is mostly used in research, often in combination with other physiological measurements. Recently, EDA has been used in research on epilepsy [Poh et al 2012], post-traumatic stress disorder [Fletcher et al 2011], sleep research [Michael 2011] and disabled patients [Kushki et al 2012] with promising potential for clinical applications.

The Sudologger is directly usable for EDA measurement in a clinical setting. It is however not the only sensor available. In 2010, Poh et al presented what has become the Q-Sensor from the MiT Media Lab [Poh et al 2010, www.affectiva.com], which is superior in technical design to the current version of the Sudologger. It has an elegant design as a wristband with wireless communication for unobtrusive wearable use. There are however methodological differences in the way measurements are done, such as the electrical property measured, the site of measurement and the type of electrodes which may or may not be significant with respect to the intended use. These issues are not further discussed without research on the impact of these methodological differences. The rationales for the Sudologger methodology is given in this thesis, and the innovation lies in the measurement methodology.

Figure 16 shows the result from Paper III where 17 volunteers were subjected to different levels of stress while EDA was measured using the Sudologger method and later compared with the subjective stress scoring.

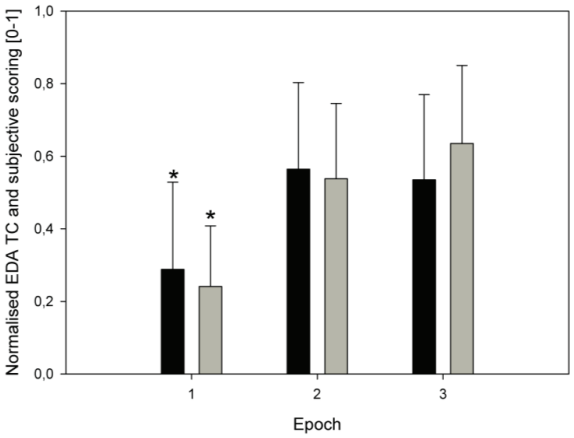

*Figure 16. Means and standard deviations of the number of EDA responses (black) and the subjective scoring (grey) for the three epochs. *p<0.05.*

In addition to the development of the Sudologger, the work in this thesis has contributed to the field of EDA measurement by the following points:

- Investigation of how different types of electrode gels influence the SC measurement (Paper IV)

- Contributed to a better understanding of the biophysical mechanism of EDA through basal research on different electrical properties of skin (Paper X).
- Findings suggesting improved detection of EDRs by using the Grimnes measurement method (Paper X).
- Sharing of a PC-based instrumentation solution for EDA measurement (Paper III).

6.4 Organ ischemia

6.4.1 Introduction

Ischemia means inadequate blood supply to an organ or local area due to constriction or obstruction of arterial blood vessels leading to that area or venous blood vessels draining the respective area. Myocardial infarction, cerebral infarction and shock are examples, and ischemia is a major cause of death in the western world. Since ischemia is reversible in many cases, an early detection could lead to earlier treatment to save the organ as well as the patient's life [Tønnessen 1997].

6.4.2 The link between ischemia and pCO_2

The function of every organ is dependent on adequate blood supply, in particular the demand of oxygen for cellular metabolism. If blood supply is reduced, and the oxygen supply becomes lower than the demand, the cellular metabolic biochemistry changes in order to produce energy differently. An increase in the partial pressure of CO_2 (pCO_2) then occurs, explained by two mechanisms: First an initial rise due to flow stagnation and thereby impeded pCO_2 removal by effluent venous blood and later a rise when cell metabolism shifts from aerobic to anaerobic state [Venkatesh and Morgan 2002, Wælgaard et al 2012]. In all tissues, CO_2 is generated under anaerobic conditions as a result of bicarbonate buffering an increase of protons due to anaerobically produced lactic acid [Tønnessen 1997] and degradation of energy-rich phosphate compounds like adenosine-triphosphate and creatine-phosphate [Rosano et al 2008].

6.4.3 Biomedical sensor for early detection of organ ischemia

The development of a biomedical sensor for early detection of organ ischemia started with the PhD work of Peyman Mirtaheri, supervised by Tor Inge Tønnessen, Sverre Grimnes and Ørjan G. Martinsen [Mirtaheri 2004]. This work led to the development of a miniaturized conductivity-based pCO_2 sensor suitable for clinical monitoring, which is today called the IscAlert™ sensor, shown in figure 17 as of 2009. The work in this thesis (Papers VI, XIII and XIV) concerns the further development and pre-clinical testing of this sensor.

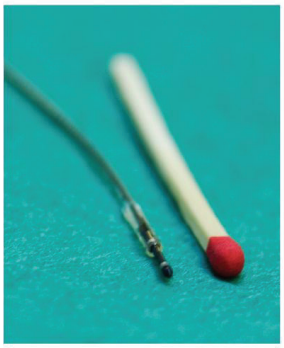

Figure 17. Picture of the IscAlert sensor, showing the sensor tip and wire.

6.4.4 The potential for clinical use

In paper VI, calibration and signal processing methods were developed in order to remove sensor drift and increase the detection accuracy of the sensor for cardiac ischemia. These methods were used on the same data in paper XIII by Pischke et al, where the diagnostic potential of pCO_2 and the IscAlert sensor was evaluated with comparison to reference pCO_2 measurements, systemic haemodynamic parameters and regional metabolic parameters. An occlusion-reperfusion animal model for myocardial ischemia was used with sensors placed in the occluded area and a control area of the myocardium. As shown in figure 18a, pCO_2 measured by IscAlert sensors increased during each occlusion and was significantly different from the pCO_2 measured in the control region. Figure 18b shows the reference pCO_2 sensor measurements, which correlated well with the drift corrected IscAlert values ($R=0.93 \pm 0.05$, $p<0.001$). The baselines are however different, as drift correction was not possible between sensor calibration and use, and the sensors were given a zero as baseline. This was however not important, as pCO_2 increases were the hypothesized ischemic reaction, and the resulting detection accuracy was high (24%, 82%, 91% and 100% sensitivity for 1, 3, 5 and 15 min occlusions, all 100% specificity).

Figure 18b also shows a new parameter which was calculated from the measurements: the time-derivative of the pCO_2 curve ($TDpCO_2$), representing the CO_2 generation rate. This parameter was found to correlate strongly with the decrease in pO_2, and reached is maximum as pO_2 reached zero (anoxia). This suggested that this novel parameter may be important in determining the transition between aerobic to anaerobic metabolism.

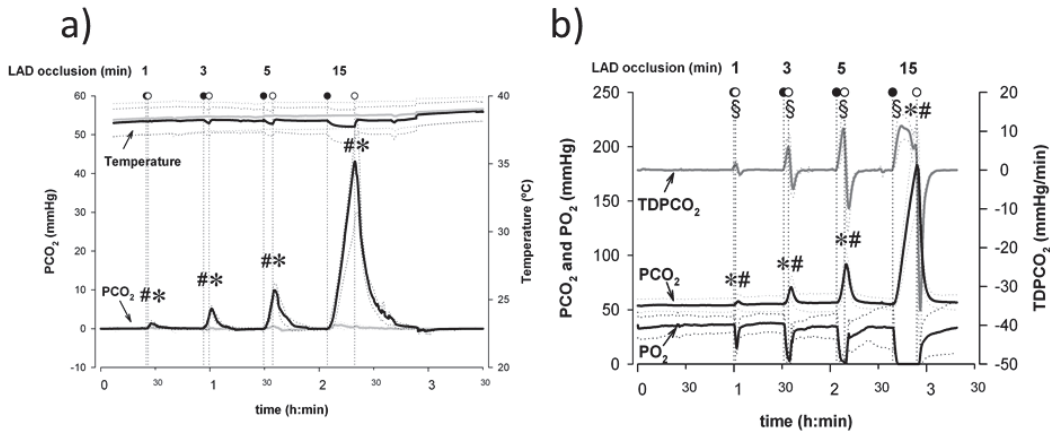

Figure 18. pCO_2 measurements during 1,3,5 and 15 minutes of induced ischemia by occlusion for IscAlert (a) and Neurotrend (b) sensors. In a) pCO_2 in the occluded region (black line) is compared to pCO_2 in a control region (grey line). In b) pCO_2 and pO_2 are compared to the $TDpCO_2$. (See paper XIII for complete figure explanations).

In comparison, no significant changes in systemic haemodynamic parameters were measured during ischemia. The ischemia was verified by regional metabolic parameters measured by microdialysis. It was concluded that the IscAlert sensors are applicable and enable immediate reliable recognition of ischaemic cardiac events. The main intended clinical application is for monitoring during and after cardiac surgery and especially coronary-artery bypass grafting.

In paper XIV by Pischke et al, the IscAlert sensors were used in an animal model for liver transplantation. After liver transplantation procedures, it is important that the blood supply to the new liver is correctly established, and the aim of the study was to evaluate pCO_2 as a real-time diagnostic tool to detect occlusion of the hepatic artery (HA) or the portal vein (PV). Sensors were placed inside the liver in order to detect HA occlusion and between intestinal loops to detect PV occlusion. As shown in figure 19, HA occlusion caused significant liver pCO_2 increase, and PV occlusion caused significant intestinal pCO_2 increase. It was concluded that a combination of hepatic and intestinal pCO_2 measurement reliably diagnoses the affected vessel, depicts the severity of the occlusion and emerges as a clinical monitoring tool in the per- and postoperative course of liver transplantation, enabling early intervention.

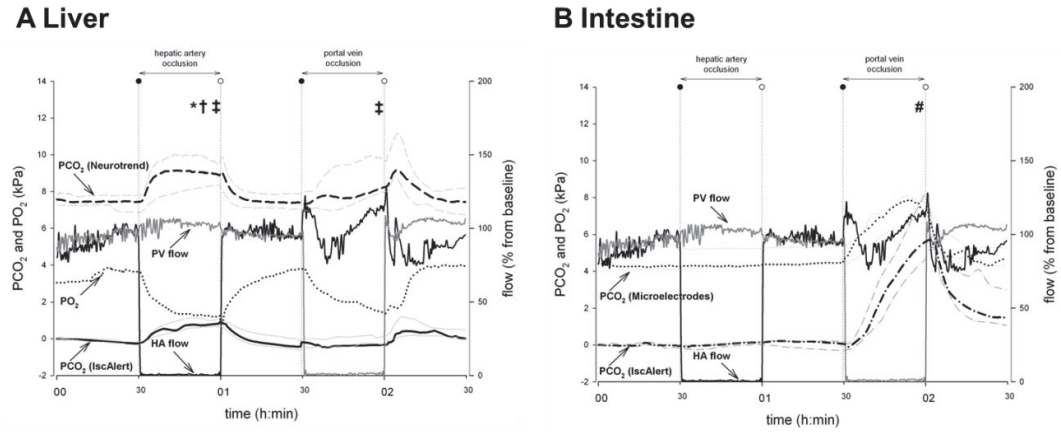

Figure 19. pCO_2 increase detected by IscAlert sensors in liver during HA occlusion (A) and in intestine during PV occlusion (B). (See paper XIV for complete figure explanations).

In conclusion, there is considerable potential for clinical use of the IscAlert sensor. There have already been many steps both in the medical basis and the technological development of the sensor, and there are still a few left before introduction to clinical trials. The work in this thesis has contributed to a few of these steps along the way, and some of the further steps on the technological side are discussed in CH 7.

6.5 Needle guidance and tissue discrimination

Paper V was part of a project for needle guidance in clinical applications based on electrical impedance, led by Håvard Kalvøy, PhD. Briefly explained, Kalvøy et al found that the sensitivity zone of impedance measurement using a medical needle electrode is approx. 3mm in radius, which enabled tissue bioimpedance measurement with high spatial resolution [Kalvøy et al 2009]. 100% tissue discrimination accuracy was obtained in this study for porcine muscle and fat/subdermis data by multivariate analysis. The picture of the prototype in CH3.4.3, figure 4b gives an idea about the use of the sensor. Early suggestions for clinical applications were biopsies and ablation in small volumes, drug delivery transcutaneously into a vessel or a small volume of muscle, nerve or adipose tissue. The work in Paper V on needle impedance properties led to a better accuracy of the method based on needle type selection. Later, Martinsen et al described an application using the needle impedance method for blood vessel detection by invasive electrical impedance tomography [Martinsen et al 2010]. The intended clinical application was rapid localization of large blood vessels for resuscitation during cardiac arrest, and the preliminary results showed that blood vessel localization was feasible, according to the authors. The needle bioimpedance method also has potential for clinical use in delivery of epidural anesthesia, which is currently undergoing pilot studies for feasibility.

In conclusion, this method has potential for several different clinical applications, but is still in its early stages and the focus application has not yet been determined.

6.6 Body composition analysis

Paper XI by Nordbotten et al concerns the improvement of bioimpedance spectroscopy (BIS) signals from some existing devices intended to estimate body composition. This bioimpedance-based method is an existing technology available on the market and has already come very far with respect to a clinical application. As already shown in table 1, the technology is already available for clinical use. This method has a great potential, as it *is the only technology available that has the potential to measure body water volumes (total body water (TBW), extracellular water (ECW) and intracellular water (ICW)) and body cell mass in the clinical setting,* according to a 2007 review article by Earthman et al by 2007. The method is non-invasive and requires only placements of four skin surface electrodes on the hand/wrist and the foot/ankle. Specific clinical applications include outcome prediction of patients with lymphedema [Kim et al 2011], assessment of fluid status in hemodialysis patients [Dou et al 2012] and the diagnosis of metabolic syndrome [Ozhan et al 2012]. BIS can accurately measure TBW and ECW in healthy, normal-weight adults with normal fluid volumes and distribution [Earthman et al 2007], but the results are mixed in clinical populations, and the method was not recommended for routine assessment of patients until further validation, in a 2004 review by Kyle et al. As discussed thoroughly in a 2008 review article by Matthie, the method still has several technical issues regarding accuracy, which are related to the choice of measurement frequencies, current density, the skin impedance and the parameterization of the measurement. In other words: electrodes, instrumentation and signal processing. The work in this thesis contributed mainly on the parameterization of BIS, but the findings from the skin surface electrode study (Paper IV) is also relevant, as it shows which electrode gel type that most effectively reduces the skin impedance, which is a source of error in BIS. The instrumentation solution presented in Paper I may also be relevant, as reduced size and cost of devices is an expected development in this field [Matthie 2008].

6.7 Conclusion on the potential for clinical applications

In conclusion, the work in this thesis has contributed both to the development of new clinical applications, and improvement of existing applications. The potential for each of these is dependent on many factors, such as the number of patients and clinical significance, the accuracy of the estimated biological parameter, the invasiveness of the measurement and the cost of the equipment. In order to give a very simplified overview, the applications are presented in a scatterplot of clinical significance and accuracy, shown in figure 20. The position and borders of each ellipse is based on the author's impression of the accuracy, which also depends on the intended use, and the author's impression of the clinical significance based on recent literature.

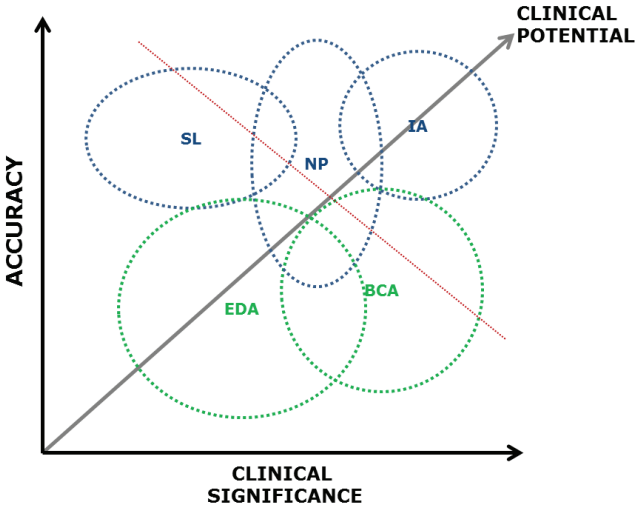

Figure 20. Clinical potential evaluated by the clinical significance and the accuracy of the applications (SL=Sudologger, NP=Needle Positioning, IA=IscAlert, EDA=Electrodermal Activity and BCA=Body Composition Analysis). Green represents technologies already available, while blue represents emerging technologies.

In the coming years, these ellipses will narrow and their position will converge somewhere within their borders when the best possible accuracy is achieved and the application is completely specified. Whether or not the end-points cross a hypothetical line (red line in figure 20) will decide whether or not the application will be a success for clinical use.

It is thus likely that the three new technologies will end up in routine clinical use.

6.8 Disclosure

A disclosure is relevant to this chapter, as the evaluations given beyond the referenced opinions reflect the view of the author only from his technological perspective. The author has earlier been financed by the company selling the Sudologger (BioGauge AS), and also the earlier company developing the IscAlert sensor (Alertis Medical ASA) for consulting work. The author has currently no interests in the discussed technologies other than scientific.

7.0 FUTURE WORK

As the technology is not yet completely in the hands of the physicians, there is still work to be done. This chapter sums up the most important future directions for the different biomedical sensor projects related to the presented work. Suggestions are given for further investigations on electrodes, instrumentation and signal processing. Apart from the main goals of clinical applications, some ongoing work on basal research and new sensor ideas are also shared.

7.1 Further work on electrodes

- As textile, rubber, conductive polymer, and other new types of electrode materials are emerging for wearable sensor applications, these should also be assessed for skin impedance measurement with regard to long-term recording with the Sudologger.
- Based on the results in Paper V, different electrode materials, and electrolytic treatments of them, must be studied with respect to impedance stability in experimental models specific for the IscAlert sensor.

7.2 Further work on instrumentation

- Due to the usefulness of the Grimnes method for simultaneous measurement of skin conductance, potential and susceptance, a microcontrolled-based design will be made for this method in an upcoming version of the Sudologger.
- The practical difference in electrodermal activity measured by DC or AC methods needs to be determined by proper experimental comparison with a relevance to clinical use.
- A special version of the Sudologger for use together with fMRI is under development.

7.3 Further work in signal processing

- The model for estimation of sweat production needs validation for repeatability and reproducibility under different conditions.
- The mechanisms of electrodermal activity (EDA) is still not completely understood, and further investigations with the Grimnes method and the SPRET from paper X together with microneurography could shed light on the last parts of this puzzle and also improve the estimation of sympatethic nervous system activity by the EDA signals.
- Ischemia detection algorithms for the IscAlert sensor need validation in clinical settings.

7.4 Future outlook on clinical applications

7.4.1 Hyperhidrosis

A study on objective evaluation of botulinum toxin treatment of palmar hyperhidrosis is in the pipeline, in collaboration with the Department of Dermatology by Prof.Anne-Lene Krogstad.

7.4.2 Night sweats

A group of researchers from the University of Oklahoma Health Sciences Center and Lynn Health Science Institute, Oklahoma, led by Dr. James Mold, are currently using the Sudologger in night sweats research.

7.4.3 Post-traumatic stress disorder (PTSD)

An fMRI-compatible version of the Sudologger is under development for research on PTSD in collaboration with Bjørn Christian Østberg, MD from the division of Mental Health and Addiction, Oslo University Hospital and the Institute of Psychiatry, King's College London. So far, we have obtained undistorted recordings in the 1.5T MR, but not in the 3T MR.

7.4.4 Diabetes: Sweating and unawareness of severe hypoglycaemia

An idea for a potential application for the Sudologger originated from Prof. Trond Geir Jenssen at the Department of Nephrology, Oslo University Hospital. In treating diabetes patients, he had often heard reports of sweating during severe blood sugar falls, even in patients who had lost their normal prewarning senses of these blood sugar falls. In order to verify this physiological assumption and thereby the feasibility for early detection of severe hypoglycaemia (SH), a pilot study, funded by the Norwegian Diabetes Association and in collaboration with Marit Bjørgaas from St.Olavs Hospital in Trondheim, was initiated in 2011 and will finish in 2012. The experimental part of 48h recording of 10 hospitalized patients is completed, and figure 21 shows a recording during one special episode in which the blood sugar of a patient dropped to dangerously low levels during sleep. In this example, the sweating reaction occurred 1h earlier than the critical point. Although the data analysis is not yet completed, several other incidents of low blood sugar coincided with increases in sweat activity.

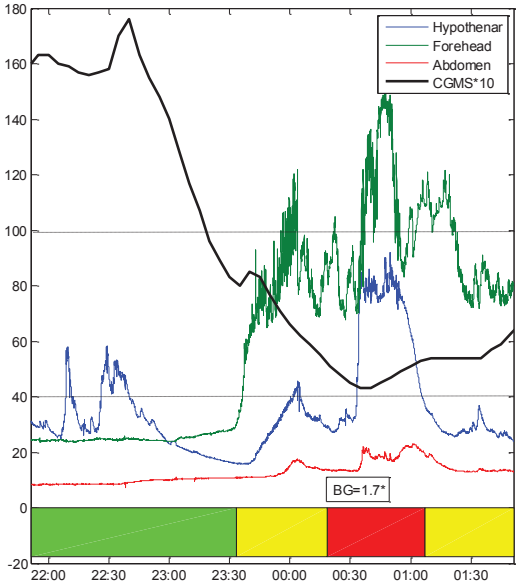

*Figure 21. Sweat activity at palmar (blue), forehead (green) and abdomen (red) skin sites and tissue glucose*10(black) during the night. The patient fell asleep at 22:30 and was awakened at 00:32 with cramps and impaired consciousness. *Blood glucose was measured to be 1.7 mmol/l at 00:32. Strong sweat activity at the forehead started at 23:33.*

However, sweating can come from other causes as well, and expectedly, the specificity seems to be very low during the waking hours. We believe that this project is well worth pursuing, as it can enable early warning of very harmful events, and we are currently seeking funding for a 3-year project. On the technical side of this project, a multisensor approach will be used to control for other causes of sweating by adding an accelerometer and temperature sensor. Further improvements in accuracy will be considered by inclusion of ECG parameters, continuous tissue bioimpedance and optical sensor methods.

8.0 GENERAL DISCUSSION AND CONCLUSION

The general aim was *improvements in electrodes, instrumentation and signal processing for biomedical sensors based on electrical impedance.* In order to discuss the significance of this work with respect to improvements in these parts, the contribution to each are summarized as follows:

8.1 Electrodes

Electrode properties were found to be critical both for gel-based electrodes for skin impedance measurement and for metallic electrodes for invasive tissue impedance measurement. Errors from drift or altered sensitivity can be reduced or overcome by using a suitable electrode or by using electrolytic pretreatment and the optimal measuring frequency in the case of the metallic electrodes. Electrode properties affecting the measurement in general is not a novel finding, but the findings specific for these electrode types and how they influence the measurement in view of the intended impedance-based sensors are new and relevant to many applications.

8.2 Instrumentation

Instrumentation for portable skin admittance measurement was developed which fits into a pocket, is operative for 24h, can measure at four skin sites simultaneously and satisfies the requirements for electrical safety and patient use. To the author's knowledge, this was the first portable (or wearable, depending on definition), device which could measure sweat activity at several skin sites simultaneously.

8.3 Signal processing

This work led to: Estimation of sweating amount by electrical properties of skin, a better explanation of the mechanisms of electrodermal actvity, a real-time sensor drift correction algorithm and a suggestion for parameterization of bioimpedance spectroscopy measurements. These are all new scientific contributions to the best of the Author's knowledge, and could be useful for several clinical applications.

Thus, the work has led to improvements in electrodes, instrumentation or signal processing for new or existing impedance-based biomedical sensors, thereby providing improvement of their accuracy and clinical potential.

8.4 General conclusion

This work has contributed to new biomedical sensors, and to knowledge which can lead to improvement of existing ones or in the way they are used. In light of the technical significance and the clinical potential discussed in CH6, the Author also concludes that this work is very likely to benefit the patient in the future.

9.0 REFERENCES

Aberg P, Birgersson U, Elsner P, Mohr P, Ollmar S. 2011 Electrical impedance spectroscopy and the diagnostic accuracy for malignant melanoma. Exp.Dermatol. 20:648-52.

Amoussou-Guenou KM, Martinsen ØG, Hounkponou M, Doumit J and Healy JC 2004 Basic principles for evaluation of less deformable erythrocyte subpopulations with the Microfiltrometer. Scand J Clin Lab Invest. 64:169-74.

Boucsein W. 2012. ELECTRODERMAL ACTIVITY, 2.ed. Springer New York.
Bruce EN 2001 *Biomedical Signal Processing and Signal Modeling.* John Wiley & Sons.

Chung C, Waterfall M, Pells S, Menachery A, Smith S and Pethig R 2011 Dielectrophoretic Characterisation of Mammalian Cells above 100 MHz. J Electr Bioimp 2:64-71.

Dou Y, Zhu F, Kotanko P. 2012. Assessment of Extracellular Fluid Volume and Fluid Status in Hemodialysis Patients: Current Status and Technical Advances. Semin Dial [Epub ahead of print]

Drake H.F. Treasure T 1986 Continuous clinical monitoring with ion-selective electrodes A feasible or desirable objective? Intensive Care Med 12 104-107

Earthman C, Traughber D, Dobratz J and Howell W 2007 Bioimpedance Spectroscopy for Clinical Assessment of Fluid Distribution and Body Cell Mass. Nutr Clin Pract. 22:389-405.

Edelberg, R. 1993. Electrodermal mechanisms: A critique of the two-effector hypothesis and a proposed replacement. In Roy, J. C. et al. (Eds.) PROGRESS IN ELECTRODERMAL RESEARCH (pp 7-30). Plenum Press, New York.

Fletcher RR, Tam S, Omojola O, Redemske R and Kwan J 2011 Wearable sensor platform and mobile application for use in cognitive behavioral therapy for drug addiction and PTSD. Conf Proc IEEE Eng Med Biol Soc 2011:1802-5.

Fowles DC 1974 Mechanisms of electrodermal activity. In R.F. Thompson & M.M. Patterson (Eds.), *Methods in physiological psychology* (Bioelectric recording techniques, Part C: Receptor and effector processes, 1:231-71).New York:Academic.

Franks W, Schenker I, Schmutz P, Hierlemann A 2005 Impedance characterization and modeling of electrodes for biomedical applications. IEEE Trans.Biomed.Eng. 52 1295-1302

Grimnes S 1983 Impedance measurement of individual skin surface electrodes. Med. Biol. Eng. Comput. 21:750-5.

Grimnes S and Høgetveit JO 2011 Biomedical Sensors. Chapter in *Handbook of research on Biomedical Engineering, Education and Advanced Bioengineering Learning.* Abu-Faraj ZO (Ed). IGI Global.

Grimnes S and Martinsen ØG 2008 *Bioimpedance and Bioelectricity Basics* (2nd.ed). Elsevier

Gumbrell G P, Peura R A, Kun S and Dunn R M 1997 Development of a minimally invasive microvascular ischemia monitor: drift reduction results. Proc. 10th int.conf.IEEE/EMBS Oct.30-Nov.2 30 25-27

Tolín Hernani M, Crespo Medina M, Luengo Herrero V, Martínez López C, Salcedo Posadas A, Alvarez Calatayud G, Morales Pérez JL, Sánchez Sánchez C 2011 Comparison between conventional ph measurement and multichannel intraluminal esophageal impedance in children with respiratory disorders. An Pediatr (Barc). [Epub ahead of print]

Huerta-Franco MR, Vargas-Luna M, Montes-Frausto HB, Flores-Hernández C and Morales-Mata I 2012 Electrical bioimpedance and other techniques for gastric emptying and motility evaluation. World J Gastrointest Pathophysiol. 3:10-18.

Iwase S, Ikeda T, Kitazawa H, Hakusui S, Sugenoya J and Mano T 1997 Altered response in cutaneous sympathetic outflow to mental and thermal stimuli in primary palmoplantar hyperhidrosis J.Auton.Nerv.Syst.64 65-73.

Kalvøy H 2010 *Needle Guidance in Clinical Applications based on Electrical Impedance*. PhD thesis, Faculty of Mathematics and Natural Sciences, University of Oslo 2010.

Kalvøy H, Frich L, Grimnes S, Martinsen ØG, Hol PK and Stubhaug A. 2009 Impedance-based tissue discrimination for needle guidance. Physiol Meas 30:129-40.

Kim L, Jeon JY, Sung IY, Jeong SY, Do JH, Kim HJ. 2011. Prediction of treatment outcome with bioimpedance measurements in breast cancer relatedlymphedema patients. Ann Rehabil Med. 35:687-93.

Kreyden O P 2002 Delusional hyperhidrosis as a risk for medical overtreatment: a case of botulinophilia Arch. Dermatol. 138:538-539.

Krogstad A L, Mork C, Piechnik S K 2006 Daily pattern of sweating and response to stress and exercise in patients with palmar hyperhidrosis. British Journal of Dermatology 154:1118-22.

Krogstad A L, Skymne A, Pegenius G, Elam M, Wallin G 2004 Evaluation of objective methods to diagnose palmar hyperhidrosis and monitor effects of botulinum toxin treatment. Clinical Neuropysiology 115:1909-16.

Kunimoto M, K Kirnö, M Elam and BG Wallin. Neuroeffector Characteristics of Sweat Glands in the Human Hand Activated by Regular Neural Stimuli. Journal of Physiology 442:391-411, 1991.

Kushki A, Andrews AJ, Power SD, King G, Chau T (2012) Classification of Activity Engagement in Individuals with Severe Physical Disabilities Using Signals of the Peripheral Nervous System. PLoS ONE 7(2): e30373.

Kyle UG, Bosaeus I, De Lorenzo AD, Deurenberg P, Elia M, Gomez JM, Heitmann BL, Kent-Smith L, Melchior JC, Pirlich M, Scharfetter H, Schols AMWJ, Pichard C. 2004. Bioelectrical impedance analysis – Part II: utilization in clinical practice. Clin Nutr 23:1226-43.

Martinsen ØG and Grimnes S 1999 Measuring depth depends on frequency in electrical skin impedance measurements. Skin res. techn. 5:179-181.

Martinsen ØG, Kalvøy H, Grimnes S, Nordbotten B, Hol PH, Fosse E, Myklebust H and Becker LB 2010 Invasive electrical impedance tomography for blood vessel detection. Open Biomed Eng J. 2010; 4: 135–7.

Matthie JR 2008. Bioimpedance measurements of human body composition: critical analysis and outlook. Expert Rev Med Devices 5:239-261.

Michael L, Passmann S and Becker R 2011 Electrodermal lability as an indicator for subjective sleepiness during total sleep deprivation. J Sleep Res. [Epub ahead of print]

Mindt W, Maurer H, Möller W 1978 Principle and characteristics of the ROCHE tissue pH electrode Archive of Gynecology and Obstetrics 226 9-16

Mirtaheri P, Grimnes S, Martinsen ØG and Tønnessen TI 2004 A new biomedical sensor for measuring PCO_2. Physiol.Meas.25:421-36.

Mirtaheri P, Omtveit T, Klotzbuecher T, Grimnes S, Martinsen Ø G, Tønnessen T I 2004 Miniaturization of a biomedical gas sensor Physiol.Meas.25 1511-1522.

Ojimba T A, Cameron A E P 2004 Drawbacks of endoscopic thoracic sympathectomy. British J. Surgery 91:264-69

Ozhan H, Alemdar R, Caglar O, Ordu S, Kaya A, Albayrak S, Turker Y, Bulur S. 2012. Performance of bioelectrical impedance analysis in the diagnosis of metabolic syndrome. J Investig Med. 60:587-91.

Pallàs-Areny R and Webster JG 2001 *Sensors and Signal Conditioning,* 2nd.ed,Hoboken, NJ: John Wiley and Sons.

Poh MZ, Loddenkemper T, Reinsberger C, Swenson NC, Goyal S, Sabtala MC, Madsen JR and Picard RW 2012 Convulsive seizure detection using a wrist-worn electrodermal activity and accelerometry biosensor. Epilepsia 53:93-97.

Poh, MZ, NC Swenson, RW Picard. A Wearable Sensor for Unobtrusive, Long-term Assessment of Electrodermal Activity, IEEE Trans. Biomed. Eng. 57:1243-1252, 2010.

Ramos R, Moya J, Morera R, Masuet C, Perna V, Macia I, Escobar I and Villalonga R 2006 An assessment of anxiety in patients with primary hyperhidrosis before and after endoscopic thoracic sympathicolysis. Eur.Journ.Cardio-Thoracic Surgery. 30:228-31.

Ramos R, Moya J, Turon V, Perez J, Villalonga R, Morera R, Perna V and Ferrer G. 2006 Primary hyperhidrosis and anxiety: a prospective preoperative survey of 158 patients Arch.Bronconeumologia 2:88-92.

Rosano GM, Fini M, Gaminti G and Barbaro G. 2008 Cardiac metabolism in myocardial ischemia. Curr Pharm Des. 14:2551-62.

Shepard RK 2009 Leads and longevityy: how long will your pacemaker last? Europace 11:142-143

Strutton D R, Kowalski JW, Glaser D A and Stang P E 2004. US prevalence of hyperhidrosis and impact on individuals with axillary hyperhidrosis: results from a national survey J. Am. Acad. Dermatol. 241–8.

Tronstad C 2005 *Portabelt apparat for måling av svetteaktivitet*. Master thesis, Norwegian University of Science and Technology, 2005.

Tønnessen TI 1997 Biological basis for PCO2 as a detector of ischemia. Acta Anaesthesiol Scand, 41:659-69.

Varlan A R and Sansen W 1997 Micromachined conductimetric p(CO2) sensor Sensors and Actuators B 55 309-15.
Venkatesh B and Morgan TJ 2002 Monitoring tissue gas tensions in critical illness. Crit Care Resusc. 2002 4:291-300.

Wælgaard L, Dahl BM, Kvarstein G, Tønnessen TI 2012 Tissue gas tensions and tissue metabolites for detection of organ hypoperfusion and ischemia. Acta Anaesthesiol Scand. 2012 Feb;56(2):200-9

Zhao P and Cai W.J 1997 An Improved Potentiometric pCO2 Microelectrode Anal.Chem. 69 5052-5058.

I

II

III

PC-based instrumentation for electrodermal activity measurement

Christian Tronstad[1], Sverre Grimnes[1,2], Ørjan G. Martinsen[2,1], Vegard Amundsen[2] and Slawomir Wojniusz[3,4]

[1]Department of Clinical and Biomedical Engineering, Oslo University Hospital, Rikshospitalet, Norway.
[2]Department of Physics, University of Oslo, Rikshospitalet, Norway.
[3]Department of Neuropsychiatry and Psychosomatic Medicine, Oslo University Hospital, Rikshospitalet, Norway.
[4]Faculty of Health Sciences, Oslo University College, Norway

E-mail: christian.tronstad@gmail.com

Abstract. A PC-based EDA measuring system is presented. The system is composed of a laptop with a PCMCIA DAQ-card running LabVIEW® software, a small front-end with a dual op-amp IC and a few passive components, and three skin-surface electrodes. The electrode system gives a monopolar measurement below the measuring electrode regardless of the electrode sizes, unless very small. Usage of the system is demonstrated by measurements from a mental stress experiment on 17 volunteers. There was a significant correlation ($R=0.51$, $p<0.001$) between the self-assessed stress-level and the EDA response frequency. The system allows easy on-site customization in software of measuring parameters, signal-quality monitoring and non-linearity detection in real time. We believe that the most suited use for the system is for stationary experimental purposes where this flexibility is desired. The system is easy to reproduce by engineers interested in doing EDA research.

1. Introduction

The activity from the sympathetic nervous system (SNS) regulates the secretory part of the sweat glands, which in turn changes the electrical properties of the skin due to the filling of electrolyte-containing sweat in the ducts. These changes are mostly in the stratum corneum (SC) layer of the skin, and by measuring the SC conductance we can obtain a link to the SNS activity. This phenomenon is usually called electrodermal activity (EDA). The best sites for measuring EDA are known to be the palmar and plantar dermatomes, which probably differ from the innervation of sweat glands on the rest of the body [1]. There is a wide range of uses for EDA recordings, with applications within psychophysiology, ambulatory monitoring, intensive care and biofeedback among others.

EDR instrumentation generally requires very few electronic components and can be built into small devices with low current consumption [2,3]. However, for stationary experimental purposes where a laptop is the monitor of choice, the instrumentation is easily realized by a DAQ card and a few off-the-shelf components. This paper presents one such solution. EDA is known as an indicator of stress [1], and measurements from usage of the system in a mental stress experimental setting are presented.

2. Materials and methods

2.1. Instrumentation

The measuring system is composed of three main parts, illustrated in figure 1:

- Three skin surface gel electrodes.
- Front-end electronics consisting of one dual op-amp IC, 5 resistors and two capacitors.
- A laptop with a National Instruments 6062E DAQ-card and LabVIEW® software for signal processing, display and data storage.

A low amplitude sine voltage generated by the D/A of the DAQ is applied to the skin through the E and R electrodes. Remote sensing at the current-less R electrode causes the right op-amp to drive a current through E which keeps the potential under R equal to the excitation sine, thus eliminating the SC impedance below E [4,5].

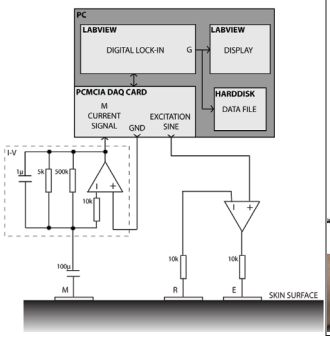

Figure 1. PC-based EDA instrumentation

Figure 2. Photo of the system in use

Because the impedance of the wet tissue is negligible compared to that of the SC, the only current-opposing element that is left is the impedance of the SC below the M electrode. Thus, the measurement is monopolar regardless of the effective electrode areas (EEA) (unless very small [4]), and confined to the SC of the EEA below M. The major contributor to changes in this impedance is the filling and reabsorption of sweat in the sweat ducts. Measuring with AC eliminates the endogenous potentials generated by the skin or electrodes. The I-V dashed box on the left constitute a current to voltage converter with a *Fc=200 Hz* RC lowpass filter. The 100µ capacitor blocks DC which may saturate the op-amp and its impedance needs to be very small compared to the SC below M, thus the large capacitance. The 10k resistors are for safety in order to reduce the current through the skin should a breakdown in the op-amp occur. The digitized current signal is demodulated by the phase-corrected excitation sine in software, giving the AC conductance G as the real part of the current divided by the excitation voltage. The voltage input and output of the DAQ is synchronized with the same sample clock. The op-amp power is supplied by the DAQ-card. Figure 2 shows a photo of the total system.

2.2. Software

Apart from the front-end with the op-amp IC as the only active component, all the measurement tasks are handled digitally in software. The digital lock-in technique is similar to that presented in [2]. For

research purposes, the aim is to preserve as much as possible of the EDR signal information, because the EDR parameters may vary depending on the feature extraction methods when the sampling frequency *Fs* is decreased below a certain threshold. Very little signal energy is lost when *Fs* is as low as 1*Hz*, but depending on the signal feature extraction method, a higher *Fs* may be required. The requirement of using a low excitation frequency *Fe* for the EDA measurement [6] decides the compensation between *Fs* and the signal quality by means of the number of periods *N* for one measurement. The software will also need a certain processing time *Tp* between each measurement for signal processing, storage etc, giving the following limit for the maximum *Fs*:

$$Fs = \left(\frac{N}{Fe} + Tp\right)^{-1} \quad (1)$$

2.3. Experimental protocol

17 volunteers (11M, 6F) who gave informed consent were subjected to three epochs of stress exposure, each lasting 10 min: Relaxation with classical music, quietly reading a text while provoked by irregular bursts of white noise and anticipation of public speaking while still receiving the white noise. The M electrode was placed on the hypothenar area of the palm, while the R and E electrodes were placed on the underarm, but the placement of these two is not critical. The skin AC conductance was sampled at *Fs=8Hz.*

2.4. Data analysis

As a measure of EDA response frequency, the number of EDA peaks (EDA TC) within a central five minute window within all the epochs was computationally determined by a top counting algorithm (A.1) and compared with a self-assessed stress score (1-10) of the volunteers using the Pearson product moment correlation. Comparison between the epochs was done using one way repeated measures ANOVA and the Holm-Sidak t-test. Normality was assumed based on the Shapiro-Wilk test.

3. Results

The SNR of the conductance measurement was 74 dB with a phase error of 0.02º, tested in a lab with a high degree of electromagnetic interference. The linear dynamic range of the system with the configuration as in fig.1 was 0 to approx 200µS. This also depends on the type of op-amp used.

There was a significant correlation between the EDA TC and the subjective stress-score ($R=0.51$, $p<0.001$). As shown in fig.3, both the EDA TC and the subjective score was significantly higher ($p<0.05$) during epoch 2 and 3 compared to epoch 1. Fig.4 shows an example measurement from epoch 2.

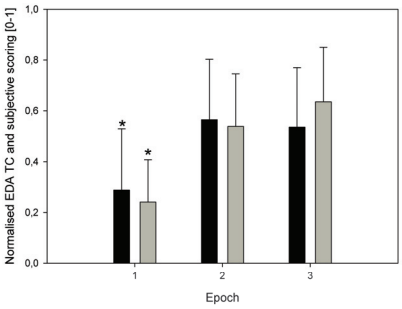

Figure 3. Mean and standard deviation of the EDA TC (black) and the subjective scoring (grey) for the three epochs. *p<0.05.

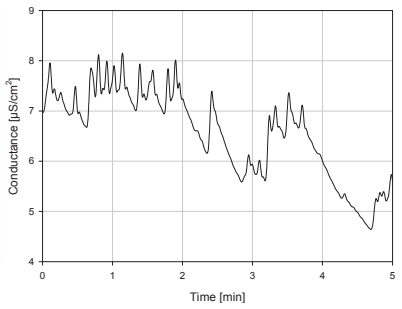

Figure 4. Example measurement from epoch 2.

Discussion

Expectedly, epoch 2 and 3 led to a higher self-assessed stress level than epoch 1. Although the protocol failed to produce a significant difference in mean stress level between the epoch 2 and 3, large intraindividual differences between these epochs were frequently observed. Thus, the correlation between the EDA parameter and the self-assessed score may be a better suited measure of the link between EDA and mental stress than the ANOVA. However, the variation in intersubjective understanding of the scoring will impact the correlation. Although the first 2.5 minutes of the epochs were excluded in the analysis to allow habituation to the noise, part of the EDA responses in epochs two and three may be directly caused by the acoustic stimulus, and whether this represents stress or not can be debated.

With this setup, measuring parameters such as the excitation voltage and frequency, phase correction, filtering and calibration is easily modified by a few mouse-clicks. In addition, the system enables automatic detection of artefacts or non-linearity from the raw input current signal, which can be important for this type of electrode system [4]. The simplicity of a laptop with only a cable, a front-end box which can be made very small and electrodes as the total measuring system makes it convenient for use in an experimental setting where a laptop is the monitor of preference. This system would be easy to reproduce by biomedical engineers interested in doing EDA research and it would work just as well with most other types of DAQ-cards, e.g. the USB-DAQ which has become more popular lately.

For electrical safety, it is important to run the laptop on battery while measuring on live subjects in order to obtain a body floating connection with the equipment.

Appendix

With FFT analysis revealing negligible energy above 1 Hz, the window length was set to $1Hz \cdot Fs =$ 8 points and the EDA TC was calculated as:

$$TC = \sum_{i=Fs/2}^{N-Fs/2} (pos\left(G[i] - G\left[i - \frac{Fs}{2}\right] - \Delta G\right)$$

$$\cdot \prod_{j=0}^{\frac{Fs}{2}} (pos(G\,[i-j] - G[i-j-1]) \cdot pos(G[i+j] - G[i+j+1]))) \qquad (A.1)$$

$$Where\ pos(x) = \begin{cases} 1, & x \geq 0 \\ 0, & x < 0 \end{cases}, \Delta G = \frac{0.01 \mu S}{cm^2}$$

References

[1] Boucsein W. 1992. *Electrodermal Activity*. NewYork: Plenum Press. 460 pages, ISBN-10: 0306442140, ISBN-13: 978-0306442148.

[2] Tronstad C., Gjein G.E., Grimnes S., Martinsen Ø.G., Krogstad A-L., Fosse E. 2008 Electrical measurement of sweat activity. *Physiol.Meas*. **29** 407-415

[3] Tronstad C., Martinsen Ø.G., Grimnes S. 2008 Embedded instrumentation for skin admittance measurement. *Engineering in Medicine and Biology Society, 2009. EMBS 2008. 30th Annural International Conference of the IEEE, Vancouver*. 2373-2376

[4] Grimnes S., Martinsen Ø.G., Tronstad C. 2009. *Noise properties of the 3-electrode skin admittance measuring circuit. 4th European Conference of the IFMBE, Antwerp. Springer Berling Heidelberd, IFMBE Proceedings* **22** 720-722.

[5] Grimnes S. 1983 Impedance measurement of individual skin surface electrodes. *Med.Biol.Eng.Comput*. **21** 750-755

[6] Martinsen Ø.G., Grimnes S., Haug E. 1999 Measuring depth depends on frequency in electrical skin impedance measurements. *Skin Res. Technol.* **5** 179-81.

IV

V

VI

VII

VIII

IX

Improved estimation of sweating based on electrical properties of skin

Christian Tronstad[a], Håvard Kalvøy[a], Sverre Grimnes[a,b] and Ørjan G. Martinsen[b,a]

[a]Department of Clinical and Biomedical Engineering, Rikshospitalet, Oslo University Hospital, Oslo, Norway
[b]Department of Physics, University of Oslo, Oslo, Norway

Corresponding author:
Christian Tronstad
Department of Research and Development, Clinical and Biomedical Engineering, Rikshospitalet, Oslo University Hospital, Oslo, Norway
Sognsvannsveien 20
0027 Oslo, Norway

Abstract

Skin conductance (SC) has previously been reported to correlate strongly with sweat rate (Swr) within subjects, but weakly between subjects. Using a new solution for simultaneous recording of skin conductance, skin susceptance (SB) and skin potential (SP) at the same skin site, the aim of this study was to assess how accurately sweat production can be estimated based on combining these electrical properties of skin. In 40 subjects, SC, SB, SP and Swr by skin water loss was measured during relaxation and mental stress. SC and Swr had high intraindividual correlations (median r=0.77). Stepwise multilinear regression with bootstrap validation lead to a sweating estimation model based on the sum of SC increases, the SP area under the curve and the SB area under the curve, yielding an interindividual accuracy of R^2=0.73, rmse=12.9%, limits of agreement of +27.6%, -30.4% and an intraclass correlation coefficient of 0.84. Bootstrapping of training and test-sets gave median rmse=15.4%, median R^2=0.66. The model was also validated for intraindividual variability. The results show that estimation of sweating is significantly improved by the addition of SB and SP measurement.

Keywords: Sweating, sweat rate, skin conductance, skin potential, skin susceptance, bioimpedance, multilinear model

Introduction

It is well known that the in vivo electrical properties of skin are heavily influenced by sweating[14]. The outermost layer of the skin, the Stratum Corneum, provides a strong electrical barrier of dead skin cells when dry, but when sweat pores are filled with sweat, pathways of ionic transport are created which greatly reduces this electrical impedance through the skin. This provides a very sensitive measurement of sweat gland activity by means of the skin conductance (SC), and is widely used as a physiological parameter within many biomedical applications [3]. Sweating also causes changes in the bioelectric potential (SP) at the skin surface, but the characteristics of this parameter is different from SC. While the SC always increases with the sweat duct filling and recovers while sweat is reabsorbed and/or pores are closed, the SP can change in both positive and negative voltage directions and produce biphasic or triphasic responses [3]. A third electrical parameter to consider is the skin capacitance, which is positively correlated with the moisture content of the stratum corneum[19], and is most accurately measured by low-frequency skin susceptance (SB)[18]. Although sweating, here defined as the amount of water loss from the skin by evaporation, and changes in the skin electrical properties both originate from the sweat gland, they are governed by completely different biophysical mechanisms. Sweating includes transport of sweat to the skin surface, evaporation and further transport of water molecules to the air.

Some of the sweat is also absorbed in the skin and later evaporates at a decreasing rate, making the evaporation also dependent on the skin sorption characteristics. SC also increases as sweat fills the pores, but this is not necessarily dependent on sweat reaching the skin surface [10]. After sweat pore filling, the SC decreases as electrolytes are reabsorbed through the sweat duct wall. The same mechanisms govern the SP response although the waveform is more complex[10]. Despite these biophysical differences, mainly the movement of water vs the movement of electrolytes, high within-subject correlations have been reported between SC and skin water loss (up to $r=0.88$[21], $r>0.85$[8]) and between the positive SP response and water loss ($r=0.93$[12]). Between-subjects correlations on the other hand, is reported to be lower than $r<0.50$ as a rule[8] and between $r=0.23$ to 0.64[21], suggesting one or more individual factors in the relation between electrical and evaporative skin properties. These factors could be differences in sweat electrolyte concentration[17], thickness of the stratum corneum[11] or the skin sorption characteristics. The SB parameter could approach some of this interindividual variance, as SB is not directly affected by sweat pore filling and reflects only the stratum corneum moisture content [18]. Recently, a method for measuring SC, SP and SB at the same skin site was introduced by Grimnes[15], enabling a new look on the relation between sweating and electrical properties of skin by inclusion of more parameters.
The aim of this study was to assess how accurately sweat production can be estimated based on combining these three electrical properties of skin. This was implemented by the following list:

1. Measure sweat rate (Swr) and the electrical properties SC, SB and SP during variations in sweating within and between subjects.
2. Analyze individual temporal correlations between changes in Swr and electrical properties.
3. Investigate between-subjects correlations between sweating and electrical parameters.
4. Develop a model for estimating sweat production based on significant parameters.
5. Validate the model for both between-subjects and within-subject variance.

Materials and methods

Skin admittance and potential measurement

Based on the solution described in Grimnes et al 2011, a PC-based EDA measuring system for simultaneous recording of skin complex admittance (SY) and SP at the same electrode was developed, consisting of front-end electronics connected via a National Instruments® DAQ-card to a laptop running software written in LabVIEW® v8.5, similar to the instrumentation presented in Tronstad et al 2010[28]. Instead of a saline bath immersion of the underarm as a reference electrode, a novel three-electrode system was used which ensures unipolar recording of SC regardless of electrode areas, thus allowing the use of the same electrode type at all sites. The constant current control was replaced by a Howland current source giving a 10 Hz AC current of 14μA to the skin. In addition to SC and SP measurements, the quadrature component of the SY signal was used to aquire SB. The differential amplifier was replaced by voltage sensing by analog-to-digital conversion at both terminals with software differencing, enabling control of the electrodermal inactivity at the reference site, which is a requirement for accurate SP recording[3]. Although abrasion[9] or skin drilling[30] is a recommended pretreatment for the inactive site, no pretreatment of the skin was used in this study to avoid risk of contamination and the need for associated procedures. The measuring electrode was attached at the hypothenar site of the palm, the SP reference electrode was attached to the apex of the elbow and a current sink electrode was placed on the underarm. The electrode type used was Arbo® Kittycat™, according to recommendations in Tronstad et al 2010[29].

Sweat rate measurement

Sweat rate (Swr) was measured by using the Q-sweat (WR Medical Electronics Co, Stillwater, USA). The Q-Sweat uses dry air (room air, drawn across a desiccant) to pick up moisture from a measurement capsule (5.06 cm^2 circular measurement area) placed on the skin. Constant airflow (60 cm^3/min) through the capsule transports the captured moisture to the temperature and humidity sensors in the device. The airflow back and forth from the capsule to the Q-sweat passes through two 2.4 m air hoses.

The skin capsule was attached on the hypothenar eminence of a randomly picked hand on each test subject (the opposite of the bioelectrical electrode). This was done by first attaching the end of the silicone band to the capsule and turn the silicone band around the wrist and back over mounting spikes on the capsule. Then the remaining half of the silicone band was turned around the palm distal to the thumb and back to the capsule, where the end of the band was attached to the mounting spikes. This way the silicone band formed a figure of eight with the middle cross attached to the capsule. One of the circles forming the figure of eight was wrapped around the wrist, similar to a wrist band. The other half was the silicone band on the meta carpus, passing to the dorsal side of the hand distal to the thumb. The capsule position was adjusted by varying the tension in the silicone band in the four directions of the cross covering the capsule. This was done to even out the pressure between the capsule and the skin around the capsule, until a thigh fit was obtained and no leakage could be detected by the Q-sweat software (WR-TestWorks 2.0.1). To further prevent air leakage, the test subject was asked to find a comfortable position for the hand and move it as little as possible during the measurements.

A step-response test of the QSweat system was done before the experiments started to test its responsiveness. By sliding a probe from a dry to a wet surface, a response delay of 8s and a time-constant of 19.2s was found.

Experimental protocol

40 healthy volunteers (31 male, 9 female, age 17-64), were recruited from Oslo University Hospital and University of Oslo and gave informed consent before participation. The study was approved by the regional ethics committee (REK #2010/1927a).

The experiments were done in silent laboratory or meeting rooms with only the test subject and two operators present. Room temperature was 22.5±1˚C. After bilateral fixation of EDA and QSweat sensors to the hypothenar area on both palms, the Swr measurement was monitored until stable levels were attained. The experiment was aborted if the Swr stabilized above the maximum of the QSweat measuring range (1000nL/min). At least 5 minutes were allowed for stabilization of EDA electrodes before the recording started. In order to produce variations in sweating and thereby duct filling over time, intervals of relaxation and mental stress were alternated. The subjects were sitting comfortably in a chair and were not allowed to speak with the operators. Mental stress was induced by asking the subject to repeatedly subtract seven from a starting number of 1000. This was repeated in three two-minute intervals, with 5 minutes for relaxation before and after, giving a total recording session of 26 minutes.

Data analysis and statistics

Signal conditioning

Due to noisy QSweat recordings, the time-series were low-pass filtered with a third-order zero-phase Butterworth filter with a 0.025 Hz cutoff frequency in order to dampen all noisy fluctuations sufficiently. The response delay and time-constant found from the step-test was used to correct the phase of the signal and the responsiveness by backwards-filtering through an inverted RC-filter with the measured time-constant.

The Swr recording with a sampling frequency of Fs=4Hz were aligned with the EDA recordings with Fs=10 Hz by resampling to 10Hz by linear interpolation using the time-series tools in Matlab.

Intraindividual time-series analysis
To assess the synchronicity between the SC and Swr recordings, the cross-covariance matrix between the two signals was calculated for each subject and the relative time-shift at the maximum was used to estimate the lag between each signal pair. A one-sample t-test was used to evaluate the significance of the lag.
Based on an insignificant lag, the correlation between the SC and Sw time-series were evaluated by the Pearson product-moment correlation coefficient.
12 Swr recordings which either saturated the measurement range (>1000 nL/min) or produced no increase above the measuring noise (5% threshold of 50 nL/min) during the stress provocation were excluded from the time-series correlation analysis.

Interindividual correlations
Similar to the time-series analysis, the recordings which saturated the Swr measurement range were excluded, but those with low responses (<50 nL/min) were included, giving a total of 33 subjects used in this analysis.
Total sweating (Sw) in µL/5 cm^2 for each subject was calculated by the area under the curve (AUC) of the Swr recording for the whole duration of the session and was used as a dependent variable in a multilinear regression with EDA parameters as independent variables. Table 1 gives a complete list of all the variables used in the analysis.
The NSCR parameter was calculated from a peak recognition algorithm using Matlab® where a peak at time t was recognized if there was 0.5s or more of continuous increase above 0.01 µS on the left side and a decrease or flat 0.5s to the right side of t.
The correlation between each pair of variables was determined by the Pearson product-moment correlation coefficient.

Table 1. Overview of all parameters extracted from the recordings and used in the statistical analyses.

Parameter	Description	Function	Unit
Swr	Sweat rate	Dependent variable	nL/min
SC	Skin conductance	Intraindividual covariate	µS
Sw	Sweating (Swr area under curve)	Dependent variable	µL
AUC SC	SC area under curve	Interindividual covariate	µSmin
AUC SB	SB area under curve	Interindividual covariate	µSmin
AUC SP	SP area under curve	Interindividual covariate	mVmin
NSCR	Number of SC responses	Interindividual covariate	dimensionless
SCpos	Sum of positive SC responses	Interindividual covariate	µS
SPpos	Sum of positive SP responses	Interindividual covariate	mV
SPneg	Sum of negative SP responses	Interindividual covariate	mV

Model development
In order to sift out reduntant independent variables and avoid overfitting, stepwise regression was first used to find the best explanatory model. The stepwise regression method adds or removes terms from a multilinear model based on their statistical significance in a regression. Beginning with no terms, one independent variable was added at a time based on the lowest p-

value of its coefficients being zero if added to the model, until the model could no longer be improved by including more terms within the significance level ($p<0.05$).
In order to validate the model suggested by the stepwise regression procedure, the model from each step was evaluated by bootstrapping. Random permutations were used to assign half of the dataset to a training set and the other half to a test set. The regression coefficients were then found from the training set and applied on the test set to calculate the root mean square error (rmse) of the estimation. This was also done on the model with all parameters for comparison. Distributions of the rmse for each model from 1000 bootstrap iterations were compared by a Kruskal-Wallis one way ANOVA on Ranks with Tukey post-hoc pairwise multiple comparison tests. The final model was selected based on the fewest number of terms and an rmse not significantly higher than any other model.

Model validation
Agreement between the model and the Sw was presented as a scatterplot using the mean coefficients from the bootstrapping, together with the coefficient of determination, R^2, the Pearson product-moment correlation coefficient, r, the rmse and percent-wise rmse. A Bland-Altman plot was constructed from the mean and differences between the measured and estimated sweating, with 1.96 std.dev limits of agreement. Reliability was assessed by the two-way mixed intraclass correlation coefficient for absolute agreement (ICC).
In order to test the validity of the model upon intraindividual variability, estimation was assessed both during periods of high and low sweating according to the ends of the stress and relaxation intervals. Sw and all model parameters were extracted from the last minutes of all stress periods for the high sweating dataset, and during the last minutes for all relaxation periods, except the last, for the low sweating dataset. Sweating was estimated from the same mean coefficients from the total dataset. The two estimations were compared by their linear regression trend-lines from scatterplots between measured and estimated sweating within the same graph.
All data-analysis was done using Matlab R2011 a, Sigmaplot 11.0 and SPSS 19.

Results

Intraindividual time-series analysis
Based on the cross-covariance, the SC and Swr signal was highly synchronized, with an insignificant ($p=0.19$, One-Sample t-test against zero) lag of the Swr with median 1.05s, 25% percentile -3.6s and 75% percentile of 12.05 s.
The temporal correlation between the SC and Swr time-series was median 0.77 ($p<0.001$), 25 % percentile 0.67 and 75 % percentile 0.84. The correlation between the means of SC and Swr was 0.94 ($p<0.001$).

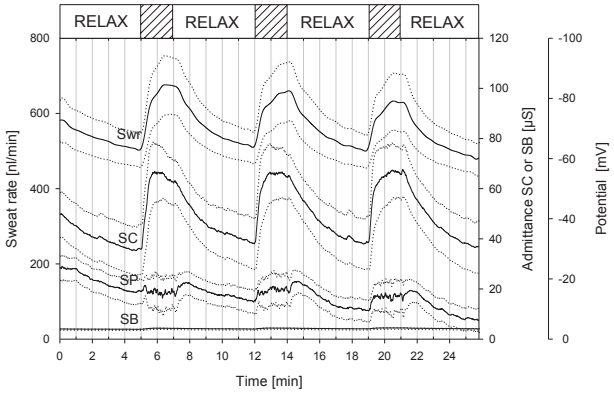

Figure 1. Mean time series of sweat rate (Swr), skin conductance (SC), skin potential (SP) and skin susceptance (SB) with 95% confidence intervals (dotted lines). The upper boxes indicates the intervals of relaxation and stress by arithmetics (hatched).

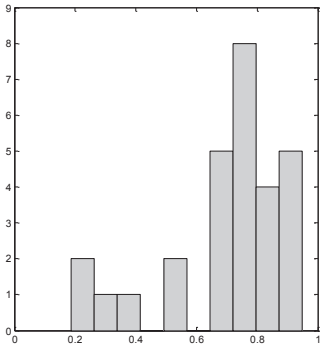

Figure 2. Histogram of intraindividual correlation coefficients between Swr and SC (N=28).

Interindividual correlations

Pearson product-moment correlation coefficients for all interindividual parameters are presented in table 2 (N=40). Sw correlated strongest with SCpos (r=0.76) and NSCR (r=0.65), and these two parameters were strongly correlated to each other (r=0.77).

Table 2. Pearson product moment correlation coefficients between all interindividual parameters.

Pearson's r	**AUC SC**	**AUC SB**	**AUC SP**	**NSCR**	**SCpos**	**SPpos**	**SPneg**
Sw	0.49**	0.39*	0.29	0.65***	0.76***	0.43**	0.17
AUC SC		0.48**	0.02	0.79***	0.66***	0.02	0.014
AUC SB			*0.13*	0.23	*0.22*	0.11	0.35*
AUC SP				-0.08	*0.19*	0.28	-0.02
NSCR					0.77***	0.2	0.12
SCpos						0.55***	-0.17
SPpos							-0.21

*p<0.05 **p<0.01 ***p<0.001

Model development

Multilinear regression using all parameters gave an R^2=0.84, r=0.91, rmse=1.7 µL. The stepwise regression lead to a model including the significant terms of SCpos, AUC SP, AUC SB and AUC SC in the given order (R^2=0.82, r=0.90, rmse=1.7 µL). Validation of this model by bootstrapping lead to rmse distributions as shown in figure 3. Based on the ANOVA with pairwise comparisons, each step lead to a significant model improvement except for the last step with the inclusion of AUC SC, which significantly increased the rmse. Thus, the SCpos+AUC SP+AUC SB model was chosen for further assessment.

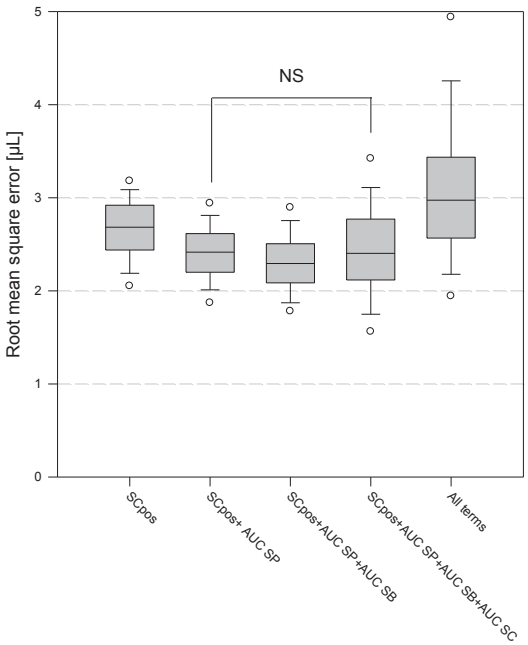

Figure 3. Distributions of rmse from 1000 bootstrap validation of models from the stepwise regression and the model including all terms. All distributions were significantly different except for model number two and four ($p<0.05$, Tukey Test for pairwise multiple comparison). Circles represent 5% and 95% percentiles.

Model validation

Table 2 also shows that none of the selected terms were significantly correlated (italic numbers). A scatterplot and a Bland-Altman plot of this model using the mean coefficients from the bootstrapping is presented in figure 4. The model estimated the measured sweating with an R^2=0.73, r=0.85 and rmse=1.9 µL, which equals 12.9% of the measurement range. The limits of agreement was 27.6% above and 30.4% below the mean, which was close to zero due to the use of averaged coefficients. The reliability test of measured vs estimated sweating gave an ICC of 0.84.

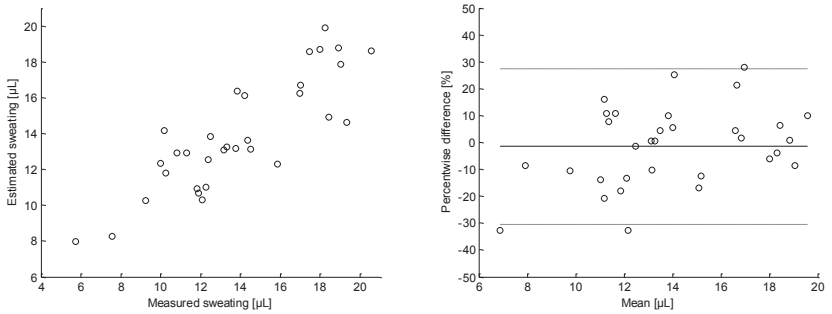

Figure 4. Scatterplot of measured vs estimated sweating based on the selected model (SCpos+AUC SP+AUC SB) with R^2=0.73, r=0.85, rmse=1.9 µL (left) and Bland-Altman plot (right) showing the mean of the measured and estimated sweating vs their percent-wise difference. The solid line represents the mean percentwise difference (-1.42%) while the dashed lines show the upper (27.6%) and lower (-30.4%) limits of agreement.

Testing of the model on the datasets from the last minutes of provoked sweating and of relaxation gave parallel (slope difference of 0.03) trend-lines with a bias of 0.28 µL. The lower R^2 for the relaxation dataset is due to a reduced range in sweating.

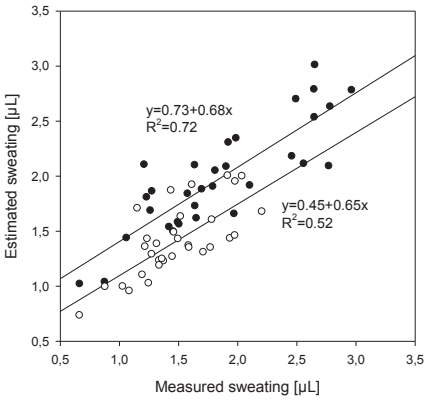

Figure 5. Scatterplots of sweating estimated by the SCpos+AUC SP+AUC SB model for periods of provoked sweating (●) and relaxation (○).

Discussion

The results from this study show that there was a high temporal correlation between sweat rate and SC, that inclusion of SV and SB parameters could explain some of the between-subjects variance, and that sweat production could be estimated with 12.9% average error by a model using a combination of the sum of SC increases, the SP and the SB areas under the curves.

The high temporal correlation between Swr and SC within subjects was not entirely expected in spite of the agreement with Muthny[21] and Edelberg[8]. Most previous studies have compared changes in evaporation to SC or SP during single sweat gland responses. A high correlation in this sense should lead to a similar correlation in this study assuming that both processes are equally linearly or non-linearly additive. Inspection of figure 1 suggests that this does not hold completely, as the SC tends to rise sharper and plateau earlier than the Swr. This could

be due to a reduction in SC as the skin is hydrated, leading to swelling of the stratum corneum and sweat pore closure, an effect explained in Edelberg 1993[10]. It is also known that evaporation follows the electrical response by roughly 5s [22,16]. The last factor to consider is the responsiveness of the QSweat device used to measure Sw in this study, which may have provided slow recordings despite the backwards filtering correction and due to the necessary aggressive low-pass filtering.

The interindividual correlation between sweating and SC was not as high (r=0.49), in agreement with both Edelberg [8] (r<0.50) and Muthny [21] (r=0.23 to 0.64), although significant (p<0.01). Stronger correlations were found between sweating and the sum of SC increases and the number of these responses (NSCR). In agreement with Ellaway [12], the positive SP responses correlated better with sweating than the negative SP responses.

Some indications of parameter redundancy could already be seen from table 2 with the combinations AUC SC+NSCR, AUC SC+SCpos, NSCR+SCpos and SPpos+SCpos. Multilinear regression including all parameters produced an overfitting with R^2=0.84 which was reduced to 0.82 through elimination of the insignificant model parameters NSCR, SPpos and SPneg by means of stepwise regression. Validation of the suggested model from the stepwise regression by bootstrapping lead to elimination of also AUC SC. The remaining terms of SCpos+AUC SP+AUC SB was able to estimate total sweat production with a median R^2=0.66 and median rmse error of 2.28 µL, which represents 15.4% of the measurement range or 8.7% of the QSweat device range, from validation by bootstrapping. We believe that the magnitude of this error needs to be considered with respect to the intended use. This accuracy is nevertheless a significant improvement compared to conventional SC measurement (Bootstrap validation of a model based on only AUC SC gave R^2=0.09). The approximately ±30 limits of agreement between measured and estimated sweating (figure 4) is also difficult to evaluate due to lack of similar studies. As an example, within cardiac output measurements, a limit of agreement up to ±30% has been suggested to be acceptable [6]. This study may also be compared with Gagnon et al [13], where sweat gland activation was determined by a modified iodine-paper technique, in which a computerized method was compared with manual counts by the correlation coefficient and a Bland-Altman plot with the results of r=0.77 and ±38 glands/cm^2 limits of agreement in a pool with a 70 glands/cm^2 mean.

The limits of agreement and the ICC can provide inconsistent results in agreement studies, and both are reported here according to the recommendation of [5]. Similar to the Pearson's r, an ICC close to 1 indicated 'excellent' reliability, but no agreement exists on the interpretation of the ICC. A value >0.9 has been proposed as high agreement between measurements, with an ICC between 0.7 and 0.8 representing questionable agreement in sports medicine [1]. Within psychometrics, ICCs >0.75 to >0.81 have been suggested as excellent agreement [4, 2, 31]. Portney and Watkins [25] suggested 0.75 as a threshold from 'poor to moderate' to 'good' reliability. Thus, we suggest that the ICC=0.84 in this study represents 'good' reliability between measured sweating and what could be estimated from model.

The same dataset was used to develop and to test the model in this study. Although the dataset was randomly divided in training and test sets in the bootstrap validation, all measurements were done by the same operators using the same methods and equipment on different subjects, hence this study does not assess repeatability or reproducibility. The ICC and the Bland-Altman plot, being based on an estimation from the mean model coefficients from the bootstrapping, is a best-case representation of the agreement.

There are numerous advantages of using the electrical methods in favor of the evaporative, as it enables miniaturization [27] and long-term ambulatory recording [24], lower costs of production and is much less susceptible to movement artifacts as the water loss measurement method requires a constant contact pressure of the probe onto the skin [23]. We believe that the proposed method is useful for measurements of sweat production for both intra- and interindividual

comparisons in situations where variations are large. Examples of such large variations include before-after treatment or treatment vs control of hyperhidrosis, exercise physiology studies, night-sweats, or psychological studies involving moderate to strong stressors. Validation of the model during stress and relaxation periods gave a bias in the scatterplot (figure 5) intercept of 0.28 µL, indicating that the model slightly (approx. 10%) overestimates the Sw during heavy sweating. This could be due to a slightly nonlinear relation between the electrical and evaporative changes, and suggests that a more advanced model should be considered based on a larger range in Swr, which was limited in this study due to the measurement range of the QSweat® device. The slopes for sweating during stress and relaxation however, were parallel, indicating that the model's explanation of between-subjects variance is valid in both cases.

The SC alone had a strong correlation to the individual variations, but both the SB and SV significantly helped explain the between-subjects factors, also with positive signs of their linear model coefficients. As mentioned in the introduction, the SB is known to reflect the moisture content of the stratum corneum separately from the sweat duct filling, and the water uptake of the corneum is known to differ among individuals [26]. The SP contribution is more difficult to interpret, as the relation between SC and SP have previously been studied only to small extent due to lack of methods to measure them simultaneously. Contrary to the SC and SB, the palmar SP is negative with respect to an electrodermally inactive skin site and increases initially in the negative voltage direction when a sweat gland response occurs, but may shortly be followed by a response in the opposite direction towards 0V. A positive SP model coefficient thus means that sweat production is estimated to increase as the SP approaches zero. In view of figure 1, SC and SP (with an opposite sign) seems to correlate well during the relaxation intervals, but as sweating increases, the SP reacts in both directions, giving a very different change in the area under curve than for the SC. Along with the low between-subjects correlation between the two parameters (r=0.02), the results suggest that the two parameters bring complementary physiological information on the skin and sweating. The results in total speak in favor of utilizing simultaneous recording of SC, SP and SB for electrical measurement of sweat activity.

The results indicate that roughly 30% of the interindividual variance in sweating could not be explained by the electrical parameters. The electrolyte concentration of sweat will directly influence the magnitude of the SC and SP responses, and relatively large variations in Na and K concentrations have been reported among healthy adults (51.9±21.1 meq for males, 36.5±18.7 meq for females, mean±std.dev) [17]. A sweat collector attached to the skin performing continuous conductivity measurement within a fixed volume could be included in order to increase the accuracy of the electrical measurement of sweating, and was considered in the planning of this study. Piloting however, revealed that insufficient amounts for analysis were collected during the experimental session when testing the Macroduct™ Sweat Collector. Another factor is the thickness of the corneum, which will influence both the Sw and electrical measurement, but in different ways. Egawa et al [11] reported a std.dev of 37 µm from a 173 µm mean for palmar corneum thickness. Only palmar skin was measured in this study, which is different from non-glabrous skin with respect to innervation, sweat gland count [20], corneum thickness [11], and electrical properties [7, 29]. Due to these differences, the model will not likely be valid on non-palmar skin without new calibration. A future study is suggested including sweat electrolyte concentration measurement, measurements of larger ranges in Swr, and SC, SP and SB at additional skin sites with different corneum thickness, and repeated measurements over different seasons in order to assess the repeatability of the estimation.

In conclusion, estimation of sweating, defined as water loss from the skin, is significantly improved by the addition of SB and SP measurement to the SC measurement only, yielding a model for estimation of sweating with approximately 15% average error.

References

1. Atkinson G, AM Nevill. Statistical methods for assessing measurement error (reliability) in variables relevant to sports medicine. Sports Med. 26:217-238, 1998.
2. Batko JJ.The intraclass correlation coefficient as a measure of reliability. Psychological Reports. 19:3-11, 1966.
3. Boucsein W. ELECTRODERMAL ACTIVITY, 2.ed. Springer New York, 2012.
4. Cicchetti DV and SA Sparrow. Developing criteria for establishing interrater reliability of specific items: applications to assessment of adaptive behavior. Am. J. Ment. Defic. 86:127-137, 1981.
5. Costa-Santos C, J Bernardes, D Ayres-de-Campos, A Costa and C Costa. The limits of agreement and the intraclass correlation coefficient may be inconsistent in the interpretation of agreement. Comment in J. Clin. Epidemiol. Jun 64:701-2, 2011.
6. Critchley LAH and JAJH Critchley. A meta-analysis of studies using bias and precision statistics to compare cardiac output measurement techniques. J. Clin. Monit. 15:85-91, 1999.
7. Dooren M, JJG Vries and JH Janssen Emotional sweating across the body: Comparing 16 different skin conductance measurement locations. Physiology & Behavior 106: 298-304, 2012.
8. Edelberg, R. Electrical activity of the skin: Its measurement and uses in psychophysiology. In Greenfield, N. S. & Sternbach, R. A. (Eds.), Handbook of psychophysiology (pp. 367-418). New York: Hold, Rinehart & Winston, 1972.
9. Edelberg, R. Electrical Properties of the Skin. In Brown, C. C. (Ed.), METHODS IN PSYCHOPHYSIOLOGY (pp. 1-53). Baltimore: Williams & Wilkins, 1967.
10. Edelberg, R. Electrodermal mechanisms: A critique of the two-effector hypothesis and a proposed replacement. In Roy, J. C. et al. (Eds.) PROGRESS IN ELECTRODERMAL RESEARCH (pp 7-30). Plenum Press, New York, 1993.
11. Egawa M. In vivo estimation of stratum corneum thickness from water concentration profiles obtained with raman spectroscopy. Acta. Derm. Venereol. 87:4-8, 2007.
12. Ellaway PH, A Kuppuswamy, A Nicotra and CJ Mathias. Sweat production and the sympathetic skin response: Improving the clinical assessment of autonomic function. Autonomic Neuroscience: Basic and Clinical. 155:109-114, 2010.
13. Gagnon D, M Ganio, RAI Lucas, J Pearson, CG Crandall and GP Kenny. The modified iodine-paper technique for the standardized determination of sweat gland activation. J. Appl. Physiol. In press, 2012.
14. Grimnes S and Martinsen ØG. BIOIMPEDANCE AND BIOELECTRICITY BASICS, 2nd. ed. Academic Press. 488 p. 2008.
15. Grimnes S, A Jabbari, ØG Martinsen and C Tronstad. Electrodermal activity by DC potential and AC conductance measured simultaneously at the same skin site. Skin research and technology. 17:26-34, 2011.
16. Kunimoto M, K Kirnö, M Elam and BG Wallin. Neuroeffector Characteristics of Sweat Glands in the Human Hand Activated by Regular Neural Stimuli. Journal of Physiology 442:391-411, 1991.
17. Lobeck CC and D Huebner. Effect of age, sex, and cystic fibrosis on the sodium and potassium content of human sweat. Pediatrics. 30:172-179, 1962.
18. Martinsen ØG, S Grimnes S, J Karlsen. Electrical methods for skin moisture assessment. Skin Pharmacol. 8: 237-245, 1995.

19. Martinsen ØG, S Grimnes, JK Nilsen, C Tronstad, W Jang, H Kin, K Shin and M Naderi Gravimetric method for calibration of skin hydration measurements. IEEE Trans.Biomed.Eng. 55:728-732, 2008.
20. Montagna W and PF Parakkal. THE STRUCTURE AND FUNCTION OF SKIN 3rd ed. ‚New York: Academic, 1974.
21. Muthny FA. Elektrodermale Aktivität und palmare Schwitzaktivität als Biosignale der Haut in der psychophysiologischen Grundlagenforschung. Freiburg:Dreisam, 1984.
22. Nishiyama T, J Sugenoya, T Matsumoto, S Iwase and T Mano. Irregular activation of individual sweat glands in human sole observed by a videomicroscopy. Autonomic Neuroscience: Basic and Clinical 88:117-126, 2001.
23. Pinnagoda J, A Tupker, T Agner and J Serup. Guidelines for transepidermal water loss (TEWL) measurement. Contact Dermatitis. 22:164-178, 1990.
24. Poh, MZ, NC Swenson, RW Picard. A Wearable Sensor for Unobtrusive, Long-term Assessment of Electrodermal Activity, IEEE Trans. Biomed. Eng. 57:1243-1252, 2010.
25. Portney L and M Watkins. FOUNDATIONS OF CLINICAL RESEARCH: applications to practice. Prentice Hall Health, New Jersey, 2000.
26. Treffel P and B Gabard. Stratum corneum dynamic function measurements after moisturizer or irritant application. Arch. Dermatol. Res. 287:474-479, 1995.
27. Tronstad C, ØG Martinsen and S Grimnes. Embedded instrumentation for skin admittance measurement. Engineering in Medicine and Biology Society. EMBS 2008. 30th Annual International Conference of the IEEE. 2008.
28. Tronstad C, S Grimnes, ØG Martinsen, V Amundsen and S Wojniusz. PC-based instrumentation for electrodermal activity measurement. J. Phys.: Conf. Ser. 224, 2010.
29. Tronstad, C, GK Johnsen, S Grimnes and ØG Martinsen. A study on electrode gels for skin conductance measurement. Physiological Measurement 31: 1395-1410, 2010.
30. Venables, PH. and MJ Christie. Electrodermal Activity. In Martin, I. and Venables, O. H. (Eds.), TECHNIQUES IN PSYCHOPHYSIOLOGY (pp 3-67). New York: Wiley & Sons, 1980.
31. Wilson KA, AJ Dowling, M Abdolell and IF Tannock. Perception of quality of life by patients, partners and treating physicians. Quality of life research. 9:1041-1052, 2001.

X

XI

XII

Hepatic and Abdominal PCO_2 Measurement Detects and Discriminates Hepatic Artery and Portal Vein Occlusion in Pigs

Soeren Erik Pischke[1,2,5] Christian Tronstad[3]; Lars Holhjem[1]; Pål Dag Line[4]; Håkon Haugaa[1,5] and Tor Inge Tønnessen[1,2,5]

[1]Division of Emergencies and Critical Care, Department of Anesthesiology; [2]Intervention Centre; [3]Department of Clinical and Biomedical Engineering; [4] Division of Cancer Medicine, Surgery and Transplantation, Department of Transplantation Surgery, Oslo University Hospital and [5]Division of Clinical Medicine, Faculty of Medicine, University of Oslo, Norway

Running title:

Hepatic and Abdominal PCO_2 detects portal occlusion

Keywords:

Orthotopic liver transplantation, ischemia, lactate, sensor, microdialysis

Corresponding author:

Tor Inge Tønnessen
Oslo University Hospital Rikshospitalet
P.O. Box 4950
0424 Oslo
Norway
tel: +47-230 73692
fax: +47-230 73681
e-mail: t.i.tonnessen@medisin.uio.no

Abbreviations:

HA	: hepatic artery
PV	: portal vein
OLT	: orthotopic liver transplantation
PO_2	: partial pressure of oxygen
PCO_2	: partial pressure of carbon dioxide
CI	: cardiac index
HV	: hepatic vein
AST	: aspartate-amino-transferase
ALT	: alanine amino-transferase
LDH	: lactate-dehydrogenase
ALP	: alkaline phosphatase
γ-GT	: gamma-glutamyl-transferase

Financial support:

S.E.P. and H.H. were supported by unlimited research grants from the South-Eastern Norwegian Health Authority (Helse Sør-Øst).

Abstract

Hepatic artery (HA) and portal vein (PV) occlusion are the most common vascular complications after liver transplantation with impact on mortality and re-transplantation rate. Detection of severe hypoperfusion may be delayed with currently available diagnostic tools. Hypoperfusion and anaerobically produced lactic acid lead to tissue CO_2 increase. We aimed to investigate if continuous assessment of intrahepatic and intra-abdominal PCO_2 may detect and distinguish HA and PV occlusion in real-time.

In thirteen pigs HA and PV were fully (n=7) or gradually (n=6) occluded. PCO_2 was monitored intrahepatically and between loops of small intestine. Hepatic and intestinal metabolism was assessed by microdialysis, portal and hepatic vein blood samples and compared to clinical parameters of systemic circulation and blood gas analysis.

Total HA occlusion led to significant increases of hepatic PCO_2 and lactate, accompanied by significant PO_2 and glucose decrease. PV occlusion induced significant intestinal but not hepatic PCO_2 increase along with significant intestinal increase of lactate and glycerol. Gradual HA and PV occlusion caused steady hepatic and intestinal PCO_2 increase, respectively. Systemic clinical parameters like blood pressure, heart rate and cardiac output were affected only by PV occlusion.

In conclusion, even gradual occlusion of HA affects liver metabolism and is reliably identified by hepatic PCO_2 measurement. Intestinal PCO_2 increases only during PV occlusion. A combination of hepatic and intestinal PCO_2 measurement reliably diagnoses the affected vessel, depicts the severity of the occlusion and emerges as a potential real-time clinical monitoring tool in the postoperative course of liver transplantation, enabling early intervention.

249 words

Introduction

Vascular complications in the course of orthotopic liver transplantation (OLT) lead to liver ischemia, which might constitute a life-threatening state for both patient and allograft (1, 2). Hepatic artery (HA) stenosis and occlusion is the most common complication (incidence in adults up to 12%, in children up to 40%) (1), demands retransplantation in > 50% of all cases and is associated with a high mortality (3, 4). The incidence of portal vein (PV) obstruction is 1-2% (1, 2), higher in patients with splanchnic thrombosis prior to OLT (up to 15%) (5), and carries a high morbidity and mortality (2).

The high impact of vascular occlusion on mortality and retransplantation rates underscores the importance of early detection of vascular complications in the first week after transplantation when most of the vascular insults occur (3). Current standard of care is arterial blood lactate assessment, Doppler ultrasound and laboratory liver enzyme assessment daily (6). However, regular blood lactate measurement is not carried out after arterial line withdrawal. Furthermore, there is no consensus on the frequency and timing of Doppler ultrasound, the method does currently not allow continuous monitoring and cannot reliably assess whether blood flow decrease is detrimental to the graft (3). Liver enzyme release reflects hepatic cell damage, is thus unspecific with respect to the cause and increases several hours after the vascular occlusion has occurred (3). Accordingly, detection of severe hypoperfusion may be delayed and as a consequence irreversible graft injury may be inevitable.

Various experimental approaches aiming at continuous surveillance of hepatic metabolism have been evaluated for early detection of liver ischemia. Microdialysis was successfully used in liver transplant patients (7-9) and could detect liver ischemia by increasing lactate levels (8, 9). However, hepatic microdialysis was only capable in detecting HA and not PV occlusion in a porcine model (10) and clinical studies (9). Continuous measurement of hepatic oxygen and carbon dioxide partial pressure (PO_2, PCO_2) in animals was shown to be feasible and detected liver hypoxia and ischemia in models of global hypoxia (11) and hemorrhagic shock (12, 13). Likewise, intestinal PCO_2 was shown to reflect intestinal ischemia (13).

Tissue PCO_2 increase reflects organ hypoperfusion, predicts organ failure and serves both as a measure of anaerobic metabolism (PCO_2 is produced when bicarbonate buffers protons) and blood flow stagnation (impaired removal of both aerobically and anaerobically produced PCO_2) (13-16).

In a prior study, we evaluated a new miniature PCO_2 sensor (IscAlert) in a model of myocardial ischemia/reperfusion and could report that ischemic episodes were successfully identified (17). The results challenged us to consider whether the FDA approved IscAlert sensor could also be used for detection of hepatic and intestinal ischemia. Neurotrend sensors and microelectrodes were used to verify IscAlert obtained values and to obtain tissue PO_2 values.

In this study, we aimed to evaluate PCO_2 as a real-time diagnostic tool to detect HA and PV occlusion. We hypothesized (a) that intrahepatic and intraperitoneal PCO_2 measurement enables distinct detection of and discrimination between HA and PV occlusion in real time and (b) that even gradual HA and PV occlusion leads to metabolic changes reflected by PCO_2 raise in liver and intestine, respectively.

Materials and Methods

Experimental setup

The Norwegian Animal Care and Use Committee approved the following protocol and animals were handled according to local guidelines and the Revised Guide for the Care and Use of Laboratory Animals (NIH GUIDE, 1996).

Thirteen conventional landrace pigs (sus scrofa, Noroc), mean weight 59.3 kg (range 54 – 62.5 kg), male or female, without any signs of infection were anesthetized by intramuscular injection of ketamine (30 $mgkg^{-1}$) and azaperone (3 $mgkg^{-1}$). Anesthesia and analgesia were maintained by continuous isoflurane (1-1.5% inspired fraction) and infusion of morphine (0.5-1 $mgkg^{-1}h^{-1}$).

After tracheotomy, mechanical ventilation (Servo ventilator system 900 C, Siemens, Germany) was carried out with a mixture of room air and oxygen aiming to keep arterial PO_2 above 90 mmHg (12 kPa). Tidal volume and ventilation rate were adjusted to keep arterial PCO_2 close to 40 mmHg (5.5 kPa).

One catheter was inserted in the right internal jugular vein for intravenous injection and measurement of central venous pressure, another catheter in the right carotid artery for assessment of arterial blood pressure and arterial blood sampling. Cardiac index (CI) was obtained from a femoral artery PiCCO catheter, (PULSION Medical Systems, Munich, Germany) after thermal dilution calibration.

After median laparotomy the PV and HA proximal to splitting into lobe arteries were identified in the portal hiatus of the liver. Blood flow measurement using transit time flow-probes (PeriVascular probe, MediStim, Oslo, Norway) was established. Inflatable vascular occluders (In Vivo Metric, Healdsburg, CA, USA) were placed around the PV and HA. It was assured that the deflated occluder did not reduce blood flow and that maximal inflation totally obliterated blood flow. Regulation of the grade of occlusion was achieved using a manually adjustable syringe pump.

Catheters enabling blood sampling from the PV and hepatic vein (HV) were established using the Seldinger technique by penetrating the peripancreatic fat and anterior middle liver lobe, respectively.

Four to six miniature sensors (<1 mm diameter) measuring PCO_2 (IscAlert, SensoCure AS, Horten, Norway) were placed in the liver via a split needle 5 - 10 mm below the surface. Up to three sensors were freely placed into the abdominal cavity, lying in between loops of small intestine. IscAlert sensors detect changes in PCO_2 from an automatically calculated baseline at zero based on a conductometric method described elsewhere (18). Briefly, a gas-permeable membrane allows tissue CO_2 diffusion into the water-filled sensor where CO_2 dissolves to HCO_3^- and H^+. This leads to a change in the conductivity of the water, which is continuously measured by the electrical impedance between two electrodes in the sensor.

To verify the IscAlert derived PCO_2 changes and to obtain tissue PO_2 values a fiber-optical sensor measuring tissue PO_2, PCO_2 and temperature (Neurotrend®, Codman, MA) was inserted into the anterior middle lobe of the liver in the same manner as the IscAlert sensors. Neurotrend sensors do not tolerate intestinal movements, which can lead to bending of the sensors' optical fibers. Thus, three dip-type CO_2 microelectrodes (Microelectrodes Inc, Bedford, NH, USA) were placed in the abdominal cavity in two animals for comparison to IscAlert obtained values.

Up to three microdialysis catheters (CMA 65, 100 kDa cutoff, 3 cm membrane, 1 $\mu lmin^{-1}$ flow, M Dialysis, Solna, Sweden) were inserted in the proximity of the Neurotrend® and IscAlert sensors in the liver and up to two were placed intraluminally into the jejunum. Microdialysis allows determination of tissue levels of substances important in cellular metabolism. The microdialysis catheter consists of a semi-permeable membrane with a

defined pore-size allowing recovery of substances from the tissue. Tissue metabolites equilibrate into a dextrane containing fluid (Plasmodex, Meda AB, Solna, Sweden) on the inner side of the membrane. The fluid is pumped continuously into a collection tube (microvial, M Dialysis, Solna, Sweden). The collection tube is disconnected for analysis of lactate, glucose, pyruvate and glycerol in an analysis machine (CMA 600, M Dialysis, Solna, Sweden).

After instrumentation the abdomen was loosely closed using surgical metal clamps preventing temperature decline and excessive fluid loss due to perspiration, while allowing intermittent observation of the liver and intestine. The abdominal wall was elevated using a lifting bandage to avoid increased intraabdominal pressure.

To compensate for fluid loss due to surgery and basic metabolism crystalloids were administered at 10 - 13 $mlkg^{-1}h^{-1}$ to achieve isovolemia as judged by central venous pressure (4-12 cm H_2O), cardiac index (< 10% change), urine production (> 1 $mlkg^{-1}h^{-1}$) and hematocrit (< 5% change). Blood glucose was regularly measured and glucose 10% was infused to ensure normoglycemia. Events of acute circulatory instability occurred in the course of PV occlusion and pigs were resuscitated with colloid infusion and continuous as well as bolus administration of epinephrine.

Experimental protocol

Following a one hour stabilization period after surgery, subjects were assigned to either group A (7 subjects) or B (6 subjects). In group A, the HA was fully occluded for 30 minutes (min) followed by a 30 min reperfusion period (fig. 1). Thereafter PV was fully occluded for 30 minutes (min) followed by a 60 min reperfusion period. Both HA and PV were then gradually occluded to 60, 40, 30, 20, 10, and 0% blood flow with a duration of 30 min at each level (fig. 1).

In group B, hepatic artery baseline flow was recorded and thereafter gradually reduced to 60, 40, 30, 20, and 10% flow in 20 min steps and was held fully occluded for 60 min. After a 60 min reperfusion period the portal vein was gradually occluded in the same manner and 0% flow was maintained for 20 min (fig. 1).

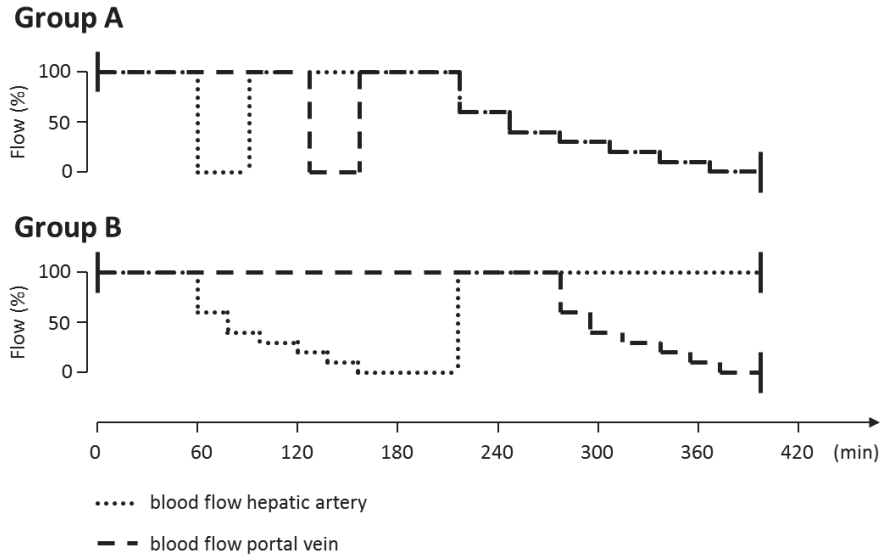

Figure 1 - Schematic time-line of the experimental design.
Blood flow was reduced in HA (dotted line) and PV (dashed line) for the designated intervals in group A (seven animals) and B (six animals).

Data collection

Global variables of circulation and respiration as well as data collected from the Neurotrend sensor were continuously recorded every 20 seconds using ICUpilot® software (M Dialysis, Solna, Sweden). IscAlert, Microelectrodes and blood flow data were acquired continuously every 20 seconds using LabView® software v8.5. Arterial, portal vein and hepatic vein blood samples were drawn for blood gas analysis (ABL 800, Radiometer Copenhagen, Denmark) at baseline, 5 min before each new occlusion, and at the end of the last reperfusion period. Microdialysis samples were obtained at the same time points and analyzed for tissue lactate, glucose and glycerol (CMA 600, M Dialysis, Stockholm, Sweden).

In the seven animals of group A IscAlert catheters were used in four animals because of sensor production stop. In the same group, data from Neurotrend sensors was used from six animals because of catheter malfunction in one animal. One subject in group A became cardiovascular instable after portal vein occlusion with subsequent death and data for combined HA and PV occlusion therefore consists of 3 IscAlert datasets. All animals in group B were monitored with both IscAlert and Neurotrend sensors in liver and intestine.

Arterial blood samples were drawn at baseline, at the end of each reperfusion period and at the end of 0% flow in HA and PV for analyses of bilirubin, aspartate-amino-transferase (AST), alanine amino-transferase (ALT), lactate-dehydrogenase (LDH), alkaline phosphatase (ALP) and gamma-glutamyl-transferase (γ-GT).

Statistics

Pilot experiments in animals undergoing identical anesthesia, surgery and insertion of measurement devices but without vascular occlusion revealed no changes in parameters of cardiovascular function or intra-organ metabolism when observed for as long as the experiment lasted in this study. Based on these findings we decided that a control group would be unnecessary both for ethical and economic reasons and reduction in the number of animals used. Thus, each animal serves as its own control and values at the end of the stabilization period and prior to gradual occlusion of HA, PV or both were used as controls for each parameter in order to monitor biological changes. Maximum values during the experimental events were extracted for all parameters measured continuously (IscAlert, Neurotrend, systemic parameters). Statistical differences were tested using a linear mixed effect model. A random effects model was used and model selection was done for each variable by choosing the model achieving the lowest Information Criteria. The measured parameters were dependent variables, vascular occlusion events were assigned fixed effect and the random effects of subjects and groups were included in the model. A post-hoc comparison of all groups to baseline with Bonferroni correction for multiple testing was performed. A P-value ≤ 0.05 was considered statistically significant. Statistical analysis was done with SPSS 18 (IBM, Armonk, NY, USA). Graphs were prepared with SigmaPlot 11 (Systat Software Inc., San Jose, CA, USA) and GraphPad Prism 5 (GraphPad Software Inc., La Jolla, CA, USA).

Results

Hepatic and intestinal PCO_2 and PO_2

In group A, total HA and PV occlusion was reliably achieved (fig. 2). HA occlusion led to significant hepatic PCO_2 increase detected by both hepatic IscAlert and Neurotrend catheters ($P < 0.001$ and 0.02, respectively, fig. 2 A). PCO_2 in the abdominal cavity remained unchanged (fig. 2 B). During PV occlusion, intestinal PCO_2 increased and was reliably detected by IscAlert ($P = 0.02$) and Microelectrode sensors (fig. 2 B). Hepatic PCO_2 increased slowly, but non-significantly during 30 min of PV occlusion (fig. 2 A). After reopening of the PV occlusion, intestinal PCO_2 began immediate return to baseline, while hepatic PCO_2 increased before approaching baseline values after 15 min.

During both HA and PV total occlusion, hepatic PO_2 decreased significantly ($P < 0.001$) (fig. 2 A). Anoxia was neither achieved during HA nor PV occlusion.

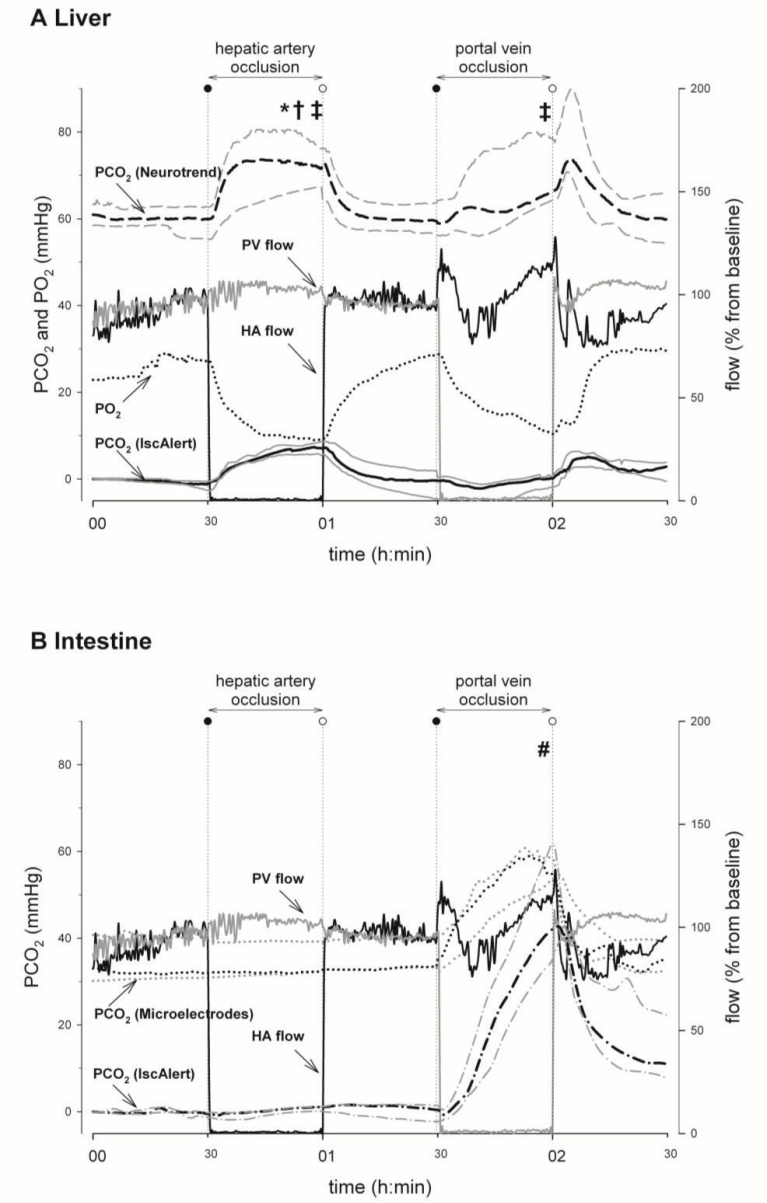

Figure 2 – HA and PV occlusion are detected by PCO_2 measurement
Blood flow in HA (black line) and PV (grey line) was reliably reduced to zero during occlusion. (A) HA occlusion but not PV occlusion led to significant increase of hepatic PCO_2 from baseline measured by IscAlert (∗; maximum change 9 mmHg (1.2 kPa)) and Neurotrend (†; maximum change 13 mmHg (1.7 kPa)). Both HA and PV occlusion led to significant reduction in hepatic PO_2 (‡). (B) Intestinal PCO_2 was significantly augmented only during PV occlusion and not HA occlusion as detected by IscAlert sensors (#; maximum change 43 mmHg (5.7 kPa)).
PCO_2 values expressed as median (black lines) and quartile range (grey lines). Blood flow and PO_2 are expressed as median. $P \leq .05$, exact values presented in text.

Hepatic and intestinal metabolism

Hepatic microdialysis in the course of HA occlusion revealed significant lactate increase (P = 0.003), accompanied by significant glucose decrease (P = 0.01; fig. 3 A). Glycerol showed a non-significant increasing trend (P = 0.21). During PV occlusion, hepatic glucose was unaffected while lactate increased significantly (P = 0.002).

Intestinal metabolism was not affected by HA occlusion, reflected by unchanged intraluminally assessed microdialysis samples (fig. 3 B). Abrogation of PV blood flow caused significant increases in intraluminal lactate (P < 0.001) and glycerol (P = 0.004, fig. 3 B).

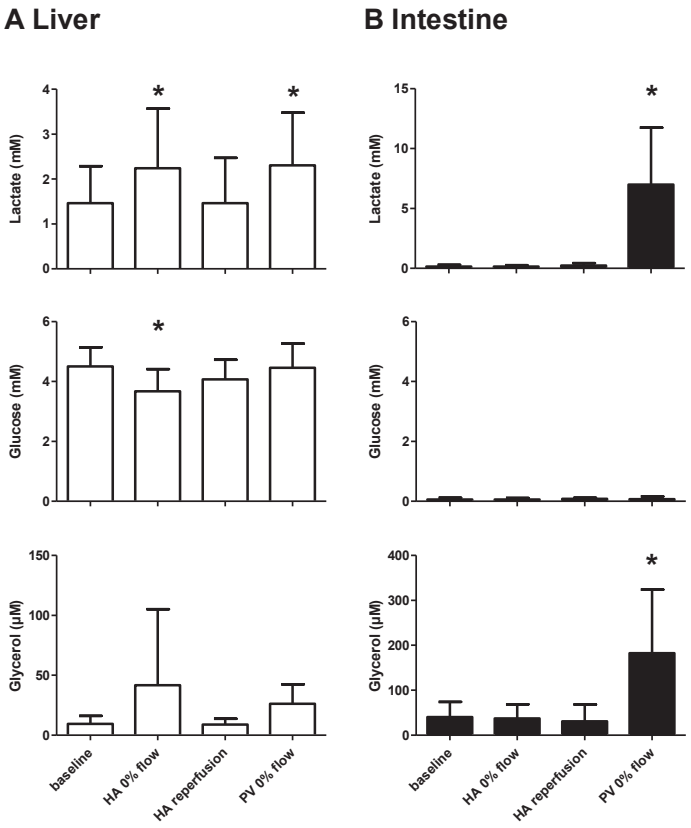

Figure 3 – Intermediate metabolism in liver and intestine is affected by HA and PV occlusion
(A) Hepatic microdialysis showed significant reduction of glucose and elevation of lactate during HA occlusion accompanied by a non-significant glycerol increase. PV occlusion led to significant hepatic lactate increase, while all other parameters were unchanged. (B) HA occlusion did not influence intestinal homeostasis. PV occlusion led to significant increases in intestinal lactate and glycerol.
All values presented as mean ± S.D.; ∗:p ≤ .05, exact values presented in text.

Blood gas analysis and laboratory assessment of hepatic cell damage

Blood gas analysis from PV, hepatic vein (HV) and arterial blood samples revealed that only PV occlusion and the following reperfusion led to significant and clinical relevant changes in PCO_2, lactate and oxygen saturation at all measurement sites (table 1).

Table 1 Blood Gas Analysis

	PCO_2 (mmHg)			Lactate (mM)			SO_2 (%)		
	arterial	portal vein	hepatic vein	arterial	portal vein	hepatic vein	arterial	portal vein	hepatic vein
Baseline	43.4 ± 3.8	52.6 ± 3.0	53.7 ± 5.3	0.70 ± 0.1	0.84 ± 0.2	0.51 ± 0.1	98.3 ± 1.3	64.2 ± 7.6	44.6 ± 11.8
Hepatic artery occlusion	43.4 ± 3.0	52.4 ± 3.0	55.7 ± 5.3	0.75 ± 0.2	0.78 ± 0.2	0.53 ± 0.1	97.9 ± 1.2	59.8 ± 11.7	34.2 ± 13.1
Reperfusion	43.1 ± 3.0	52.7 ± 2.3	53.0 ± 3.0	0.67 ± 0.1	0.83 ± 0.1	0.46 ± 0.1	97.6 ± 1.4	62.1 ± 8.4	44.3 ± 14.0
Portal vein occlusion	42.3 ± 5.3	68.9 ± 9.8*	60.4 ± 4.5	2.01 ± 0.8	3.94 ± 1.7*	2.10 ± 1.0	97.0 ± 2.2	30.9 ± 17.0*	23.5 ± 10.7*
Reperfusion	45.2 ± 4.5	55.5 ± 9.8	56.6 ± 12.0	2.66 ± 2.8*	2.81 ± 2.8	2.40 ±2.9*	92.2 ± 7.3*	61.9 ± 15.2	42.7 ± 18.5

All values: Mean ± S.D.; SO_2: saturation of oxygen
*: $p \leq 0.05$, Linear mixed-effects model with post-hoc comparison of all samples to baseline and Bonferroni correction for multiple testing

Laboratory assessment of standard clinical parameters for liver cell damage showed a significant AST increase from baseline (40.0 ± 9.5 U/l) in the course of PV occlusion (95.0 ± 52.2 U/l, P = 0.006) and PV reperfusion (123.3 ± 43.3 U/l, P < 0.001), while bilirubin, ALT, LDH, ALP and γ-GT remained unaffected and in the normal range throughout the experiment.

Systemic hemodynamics

While complete occlusion of HA had no effect, total obstruction of PV did significantly change mean arterial blood pressure, heart rate, end-tidal CO_2 and CI (P < 0.05; table 2).

Table 2 Systemic Parameters

Event	MAP (mmHg)	CI (l/min/m²)	Pulse (beats/min)	SpO_2 (%)	$etCO_2$ (mmHg)
Baseline	66.8 ± 7.8	4.2 ± 0.7	85.3 ± 13.3	99.7 ± 0.4	47.3 ± 4.5
Hepatic artery occlusion	70.3 ± 11.3	4.1 ± 0.8	85.7 ± 15.3	99.4 ± 0.9	47.3 ± 4.5
Reperfusion	66.2 ± 8.2	4.5 ± 0.8	90.3 ± 18.7	99.3 ± 0.9	47.3 ± 3.8
Portal vein occlusion	51.2 ± 9.7 *	3.2 ± 1.0 *	116.1 ± 29.4 *	99.6 ± 0.5	42.0 ± 6.8 *
Reperfusion	66.5 ± 8.5	5.1 ± 0.7	121.6 ± 11.0 *	98.1 ± 1.5	48.0 ± 3.8

All values expressed as mean ± SD of the average in the evaluated period; MAP: mean arterial pressure; CI: cardiac index; SpO2: saturation of peripheral oxygen; etCO2: end tidal CO2
*: $p \leq 0.05$, Linear mixed-effects model with post-hoc comparison of all samples to baseline and Bonferroni correction for multiple testing

Experimental clinical situations

Acute total HA or PV obstruction may occur clinically as embolization or thrombosis. Gradual stenosis also occurs due to graft kinking or incomplete thrombosis, leading to total obstruction after some time. Hence, HA and PV were gradually occluded separately (fig. 4 A & B) or in combination, the latter resembling systemic blood flow impairment as seen in cardiogenic or hemorrhagic shock (fig. 4 C). Gradual HA blood flow decrease led to a step-wise increase in the hepatic PCO_2, while intra-abdominal PCO_2 was unchanged (fig. 4 A).

Gradual PV blood flow reduction led to an immediate increase of intestinal PCO_2 with each reduction in blood flow (fig. 4 B). Combined graded HA and PV blood flow reduction led to joint increases of hepatic and intestinal PCO_2 reaching high end-point values (fig. 4 C). Hepatic lactate determined by microdialysis remained unaffected during gradual HA blood flow reduction (data not shown). PV and combined HA and PV obstruction caused immediate intestinal and hepatic lactate increase attaining significance during 10% and 0% blood flow (data not shown).

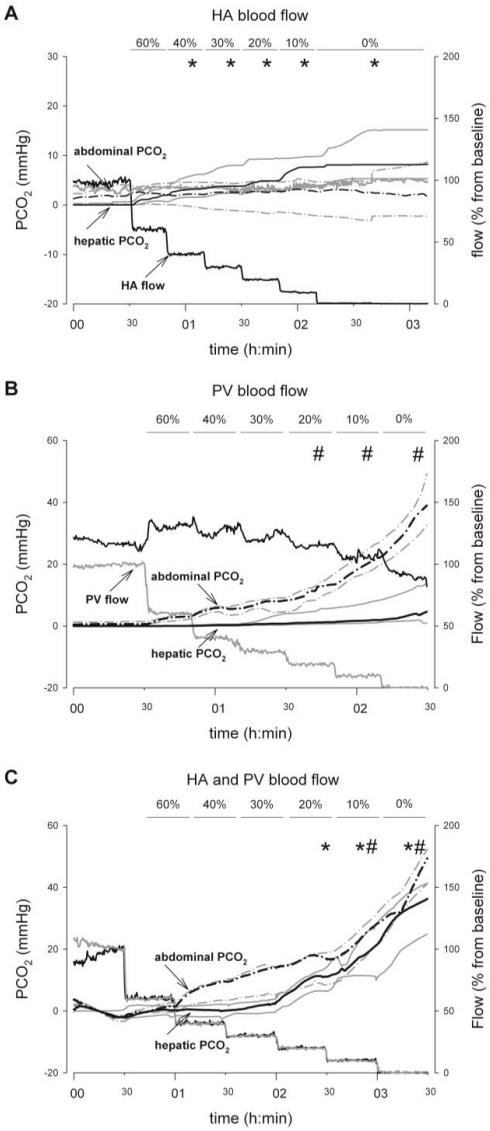

Figure 4 – Gradual blood flow decrease in HA, PV or both is detected by hepatic and intestinal PCO_2 measurement with IscAlert sensors

Blood flow in HA (black line) and PV (grey line) was reliably reduced to target values expressed as percentage of baseline blood flow. (A) Gradual decrease of HA blood flow resulted in hepatic PCO_2 increase (continuous line), reaching significance during 40% of baseline blood flow (∗; maximum change from baseline 8 mmHg (1.1 kPa)), while intraperitoneal PCO_2 (dash-dot line) was unaffected. (B) PV occlusion did not affect hepatic PCO_2 but intra-abdominal PCO_2 was significantly increased starting at 20% blood flow (#; maximum change from baseline 39 mmHg (5.2 kPa)). (C) Combined flow reduction in HA and PV resulted in significant intestinal (#; maximum 50 mmHg (6.6 kPa)) and hepatic (∗; maximum 36 mmHg (4.8 kPa)) PCO_2 increase with the highest end-point values of all situations tested. PCO_2 values expressed as median (black lines) and quartile range (grey lines). Blood flow is expressed as median. $P \leq .05$, exact values presented in text.

Discussion

In the present study, we demonstrate that selective occlusion of HA and PV leads to distinct alterations of hepatic and intestinal metabolism, respectively. HA occlusion affects hepatic energy metabolism resulting in glucose depletion, lactate and PCO_2 increase, while intestinal metabolism is unaffected. PV occlusion mainly affects intestinal metabolism leading to intraluminal increases in lactate and glycerol concomitant with an intra-abdominal PCO_2 increase. Gradual occlusion of either HA and PV alone or in combination results in specific PCO_2 changes in both liver and intestine already during states of impaired blood flow.

We detected a significant increase in hepatic PCO_2 during HA occlusion and HA stenosis when blood flow was reduced to 40% of baseline. Intestinal PCO_2 increased only during PV occlusion. PCO_2 increase might be either due to blood flow stagnation leading to accumulation of aerobically produced CO_2 or anaerobic metabolism leading to CO_2 generation by bicarbonate buffering lactate derived protons (16, 19). During complete blood flow obstruction, our study supports the latter cause since simultaneous lactate and glycerol increase indicate ischemia with cellular membrane break down. States of diminished blood flow during gradual obstruction did not lead to hepatic nor intestinal lactate increases, probably due to pre-conditioning effects of slow and stepwise reduced blood flow (20). Reduced HA and PV blood flow, however, caused hepatic and intestinal PCO_2 increase, respectively, strongly indicating that blood flow stagnation contributes to the accumulation of CO_2 in the organ (16). PCO_2 in the HV showed a modest increase during HA and PV occlusion. Greater de-oxygenation of hemoglobin during hypoxia alkalinizes hemoglobin, thus increasing proton buffering ability as well as binding of CO_2 forming carboxyhemoglobin (Haldane effect). This effect enables transport of large amounts of CO_2, while dissolved venous effluent PCO_2 gets only minimally increased (21). Blood gas analysis measures the dissolved portion of CO_2 and the increase in tissue PCO_2 will therefore be more pronounced than the increase in HV PCO_2. Tissue PCO_2 may thus serve as a parameter of blood flow assessment with slower and lower increase during blood flow decrease and fast and higher elevation during states of tissue ischemia (13).

Standard clinical monitoring using parameters of systemic hemodynamic monitoring and arterial blood gas analysis failed to detect HA occlusion. PV occlusion led to significant changes of blood pressure, pulse, end tidal CO_2 and cardiac output. These observations are unspecific as they reflect acute hypotension with compromised systemic circulation due to blood pooling in the intestine and would thus not result in reliable and exclusive diagnoses of acute PV occlusion. Only AST but not ALT and bilirubin got elevated during PV occlusion. This may imply that intestinal but not hepatic cell damage occurred (22) in accordance with AST being released during intestinal ischemia. However, the specificity of AST as a serum marker for intestinal ischemia is weak (23). The findings support the impression that postoperative HA and PV occlusions are difficult to detect with current standards of monitoring (1). Contrary to this, we show that continuous intraorgan monitoring using hepatic and intra-abdominal PCO_2 measurement provides both real-time ischemia detection as well as identification of the affected vascular territory.

Both HA and PV occlusion leads to comparable hepatic PO_2 decrease as both vessels contribute to the hepatic oxygen content. Therefore, surveillance of hepatic PO_2 does not seem to be optimal for monitoring of liver grafts as neither the metabolic state nor the affected vessel can be identified. Occurrence of anaerobic metabolism and significant PCO_2 increase seemed to be dependent on the lack of HA and not PV blood flow, confirming clinical and experimental findings (9, 10). Occurrence of anaerobic metabolism despite sufficient PV blood flow might be explained by the fact that parts of the liver, e.g. the biliary system, are dependent on HA blood flow (4, 24).

Recently, post-operative monitoring of the liver graft using microdialysis has been successfully evaluated in both experimental and clinical studies and was shown to detect acute cellular rejection and HA occlusion (8-10). In this study, we confirm that HA occlusion

leads to significant lactate production already after 30 min and is accompanied by PO_2 decrease and PCO_2 increase, indicating that lactate production is indeed due to anaerobic metabolism rather than hyper-metabolism as seen in rejection (10). PV occlusion affected intestinal metabolism and it has been shown that intestinal ischemia leads to dysfunction of the gut barrier resulting in luminal lactate and glycerol increase (25, 26). Microdialysis catheters placed between loops of intestine have been shown to reflect the intraluminal changes (26, 27). Results from the present study might therefore be translated to clinical monitoring with placement of the microdialysis catheters or IscAlert sensors between intestinal loops for reliable detection of intestinal ischemia.

PV occlusion lead to significant hepatic lactate increase, which was not observed in a different model where a portocaval shunt was used during PV occlusion (10). The discrepancy could be explained by the portocaval shunt preventing intestinal venous congestion; while in our model blood stasis and pooling in the intestine lead to intestinal ischemia with lactate production and assumed shunting to the systemic circulation. In addition to physiological and therefore normal shunts patients with portal hypertension have established collaterals pre-transplantion (28). However, these collaterals are probably not as efficient as an experimental portocaval shunt during postoperative PV occlusion. Thus, PV occlusion after OLT will lead to some degree of intestinal venous congestion with subsequent intestinal ischemia, lactate and PCO_2 increase (29).

Following liver transplantation, the most important property of a test is the ability to detect impaired hepatic artery circulation, since this is the most deleterious and common vascular complication. Consequently, both microdialysis and PCO_2 monitoring could be useful to detect and discriminate HA and PV occlusion. Currently, microdialysis has the advantage of clinical approval, at least in Europe. However, the additional workload of substance analysis combined with considerable price and uncertainty of individual catheter life span may limit future clinical application in liver transplants. IscAlert PCO_2 sensors on the other hand would have the advantage of real-time, bedside continuous monitoring without increased workload. Most importantly, based on our results partially decreased blood flow would be detected only with IscAlert sensors, while full occlusion would be detected earlier with IscAlert sensors than with microdialysis catheters.

Limitations of this study include the large variance of systemic circulatory function during PV occlusion. However, as the trend of all measured variables was consistent, statistical significance was achieved. We did not evaluate hepatic and intestinal PCO_2 during hepatic vein occlusion, a rare clinical condition caused by veno-occlusive disease or caval stenosis (1, 30). One might speculate that total hepatic vein occlusion would lead to PCO_2 rise in both liver and intestine due to blood congestion and tissue ischemia but further studies should explore this disease entity. Currently, none of the investigated PCO_2 sensors are approved for hepatic or intestinal use. Neurotrend sensors are neither produced nor commercially available, while Microelectrodes are not approved for clinical use. The IscAlert sensor is FDA approved for use in human skeletal muscle, and approval for intraabdominal use will be sought. The IscAlert sensor design has good functionality, as they were easy to insert in both liver and abdominal cavity, did not lead to bleeding or other adverse effects and were easy to retract without damage of the liver tissue at the end of the experiment.

Clinical studies will be carried out with IscAlert PCO_2 sensors inserted in the liver at the end of the transplantation surgery. Intestinal sensors could either be left in the abdominal cavity at the end of surgery, or inserted percutaneously under ultrasound guidance via a split-needle technique (27).

In conclusion, continuous real-time intraorgan monitoring of liver and intestinal PCO_2 evolves as a potential method to monitor hepatic and intestinal blood supply. Vascular complications can be revealed almost immediately, which is clearly superior to current monitoring methods. Combined hepatic and intra-abdominal sensor placement enables detection and discrimination of HA and PV occlusion.

Acknowledgments

The nursing staff of the Intervention Centre provided excellent assistance during the experiments.

Reference List

1. Vaidya S, Dighe M, Kolokythas O, Dubinsky T. Liver transplantation: vascular complications. Ultrasound Q 2007;23(4):239-253.

2. Duffy JP, Hong JC, Farmer DG, Ghobrial RM, Yersiz H, Hiatt JR, et al. Vascular complications of orthotopic liver transplantation: experience in more than 4,200 patients. J Am Coll Surg 2009;208(5):896-903.

3. Bekker J, Ploem S, de Jong KP. Early hepatic artery thrombosis after liver transplantation: a systematic review of the incidence, outcome and risk factors. Am J Transplant 2009;9(4):746-757.

4. Stange BJ, Glanemann M, Nuessler NC, Settmacher U, Steinmuller T, Neuhaus P. Hepatic artery thrombosis after adult liver transplantation. Liver Transpl 2003;9(6):612-620.

5. Llado L, Fabregat J, Castellote J, Ramos E, Torras J, Jorba R, et al. Management of portal vein thrombosis in liver transplantation: influence on morbidity and mortality. Clin Transplant 2007;21(6):716-721.

6. Mehrabi A, Fonouni H, Muller SA, Schmidt J. Current concepts in transplant surgery: liver transplantation today. Langenbecks Arch Surg 2008;393(3):245-260.

7. Nowak G, Ungerstedt J, Wernerman J, Ungerstedt U, Ericzon BG. Clinical experience in continuous graft monitoring with microdialysis early after liver transplantation. Br J Surg 2002;89(9):1169-1175.

8. Waelgaard L, Thorgersen EB, Line PD, Foss A, Mollnes TE, Tonnessen TI. Microdialysis monitoring of liver grafts by metabolic parameters, cytokine production, and complement activation. Transplantation 2008;86(8):1096-1103.

9. Haugaa H, Thorgersen EB, Pharo A, Boberg KM, Foss A, Line PD, et al. Early bedside detection of ischemia and rejection in liver transplants by microdialysis. Liver Transplantation 2012.

10. Ungerstedt J, Nowak G, Ungerstedt U, Ericzon BG. Microdialysis monitoring of porcine liver metabolism during warm ischemia with arterial and portal clamping. Liver Transpl 2009;15(3):280-286.

11. Yang WF, Hafez TF, Thompson CS FAU - Mikhailidis D, Mikhailidis DP FAU - Davidson B, Davidson BR FAU - Winslet M, Winslet MC FAU - Seifalian A, et al. Direct measurement of hepatic tissue hypoxia by using a novel $tcpO_2/pCO_2$ monitoring system in comparison with near-infrared spectroscopy. Liver Int 2003;23(3):163-170.

12. Soller BR, Heard SO, Cingo NA, Hsi C, Favreau J, Khan T, et al. Application of fiberoptic sensors for the study of hepatic dysoxia in swine hemorrhagic shock. Crit Care Med 2001;29(7):1438-1444.

13. Waelgaard L, Dahl BM, Kvarstein G, Tonnessen TI. Tissue gas tensions and tissue metabolites for detection of organ hypoperfusion and ischemia. Acta Anaesthesiol Scand 2012;56(2):200-209.

14. Venkatesh B, Morgan TJ. Monitoring tissue gas tensions in critical illness. Crit Care Resusc 2002;4(4):291-300.

15. Tonnessen TI. Biological basis for PCO_2 as a detector of ischemia. Acta Anaesthesiol Scand 1997;41(6):659-669.

16. Neviere R, Chagnon JL, Teboul JL, Vallet B, Wattel F. Small intestine intramucosal PCO(2) and microvascular blood flow during hypoxic and ischemic hypoxia. Crit Care Med 2002;30(2):379-384.

17. Pischke SE, Tronstad C, Holhjem L, Halvorsen PS, Tonnessen TI. Perioperative detection of myocardial ischaemia/reperfusion with a novel tissue CO_2 monitoring technology. Eur J Cardiothorac Surg 2012.

18. Mirtaheri P, Omtveit T, Klotzbuecher T, Grimnes S, Martinsen OG, Tonnessen TI. Miniaturization of a biomedical gas sensor. Physiol Meas 2004;25(6):1511-1522.

19. Dubin A, Murias G, Maskin B, Pozo MO, Sottile JP, Baran M, et al. Increased blood flow prevents intramucosal acidosis in sheep endotoxemia: a controlled study. Crit Care 2005;9(2):R66-R73.

20. Winbladh A, Bjornsson B, Trulsson L, Offenbartl K, Gullstrand P, Sandstrom P. Ischemic preconditioning prior to intermittent Pringle maneuver in liver resections. J Hepatobiliary Pancreat Sci 2012;19(2):159-170.

21. Deem S, Alberts MK, Bishop MJ, Bidani A, Swenson ER. CO_2 transport in normovolemic anemia: complete compensation and stability of blood CO_2 tensions. J Appl Physiol 1997;83(1):240-246.

22. Caglayan F, Caglayan O, Gunel E, Elcuman Y, Cakmak M. Intestinal ischemia-reperfusion and plasma enzyme levels. Pediatr Surg Int 2002;18(4):255-257.

23. Zhang FX, Ma BB, Liang GZ, Zhang H. Analysis of serum enzyme levels in a rabbit model of acute mesenteric ischemia. Mol Med Report 2011;4(6):1095-1099.

24. Deltenre P, Valla DC. Ischemic cholangiopathy. Semin Liver Dis 2008;28(3):235-246.

25. Solligard E, Juel IS, Bakkelund K, Johnsen H, Saether OD, Gronbech JE, et al. Gut barrier dysfunction as detected by intestinal luminal microdialysis. Intensive Care Med 2004;30(6):1188-1194.

26. Solligard E, Juel IS, Bakkelund K, Jynge P, Tvedt KE, Johnsen H, et al. Gut luminal microdialysis of glycerol as a marker of intestinal ischemic injury and recovery. Crit Care Med 2005;33(10):2278-2285.

27. Ungerstedt J, Nowak G, Ericzon BG, Ungerstedt U. Intraperitoneal microdialysis (IPM): a new technique for monitoring intestinal ischemia studied in a porcine model. Shock 2003;20(1):91-96.

28. Adam R, Hoti E. Liver transplantation: the current situation. Semin Liver Dis 2009;29(1):3-18.

29. Settmacher U, Nussler NC, Glanemann M, Haase R, Heise M, Bechstein WO, et al. Venous complications after orthotopic liver transplantation. Clin Transplant 2000;14(3):235-241.

30. Lee HJ, Kim KW, Mun HS, Kim JH, Song GW, Hwang S, et al. Uncommon causes of hepatic congestion in patients after living donor liver transplantation. AJR Am J Roentgenol 2009;193(3):772-780.

APPENDIX

ISSS 10th International Symposium on Sympathetic Surgery poster by Øvensen et al (by permission)

OBJECTIVE MEASUREMENTS OF SWEAT ACTIVITY BEFORE AND AFTER BILATERAL THORACOSCOPIC SYMPATHECTOMY IN PATIENTS WITH HYPERHIDROSIS AND FACIAL BLUSHING USING A NEW MULTICHANNEL INSTRUMENT

E.Øvensen[a], K. Toska[d], K.Kristiansen[a], O.Grenager[a], Erik Fosse[c], J.Wesche[a,b]

a.Department of Vascular and Thoracic surgery, Akershus University Hospital, Norway
b.Institute of Clinical Medicine, University of Oslo, Oslo, Norway
c.Interventional Centre, Rikshospitalet, Oslo, Norway
d.Institute of Basic Medical Sciences, Department of Physiology, University of Oslo

Akershus universitetssykehus

Introduction

Thoracoscopic sympathectomy is a well established method for treating palmar hyperhidrosis and facial blushing. Compensatory hyperhidrosis is the most common side effect and potentially disabling. The indication is based on patient complaints. No objective measurements of sweat activity are routinely used before surgery. This study investigates sweat activity in patients with hyperhidrosis and facial blushing before and after bilateral thoracoscopic sympathectomy.

Methods

A new multichannel instrument (Sudologger) was used to measure sweat activity from skin areas of the face, palms, stomach and back[1]. The sudologger uses skin surface electrodes for unipolar admittance measurement in the stratum corneum. Measurements were obtained from 46 patients pre- and postoperatively in supine and sitting position. Continuous measurements were obtained over 10 min in each position and an average value over four minutes in each period was calculated in each subject.

Palmar hyperhidrosis and facial blushing

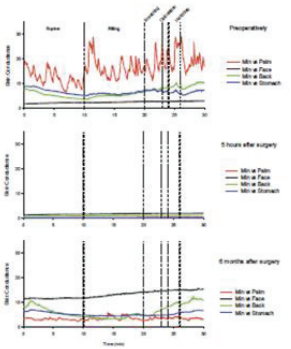

One patient with palmar hyperhidrosis an fascial blushing measured pre-operatively, 5 hours and 6 month after bilateral sympathectomy on second rib.

Results

Sweat activity was higher in the sitting than in the supine position prior to surgery(p=0,000). There was a decrease in palm sweat activity (p=0,000) after bilateral thoracoscopic sympathectomy (rib 2 and/or 3). Sweat activity was unchanged in other areas.

	Pre (Mean)	Post (Mean)	Paired Differences: Mean	95% CI of the difference Lower	Upper	P-value (2-tailed)
Back	2,91	2,41	0,50	-0,62	1,62	0,38
Palm	9,92	2,30	7,62	5,63	9,62	0,00
Face	6,34	6,32	0,02	-2,59	2,63	0,99
Stomach	3,21	2,51	0,71	-0,25	1,67	0,145

Conclusion

These results show an immediate effect on sweat activity after bilateral sympathectomy, with a decrease in the palmar area but no truncal changes. Further studies on sweat activity patterns will be performed to find the best distinguishing parameter for diagnosis and treatment evaluation.

Referance
1. Tronstad, C., et al., Electrical measurement of sweat activity. Physiol Meas, 2008. 29(6): p. S407-15.